1986

ELECTROCHEMICAL INVESTIGATION OF THE EFFECTS OF TEMPERATURE, pH, AND ELECTROLYTE ON THE ELECTRON TRANSFER REACTIONS OF CYTOCHROME C

Kent Brian Koller

COLLEGE OF HUMANITIES AND SCIENCES
VIRGINIA COMMONWEALTH UNIVERSITY

This is to certify that the dissertation prepared by Kent B. Koller entitled "Electrochemical Investigation of the Effects of Temperature, pH, and Electrolyte on the Electron Transfer Reactions of Cytochrome c" has been approved by his committee as satisfactory completion of the dissertation requirement for the degree of Doctor of Philosophy.

[redacted]
Director of Dissertation

[redacted]
Committee Member

[redacted]
Committee Member

[redacted]
Committee Member

[redacted]
Committee Member

[redacted]
Department Chairman

[redacted]
School Dean

8/12/86
Date

ELECTROCHEMICAL INVESTIGATION OF THE EFFECTS OF TEMPERATURE, pH, AND ELECTROLYTE ON THE ELECTRON TRANSFER REACTIONS OF CYTOCHROME c

A dissertation submitted in partial fulfillment of the requirements for the degree of Doctor of Philosophy at Virginia Commonwealth University.

By

Kent Brian Koller
B.S., Virginia Commonwealth University, 1981

Director: Dr. Fred M. Hawkridge
Professor of Chemistry

Virginia Commonwealth University
Richmond, Virginia
August, 1986

ACKNOWLEDGEMENTS

I welcome the opportunity to express my sincere gratitude to the faculty of the Department of Chemistry of Virginia Commonwealth University for their support and guidance. They have liberally taken time from their busy schedules to answer my many questions. First, I wish to thank my advisor Dr. Fred Hawkridge for his extraordinary patience with me during my development as a chemist. His professional ethics and careful attention to accuracy in scientific research serve as standards that I will emulate throughout by my career. Dr. Vallarino was of invaluable assistance in studying for the foreign language exam. Dr. Sneden, as Graduate Student Coordinator, made the administrative process of satisfying the degree requirements and applying for fellowships as painless as possible. My special thanks go to Dr. Topich for the guidance he provided as my research director when I was in the Master's degree program and as an instructor in three of my chemistry courses.

The friendship of my fellow graduate students is deeply appreciated. The trauma of graduate school is made more bearable by commiseration with fellow sufferers. In particular, I thank Dave Reed for setting up the spectro-

photometer that I used for spectroelectrochemical experiments and Carolyn Corcoran for proofreading this manuscript.

TABLE OF CONTENTS

page

LIST OF TABLES vi

LIST OF FIGURES vii

LIST OF SYMBOLS ix

ABSTRACT xii

I. INTRODUCTION 1

A. Overview and Objectives 1

B. Structure of Cytochrome c 5

C. Reaction Mechanism of Cytochrome c 24

D. Electron Transfer Theory 39

E. Heterogeneous Electrochemistry of Cytochrome c 48

II. EXPERIMENTAL..... 51

III. RESULTS AND DISCUSSION..... 62

A. Separation of Faradaic and Nonfaradaic Response 62

B. Temperature, Electrolyte, and pH Dependence of the Formal Potential of Cytochrome c 82
1. In pH 7.0 Buffer 82
2. In pH 5.3 Buffer 107
3. In pH 8.0 Buffer 111

C. Kinetic and Adsorption Behavior of Cytochrome c 114
1. In pH 7.0 Buffer 116
2. In pH 5.3 Buffer 158
3. In pH 8.0 Buffer 160

D. Summary 175

E. Model of Heterogeneous Electron Transfer 178

REFERENCES 185

APPENDIX: DIGITAL SIMULATION OF CYCLIC VOLTAMMETRY 198

APPENDIX REFERENCES 231

VITA 232

LIST OF TABLES

Table page

1. Temperature dependence of the cyclic voltammetric peak separation and midpoint potential of 1 mM cytochrome c in the presence of NaCl 103

2. Surface excess values for adsorbed cytochrome c ... 135

LIST OF FIGURES

Figure		page
1.	The mitochondrion	3
2.	Cytochrome c molecular structure	7
3.	Hemes b and c	9
4.	Electron transfer reaction diagrams	43
5.	Cyclic voltammetry of $K_3Fe(CN)_6$ demonstrating the effect of working electrode orientation at slow scan rates and elevated temperatures	58
6.	Cyclic voltammetry of electrolyte alone at various temperatures	65
7.	Cyclic voltammetry of electrolyte alone at various scan rates	67
8.	Cyclic voltammetry of electrolyte alone at various pH values	70
9.	Cyclic voltammetry of cytochrome c in pH 5.3 phosphate buffer	78
10.	Derivative cyclic voltammetry and cyclic voltammetry of cytochrome c	84
11.	Temperature dependence of the E°' and k°' of $K_3Fe(CN)_6$	88
12.	Temperature dependence of the E°' of cytochrome c in pH 7.0 phosphate and Tris/cacodylic acid buffers	92
13.	Temperature dependence of the E°' of cytochrome c in pH 5.3 Tris/cacodylic acid buffer and pH 8.0 phosphate and Tris/cacodylic acid buffers	110
14.	Reversible and quasi-reversible cyclic voltammetry of cytochrome c in pH 5.3 Tris/cacodylic acid buffer	118
15.	Temperature dependence of the diffusion coefficient of cytochrome c	121

16. Temperature dependence of the k°' of cytochrome c in pH 7.0 phosphate and Tris/cacodylic acid buffers and in pH 5.3 Tris/cacodylic acid buffer . 124

17. Temperature dependence of k°' of cytochrome c in pH 7.0 Tris/cacodylic acid buffer from three experiments 126

18. Temperature dependence of the $i_{p,c}$ of quasi-reversible cyclic voltammograms of cytochrome c in pH 5.3, 7.0, and 8.0 Tris/cacodylic acid buffers 128

19. Real and simulated cyclic voltammograms of cytochrome c that demonstrate the presence of reactant adsorption 134

20. Simulated cyclic voltammograms that demonstrate the effect of variation of reactant and product adsorption strength 142

21. Simulated quasi-reversible cyclic voltammograms that demonstrate the effect of variation of α 153

22. Temperature dependence of the asymmetry of the cyclic voltammetric peak potentials about E°' of cytochrome c in pH 5.3, 7.0, and 8.0 buffers 162

23. Temperature dependence of quasi-reversible cyclic voltammograms of cytochrome c in pH 8.0 buffer ... 165

24. Scan rate dependence of cyclic voltammmetry of cytochrome c in pH 8.0 buffer at 5 °C 167

25. Scan rate dependence of cyclic voltammmetry of cytochrome c in pH 8.0 buffer at 60 °C 171

LIST OF SYMBOLS

A	electrode area, absorbance
C	concentration, analytical
CV	cyclic voltammetry
D	diffusion coefficient (cm^2/s)
DCVA	derivative cyclic voltabsorptometry
E	electrode potential referenced to the normal hydrogen electrode
E°'	formal redox potential referenced to the normal hydrogen electrode
E_{mp}	midpoint potential between $E_{p,a}$ and $E_{p,c}$
$E_{p,a}$	anodic peak potential
$E_{p,c}$	cathodic peak potential
$\blacktriangle E_p$	potential difference between $E_{p,a}$ and $E_{p,c}$
F	Faraday's constant
$\blacktriangle G°$	free energy
$\blacktriangle H°$	enthalpy
i	current
iep	isoelectric point
i_p	voltammetric peak current
$i_{p,a}$	anodic peak potential
$i_{p,c}$	cathodic peak potential
k	Boltzmann's constant

$k^{\circ\prime}$	formal heterogeneous electron transfer rate constant (evaluated at $E = E^{\circ\prime}$)
k_b	back heterogeneous electron transfer rate constant (potential-dependent)
k_f	forward heterogeneous electron transfer rate constant (potential-dependent)
Γ	adsorbed material ($mole/cm^2$)
Γ_s	saturated surface coverage ($mole/cm^2$)
L	liter
n	stoichiometric number of electrons transferred
NHE	normal hydrogen electrode
O	oxidized species
OTE	optically transparent electrode
OTTLE	optically transparent thin-layer electrode
pzc	potential of zero charge on an electrode
pzzp	point of zero zeta potential
$\blacktriangle S_{rc}^{\circ}$	reaction center entropy
t	time after start of electrolysis
T	temperature
Tris	tris(hydroxymethyl)aminomethane
V	volume
x	distance from electrode surface into solution
α	reductive electrochemical transfer coefficient
ε	molar absorptivity

$\blacktriangle\varepsilon$	difference molar absorptivity between two forms of a molecule (typically $\varepsilon_{red} - \varepsilon_{ox}$)
μ	ionic strength
μA	microamps
μC	microcoulombs

ABSTRACT

ELECTROCHEMICAL INVESTIGATION OF THE EFFECTS OF TEMPERATURE, pH, AND ELECTROLYTE ON THE ELECTRON TRANSFER REACTIONS OF CYTOCHROME c.

Kent B. Koller

Virginia Commonwealth University, 1986.

Major Director: Dr. F. M. Hawkridge

Spectroelectrochemical and electrochemical methods have been used to investigate the characteristics of heterogeneous electron transfer between cytochrome c and indium oxide electrodes. Direct electron transfer between cytochrome c and solid electrodes is of interest due to the interfacial character of electron transfer between the protein and its membrane-bound physiological redox partners. The conformation of ferricytochrome c is affected more by changes in temperature or pH than is its reduced form, ferrocytochrome c. This difference in conformational stability is attributed to the +1 charge of the heme in ferricytochrome c that is largely embedded in the hydrophobic interior of the enzyme.

A linear temperature dependence of the formal potential of cytochrome c was observed from 5 to ≥ 55 °C in neutral and acidic media. This behavior is attributed to a linear variation in the conformation of ferricytochrome c that

results in an increase in solvent exposure of the solvent-exposed heme edge. A break in the linear temperature dependence of the formal potential occurred at 40 °C in alkaline media. This reflects a distinct conformational change that accompanies the onset of thermal denaturation of ferricytochrome c. The change in reaction center entropy, $\blacktriangle S_{rc}°$, of ca. -13 eu in neutral and acidic media (5 to ≥ 55 °C) and in alkaline media (below 40 °C) is appropriate for the small shift to a more stable conformation of cytochrome c that occurs upon reduction.

The heterogeneous electron transfer rate constant, k°', of cytochrome c exhibited a biphasic temperature dependence with a maximum value obtained at different temperatures, but at the same formal potential in binding and nonbinding neutral media. This indicates that there is an optimum conformation of ferricytochrome c for facile heterogeneous electron transfer. Adsorption of reactant and product was detected. The strength and type of adsorption were found to be temperature- and pH-dependent. The characteristics of electron transfer between cytochrome c and an electrode depend on bulk solvent properties and electrode surface characteristics.

CHAPTER I - INTRODUCTION

A. Overview and Objectives

Cytochrome c is a member of a diverse group of electron transfer enzymes, cytochromes, that all contain a protoheme IX, or one of its derivatives (1-3). While cytochromes are found in nearly all forms of life, this discussion will be limited to the cytochrome c found in the mitochondria of eukaryotic cells.

Oxidative phosphorylation couples the electron flow along the mitochondrial respiratory chain to the production of ATP (adenosine triphosphate), a common energy source in living cells (4). The culmination of the respiratory process is the electron transport chain that is incorporated in the inner membrane of mitochondria (Figure 1). High energy electrons enter the chain from the matrix side of the inner membrane and release free energy as they move to the terminal electron acceptor, oxygen. Cytochrome c is a small (molecular weight ca. 12,400), water soluble, peripheral enzyme that exists in the cytosol between the inner and outer membranes of mitochondria. Its function is to transfer an electron from cytochrome c reductase to cytochrome c oxidase, the terminal enzyme in the electron transport

Figure 1. The mitochondrion: (a): structure (adapted from White, A.; Handler, P.; Smith, E. L.; Hill, R. L.; Lehman, I. R. "Principles of Biochemistry", 6th Ed.; Mcgraw-Hill: New York, 1978) and (b): the electron transport chain (based on Gassotti, P. Top. Bioelectrochem. Bioenerg. **1980**, 3, 149-190).

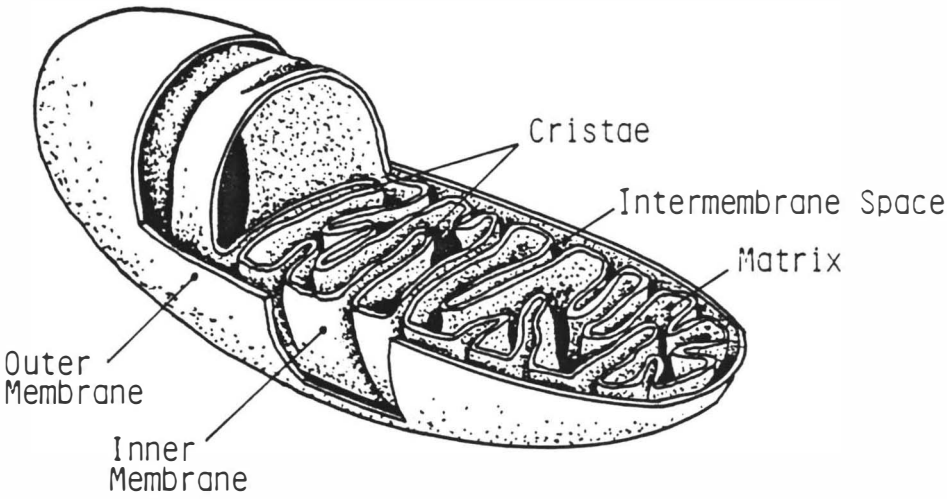
Cristae
Intermembrane Space
Matrix
Outer Membrane
Inner Membrane

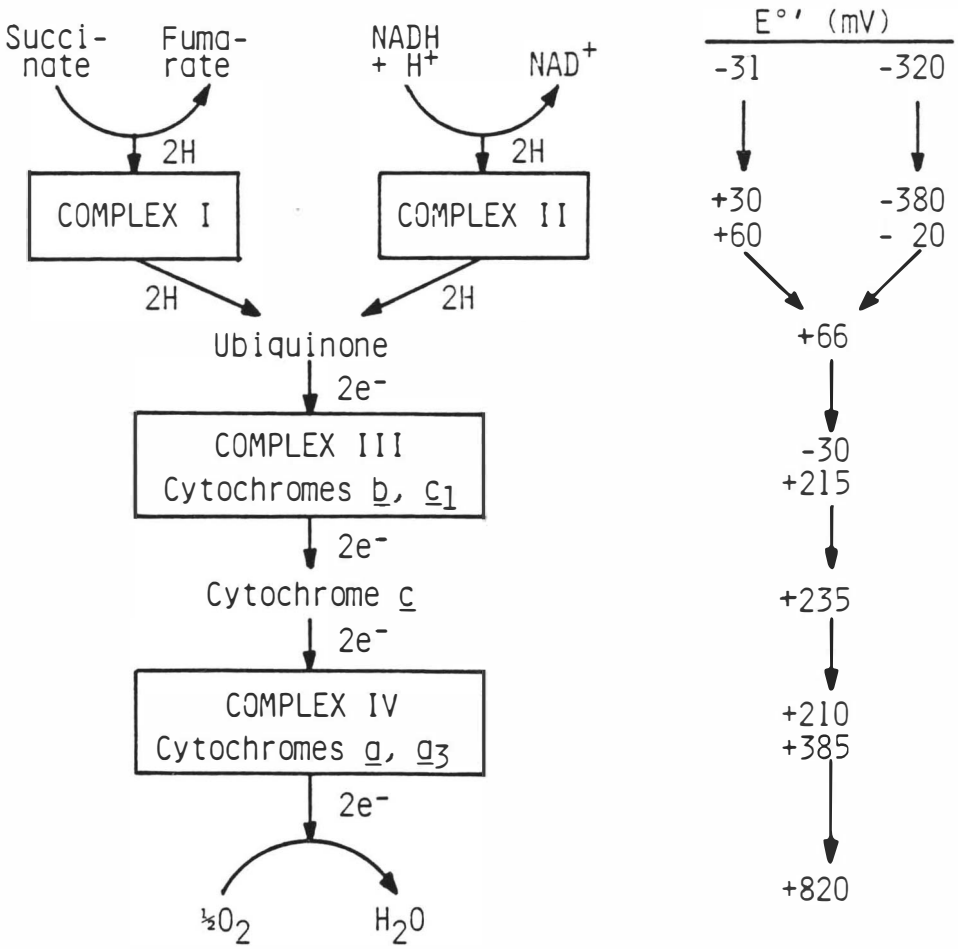
Succi-nate
Fuma-rate
NADH + H+
NAD+
2H
2H
COMPLEX I
COMPLEX II
2H
2H
Ubiquinone
2e-
COMPLEX III
Cytochromes b, c1
2e-
Cytochrome c
2e-
COMPLEX IV
Cytochromes a, a3
2e-
½O2
H2O
E°' (mV)
-31
-320
+30
+60
-380
- 20
+66
-30
+215
+235
+210
+385
+820

chain.

Cytochrome c is easily separated from its mitochondrial environment because it is soluble in water and is weakly associated with the inner membrane surface. The protein has been widely studied owing to its availability in pure, native form. The crystal structures of mitochondrial cytochrome c from several sources have been determined to atomic resolution (1). The interpretation of the physicochemical properties of cytochrome c is facilitated by the knowledge of its conformation.

The kinetics and mechanism of electron transfer between cytochrome c and its physiological redox partners is not fully understood. Electrochemistry has been applied to the study of the thermodynamic and kinetic properties of cytochrome c (5-56). While the temperature dependence of the thermodynamic properties of cytochrome c has been investigated using electrochemical methods, heterogeneous electron transfer had not been employed prior to the beginning of this research, rather, a mediator was used to link the potential of the electrode to the redox ratio of cytochrome c (14, 17, 23, 24, 44). Although heterogeneous electron transfer rate constants have been obtained for cytochrome c at various electrodes (15, 18, 27, 29, 30, 32, 35, 36, 37, 38, 41, 42, 45-56), the effects of temperature on the heterogeneous electron transfer kinetics have not been investigated. The goal of the research presented in this dissertation has been to elucidate the mechanism of the

heterogeneous electron transfer of cytochrome c at a solid electrode through the characterization of the effects of temperature, pH, and electrolyte on the thermodynamic and kinetic parameters of the reaction. The study of cytochrome c electron transfer behavior using direct electrochemical methods is of interest due to the interfacial character of the electron transfer reactions between cytochrome c and its physiological redox partners. This investigation of the mechanism of direct electron transfer of cytochrome c at an electrode also may provide useful information for the general development of amperometric biosensors.

B. Structure of Cytochrome c

Cytochrome c (Figure 2) consists of a single polypeptide chain with a globular tertiary structure and a heme (Figure 3) that is deeply embedded within the hydrophobic interior of the protein, except for a solvent-exposed heme edge (1). The redox component of cytochrome c is a low-spin iron atom located in an octahedral coordination environment. The iron atom cycles between the +3 and +2 oxidation states. A porphyrin ring provides the equatorial ligands. The iron-containing porphyrin ring is the heme group. Axial coordination sites of the iron atom are occupied by two strong field ligands: the ε-nitrogen of his-18 and the sulfur atom of met-80.

In ferricytochrome c, the five electrons in the 3d shell of the iron atom are located in the d_{xy}, d_{xz}, and d_{yz} orbitals. The z axis is normal to the heme plane. The

Figure 2. Cytochrome c molecular structure. This view of oxidized horse heart cytochrome c is towards the molecular front face, which contains the exposed heme edge (or heme crevice). The left and right sides of the molecule are as viewed. Only the α-carbon atoms are shown; amide groups are represented by straight bonds. No amino acid side chains are shown except for those bonded to the heme, i.e., met-80, his-18, cys-14, cys-17. (Adapted from Dickerson, R. E.; Timkovich, R. In "The Enzymes", Boyer, P. E., Ed.; Academic Press: New York, 1975; Vol. XI-A, 397-547).

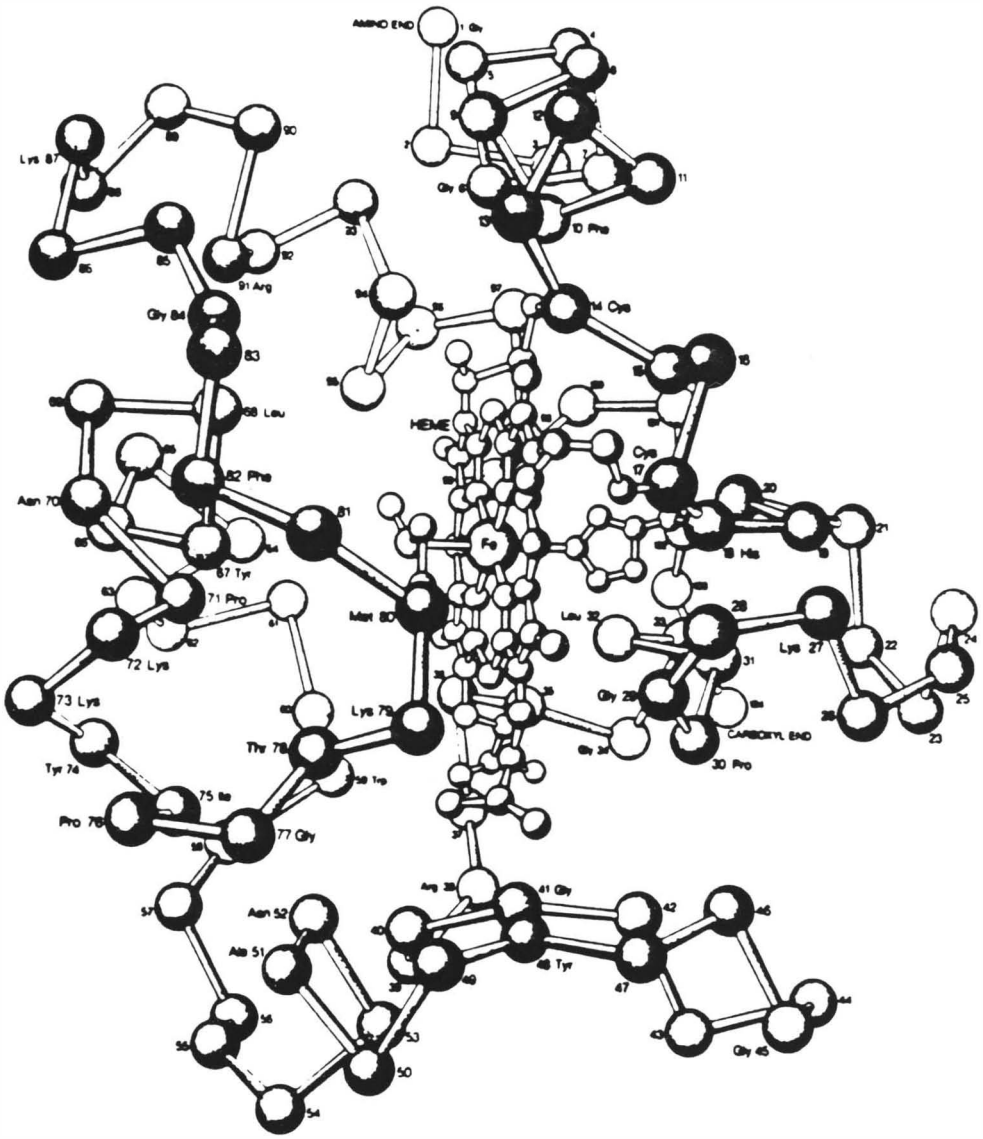
AMINO END
1 Gly
10 Phe
14 Cys
HEME
Fe
8 His
CARBOXYL END
30 Pro
Lys 27
Gly 25
Leu 32
Met 80
Lys 79
Thr 78
77 Gly
Pro 76
75 Ile
Tyr 74
73 Lys
72 Lys
71 Pro
67 Tyr
82 Phe
68 Leu
Gly 84
91 Arg
Lys 87
Asn 70
Asn 52
Ala 51
41 Gly
45 Tyr
Gly 45

Figure 3. Hemes b and c

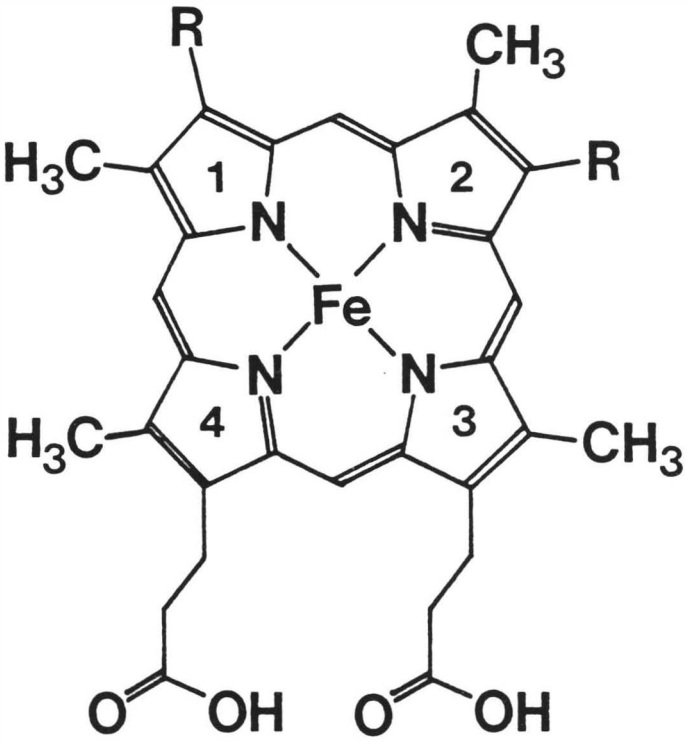

heme b, R: $-C(=CH_2)-H$

heme c, R: $-C(CH_3)(H)-S-$

unpaired spin density is located primarily in the d_{xz} and d_{yz} orbitals (57), which are mixed with the π-orbitals of the porphyrin ring. A proton NMR study of horse heart ferricytochrome c (58) revealed that there is a pronounced asymmetry to the spin density distribution, i.e., 2% of an unpaired electron is localized on the porphyrin ring carbon atoms 3 and 8, whereas only 0.5% of the unpaired electron is on ring carbon atoms 1 and 5. Carbon atom 3 is at the solvent-exposed heme edge. Thus, the asymmetry of the unpaired electron spin distribution on the heme may facilitate direct electron transfer at the solvent-exposed heme edge of cytochrome c. The importance of the spin density asymmetry to physiological function is reinforced by the fact that a chemical modification of cytochrome c caused a change in the spin density distribution and a concomitant loss of physiological activity (59). The direction of the spin density distribution asymmetry may be controlled by the chirality of the axially bound met-80 sulfur (R in horse heart) (60). The chirality of the met-80 sulfur atom controls the direction of the lone pair orbital on the sulfur atom (directed along pyrrole rings II and IV in mitochondrial-type cytochrome c). The orientation of this lone pair orbital imparts different energies to the molecular orbitals formed from the d_{xz} and d_{yz} atomic orbitals of the iron in which the unpaired electron resides, affecting the distribution of the unpaired electron spin density.

The crystal structures of horse heart and bonito ferri-

cytochrome c have been determined to 2.8 Å resolution (61). Horse heart and bonito cytochrome c consist of 104 amino acids in one continuous polypeptide chain, with no disulfide bridges. The heme seems to be the controlling feature of the folding of the polypeptide chain. Only one group of residues, 92 to 102, is strictly alpha-helical. There are six abrupt bends in the chain, each at a location required to attain a globular structure about the heme. Residues 1 through 47 are on the right side of the heme (as shown in figure 2), while residues 48 through 91 are on the left side with the heme placed deeply within the pocket formed by the halves. The remaining residues, 92 to 104, form an alpha-helical chain that extends from the top rear to the right side of the enzyme. The halves of the polypeptide chain are held together by four bonds to the heme. The right side of the polypeptide chain is covalently attached to the heme by thioether linkages between cys-14 and cys-17 and the vinyl groups at positions 2 and 4, respectively, and by a coordinate bond between a nitrogen of his-18 and the iron atom of the heme. The left side is attached to the heme by the coordinate bond between the met-80 sulfur and the iron atom. Thus, the heme plays a major role in the stabilization of the enzyme structure. Substitution of synthetic prosthetic groups that are incapable of covalent linkage to the polypeptide chain results in a looser structure due to a weakening of the heme crevice (62). The structure of the enzyme is further stabilized by an extensive series of hydrogen

bonds. A hydrogen bond from the carbonyl oxygen of pro-30 to the δ-nitrogen of his-18 stabilizes the orientation of the imidazole ring relative to the heme. The sulfur of met-80 is hydrogen bonded to tyr-67. One of the propionic acid side chains of the heme group is buried deeply in the hydrophobic interior of the enzyme. This polar group promotes hydrogen bonds to tyr-48, trp-59, and thr-40. It has been estimated, by a proximity analysis from crystal structure data, that there are 37 backbone, 23 backbone-to-side chain, and 10 side chain-to-side chain hydrogen bonds (63). By the same analysis, it was calculated that there are 136 nonpolar contacts within limits of 4.0 Å and 298 nonpolar contacts within limits of 4.5 Å. It was concluded from a study of the contribution of electrostatic factors to the conformational stability of cytochrome c that the major forces contributing to structural integrity are due to interactions between internal residues (64). Both sides of the heme are surrounded by hydrophobic side chains with at least two approximately parallel aromatic groups on each side, creating a hydrophobic environment for the heme. The crevice about the solvent-exposed heme edge is circled by several positively charged lysine groups. A cluster of nine negatively charged acidic residues is located at the opposite end of the molecule. This asymmetric distribution of charges on the surface is an unusual feature of cytochrome c, and it will be discussed further. In all, cytochrome c has 19 positively charged lysine residues, plus two argi-

nines, also positively charged, but has only 12 acidic residues (aspartic or glutamic acids). Thus, cytochrome c is a very basic molecule with an isoelectric point near pH 10. Cytochrome c has nine aromatic residues situated in the tightly packed interior of the molecule. With the exception of the isolated aromatic residues, phe-36 and phe-82, all are positioned in a parallel configuration with at least one other aromatic group. Phe-36 fills a hydrophobic position in the rear of the molecule, and appears to serve no purpose other than to provide hydrophobicity and bulk. Phe-82, however, is close to the heme group in the center of the flexible region of residues 80 to 85. The close parallel configuration of the aromatic group of phe-82 and the heme, together with its relative freedom of movement, indicate that phe-82 may serve as a pathway for electron transfer to and from the heme (vide infra).

The crystal structures of tuna ferricytochrome c (65) and ferrocytochrome c (66) have been determined to 2.0 Å resolution. While the research presented in this dissertation used exclusively horse heart cytochrome c, the analysis of tuna cytochrome c is of interest for two reasons. First, all types of eukaryotic cytochrome c are nearly identical in structure and function, differing only in a few residue substitutions in or additions to the polypeptide chain. Second, the crystals of horse heart ferricytochrome c were of limited quality (65) such that the resolution of the X-ray crystal structure could not be extended beyond 2.8 Å and

crystals of horse heart ferrocytochrome c could not be obtained.

The analysis of tuna ferricytochrome c revealed that the phe-82 residue is located next to the heme, and closes the heme crevice. It does not extend out into the external solution as had been suggested in the 2.8 Å analysis of horse heart ferricytochrome c (61). A comparison of the crystal structures of the two redox states of tuna cytochrome c demonstrated some small differences (67). When reduced, the heme group moves 0.15 Å further into the hydrophobic interior of the molecule. Several residues that are directly involved with the heme also move. These include residues involved in heme attachment to the polypeptide chain, the residues positioned at the lower right lining of the heme crevice, those at the floor of the crevice, and groups tyr-67, met-80, phe-82, and ala-83. Also, a network of hydrogen bonding involving asn-52, thr-78, and tyr-67 with a buried water molecule located to the left of the heme is affected. When cytochrome c is reduced, the water molecule moves approximately 1.0 Å away from the heme. The residues that are hydrogen bonded to the water molecule are also shifted in position. This buried water molecule is located approximately 5 Å from the met-80 sulfur atom and lies underneath the 70 to 80 series of residues of the polypeptide chain. This region of the molecule appears to be the active site for electron transfer (vide infra). The side chains of this series of residues are either basic or

hydrophobic, and would provide a good fit to a hydrophobic region surrounded by a ring of negative charges on a reaction partner. This appears to be the mode of interaction for the reaction of cytochrome c with cytochrome c peroxidase (68).

A significant feature of cytochrome c is that while the iron atom cycles between charges of +3 and +2, the heme group has a positive charge of +1 in the oxidized form and is neutral when reduced. Therefore, the positive charge on the heme in ferricytochrome c is partially stabilized by the 1.0 Å shift of the buried water molecule toward the heme and the 0.15 Å movement of the heme out of its hydrophobic crevice.

In summary, cytochrome c consists of a heme which is enveloped by the hydrophobic groups of the polypeptide chain. The hydrophilic groups of the polypeptide chain are oriented outward, and solubilize the molecule. The protein is roughly spherical in shape, with dimensions, excluding solvent, of 30 X 34 X 34 Å, including side chains.

The protein sheath plays a crucial role in determining the reduction potential of the heme. Several explanations of the factors that determine the reduction potential have been proposed. Mitochondrial cytochrome c has a redox potential of 260 mV ± 20 mV (1-3). This value is approximately 300 mV positive of model heme compounds in aqueous solution (69, 70). The substitution of nonaqueous, low dielectric solvents for water raised the reduction potential

of the model heme complexes (69, 70). From this result, it was postulated that the hydrophobic environment of the heme group caused the high reduction potential of cytochrome c. The model was based on the difference in free energy for the ferric heme (positive charge of +1) in polar and nonpolar environments. The neutral ferrous heme was assumed to have an electrostatic free energy change of zero with change in polarity of solvents. Thus, the positively charged ferric heme is destabilized relative to the neutral ferrous heme in a nonpolar environment, resulting in a positive shift in reduction potential. Another model (71) is that the degree of heme exposure to solvent is inversely proportional to the reduction potential and that solvent exposure, rather than internal hydrophobicity, is the controlling factor. Moore and Williams (72) proposed that the reduction potential is determined by a more complex mix of factors that includes the electrostatic charge and donor and acceptor power of the ligand. Nitrogen is a better electron donor than sulphur (lowers reduction potential), and sulphur is a better π-acceptor than nitrogen (raises the reduction potential). Therefore, cytochromes with two histidine axial ligands have lower reduction potentials than cytochrome c. Myer, et al. (73) published simultaneously with Moore and Williams, and stated that neither the hydrophobicity of the heme environment nor the degree of solvent exposure controls the reduction potential. The governing factors were determined to be a combination of the integrity of the Fe-S bond and the

hydrophobicity of the trp-57 heme environment in the deepest part of the heme crevice. Substitution of various internal residues local to the heme altered the reduction potential of cytochrome c only if the hydrogen bonding network was disrupted (74). One additional contributing factor is the electrostatic interaction between one of the propionate sidechains of the heme and the positive charge on the ferric ion (75). There does not appear to be a definitive explanation for the heme reduction potential for cytochrome c.

Moore and Williams conducted an NMR study of the effect of temperature on the conformation of ferricytochrome c (76) and the effects of temperature and pH on the conformation of ferrocytochrome c (77). They found that ferrocytochrome c was extremely stable in that it maintained its native configuration from 4 to 97 °C at neutral pH and from pH 4 to 12 at 25 °C. The high activation energy required for the rotation of the aromatic group of a tyrosine residue reflected the close packing of the interior of the molecule (78). There was a linear relationship between the log of the rotation rate and temperature. This indicated that the rotation rate of aromatic residues in the interior of the enzyme could be used as a measure of the stability and conformation of a globular enzyme. Ferricytochrome c was less stable to the effects of temperature, but still maintained nativity in the wide temperature range of 20 to 77 °C at pH 5.3. (The temperature range for nativity was not studied at neutral pH.) The denaturation of ferricytochrome c was attributed

to the rupture of the iron to met-80 sulfur bond, which gradually weakened with increase in temperature. Some high-spin character begins to develop at elevated temperatures prior to denaturation. Moore and Williams found that there is about 12 % high-spin character at 67 °C. Change in oxidation state causes a small change in structure about ile-57. This region of the enzyme, the bottom half of the front face, assists in shielding the heme from solvent (79). In addition to changing with oxidation state, these residues also vary in position in a continuous manner with change in temperature and/or pH. Change of conformation of this region with change in oxidation state has also been determined by noting differences in acetylation reactivity of surface lysine residues (80). The relative change was found to be pH-dependent. Thus, the relative conformational change accompanying change in oxidation state varies with temperature and pH. The driving forces for the conformation difference are a change in the Fe-S bond length, which alters the positions of adjacent residues by a "pull-push" mechanism (76), and the change in heme charge, which produces conformational effects by electrostatic interactions.

A major difference between the two redox states of cytochrome c is the difference in the Fe-S bond strength. This bond has been determined to be much stronger in ferrocytochrome c (81). This coordinate bond is the only chemical bond holding the left side of cytochrome c to the heme. Thus, the increased rigidity and stability of ferrocyto-

chrome c can be explained by the increase in the Fe-S bond strength when ferricytochrome c is reduced.

A computer simulation study of cytochrome c, based on a complex of ferricytochrome c and cytochrome c peroxidase, illustrated that the net result of reduction of ferricytochrome c is a "clamshell-like closing of the protein envelope on the heme" (82). Residues 1-20, 27, and 28, on the right side of the heme, undergo a small movement to the left. Residues 70-80, located on the left side of the heme, shift to the right. There are three regions on the back and bottom of the molecule that simultaneously undergo a hinge-like movement that serves as an energy sink to relieve conformational strain. Another effect of reduction is a movement of phe-82. The heme also moves. The bottom half (rings 1 and 4, the points of propionate attachment) shifts to the left, and the top half (points of thioether connection to the backbone) moves to the right. The driving force for the change in heme position is the change in charge on the heme from positive to neutral upon reduction, causing change in the covalent and nonbonded interactions of the heme within its protein environment. This movement at the binding site of cytochrome c provides a mechanism for breaking away from its reaction partner following electron transfer.

The 695 nm absorption band of ferricytochrome c has been used as an indication of the condition of the Fe-S bond (60, 83-88). This absorption band can be eliminated by

increasing the temperature at neutral pH or by increasing the pH while holding temperature constant. Both processes are entirely reversible. There is ample experimental evidence that an equilibrium between two forms of ferricytochrome c (states III and IV) is being affected. The 695 nm peak area should be monitored, rather than the peak height, to accurately determine the temperature of transition from state III to state IV (86). The conversion of state III to state IV is accompanied by a very unfavorable enthalpy change and a favorable entropy change. This is consistent with the postulate that the conversion from state III to state IV occurs through the breaking of the Fe-S bond. In contrast, the Fe-S bond in ferrocytochrome c is much more stable to extremes in pH or temperature (77).

The effect of pH variation on ferricytochrome c conformation was first studied by Theorell and Akesson (89). They reported five conformations; state III exists at neutral pH, states I and II correspond to acidic forms and states IV and V to alkaline structures. The respective pKa's for the transitions from I to V are <2.0, 2.5, 8.8 to 9.6, >11. Myer et al. (90), in a resonance Raman study, reported two additional states, IIIa and IIIb. State IIIa is a precursor to the neutral form, state III, and state IIIb is a precursor to the alkaline form, state IV. They found that the only pH region where the structure of cytochrome c was not affected is from 5 to 7.

The transition from the neutral form III to the alka-

line form IV of ferricytochrome c, known as alkaline isomerization, has been well-studied. The techniques of resonance Raman spectroscopy (90, 91, 92), differential pulse polarography (31), stopped flow circular dichroism (93, 94), and pulse radiolysis (95, 96) have been applied to examining the pH-induced conformational change from neutral pH to alkaline pH. The generally accepted mechanism involves an intermediate, i.e., the structure labeled IIIb by Myer. For the transition from state III to state IV, analysis of the 695 nm absorption band (90) revealed that the first two-thirds of the loss of absorption is due to conformational change and the final one-third to disruption of the Fe-S bond. Also, the Fe-S bond breaking follows the change in conformation. The transition from state III to state IIIb involves a tightening of the pyrrole rings in the outer domain of the porphyrin ring. The heme core is unaffected. The dimensions of the heme core reflect the degree of hydrophobicity of the heme environment. As the nonpolar character increases, the porphyrin ring core size increases. The transition from state IIIb to state IV involves more pronounced changes in the coordination configuration, as well as in the porphyrin ring core dimensions. The latter reflects a loosening of the heme crevice. The change in coordination is produced by the rupturing of the Fe-S bond and the deprotonation of some group that subsequently binds to the iron in the vacated axial position. The transition from state III to state IV is also accompanied by a decrease

in reduction potential (5) to the point where ferricytochrome c can no longer react with cytochrome c reductase. All three forms have been found to be electroactive, with state IV exhibiting much slower electron transfer kinetics. The mechanism proposed for reduction of state IV ferricytochrome c involves formation of an activated complex followed by rapid electron transfer, and then a slow relaxation to the stable ferrocytochrome c where the Fe-S bond is reformed.

The identification of the group that replaces the sulfur atom upon alkaline isomerization is a point of controversy. It is known to be a strong field ligand due to the fact that the iron remains low-spin. Lys-79 and lys-72 have been found to be likely candidates through chemical modification studies (87, 97), as well as an hydroxyl group (85) and the phenolic hydroxyl group of trp-67 (98). Bosshard (99) found that the 6th ligand in state IV cannot be a lysine. Bosshard proposed that deprotonation of the buried water molecule near met-80 enables a deprotonated surface-located water molecule to move into the heme crevice and replace the sulfur atom. This would explain the higher stability of ferrocytochrome c to alkaline pH. The ferrous heme is uncharged, and the hydroxyl ion at the heme edge is therefore not drawn into the heme crevice.

Urea denaturation of horse heart ferricytochrome c at neutral pH is proposed to include two intermediate states (73, 100). The first step is associated with a general

loosening of the heme crevice, followed by solvent exposure of the polypeptide backbone, and the final transition involves the breaking of the Fe-S bond and a disruption of the tryptophan-heme domain of the molecule. No difference in bimolecular reaction kinetics was observed until the third step. It was concluded that the tryptophan domain determines the stability of the Fe-S bond, as well as the formal reduction potential of the molecule. The mechanism for the reduction of the denatured form was thought to occur through an activated complex which must revert to one of the intermediate states prior to electron transfer. Hence, the fluorescence emitted by the tryptophan-heme region has been proposed to be a better indicator of the conformation of ferricytochrome c than the 695 nm absorption band (101). An optically transparent thin layer electrode cell (OTTLE) was used to control the redox ratio of cytochrome c while simultaneously monitoring the fluorescence of the solution. A mediator was used to link the potential of the electrode to the solution cytochrome c. Analysis of the change in fluorescence intensity revealed that the tryptophan residue moves toward the heme ca. 0.7 Å upon reduction.

The OTTLE, incorporating an electrochemical mediator, has also been used to study the effect of temperature on the formal reduction potential of cytochrome c in the presence of specifically adsorbed anions (14, 17, 24). The decrease in reduction potential with increase in temperature (25 to 55 °C) was related to the extent of anion binding to ferri-

cytochrome c. Ion binding to the oxidized form reduces the charge repulsion within the molecule, and thus decreases its size, resulting in a smaller net size change during reduction. The strength of anion binding was related to the change in formal potential with change in temperature, dE°'/dT. Biphasic behavior was observed in the presence of chloride ions, with the transition point occurring at 42 °C. This was related to the change in solvation strength of the chloride ion, which occurs at the same temperature. The idea that this is an entropy effect was further reinforced by the elimination of the biphasic behavior in D_2O-chloride solutions. This biphasic behavior in the presence of chloride anions was not observed in the case of heterogeneous electron transfer between cytochrome c and a chemically modified electrode (52) or a metal oxide semiconductor electrode (56). The reason for this discrepancy has not been resolved. A possible explanation is that the chloride anions are excluded from the electron transfer active site region under heterogeneous conditions (56). This discrepancy will be discussed further in the Results and Discussion section.

C. Reaction Mechanism of Cytochrome c

Cytochrome c reacts alternatively with its membrane-bound physiological reaction partners. Electrostatic attraction provides the driving force for movement of cytochrome c to its appropriate partner. The movement of cytochrome c is probably two-dimensional along the negatively

charged membrane surface (102). The diffusion coefficient of cytochrome c in mitochondria is much slower than in aqueous solution, i.e., 1.6 X 10^{-10} cm^2/sec (102) to 7 X 10^{-10} cm^2/sec (103) versus ca. 1.2 X 10^{-6} cm^2/sec (104). This appears to be due to the interaction of cytochrome c with the phospholipid membrane (105). The rate of diffusion of cytochrome c in its physiological environment is much smaller than that required for a model involving diffusion-mediated electron transfer between randomly dispersed components (102, 103). An explanation for this discrepancy is that the cytochrome c reductase and oxidase enzymes are able to move within their membrane environment. A diffusion coefficient of 1.5 X 10^{-10} cm^2/sec for cytochrome c oxidase has been measured (103). Thus, there could be an equilibrium between cytochrome c reductase-cytochrome c-cytochrome c oxidase aggregates, partial aggregates, and separated reductase-diffusing cytochrome c oxidase systems, each participating in electron transfer (102, 103). This theory is supported by the observation that only 50% of cytochrome c oxidase in native mitochondrial membrane has rapid rotational mobility (106). Another supporting facet is the Singer-Nicholson fluid-mosaic model of biological membranes (107). Biomembranes are polar lipid bilayers with an internal fluid character due to an appropriate mixture of saturated and unsaturated fatty acids. Integral proteins have hydrophobic surface residues that allow them to dissolve in the nonpolar interior of the membrane. The membrane pro-

duces the proper three-dimensional conformation of the integral membrane for biological activity. Since there are no covalent bonds between lipid molecules of the bilayer or between the protein surface and the lipids, the integral proteins are free to move in a two dimensional manner. An interesting hypothesis is that both peripheral cytochrome c and its integral redox partners are free to diffuse in a two-dimensional mode. The active sites of the integral proteins are maintained at the membrane-cytosol interface by their placement in the membrane. Cytochrome c moves along the interface, and is oriented for effective electron transfer by electrostatic factors upon close approach to its redox partners.

Despite the very small crystal structure differences between reduced and oxidized tuna cytochrome c, there are many physicochemical properties which are affected by oxidation state (80). The X-ray crystal structure represents a time-averaged static structure. However, the structure of cytochrome c is not static in its physiological environment, rather, it is undergoing constant, thermally-induced motion. The dynamic, vibrational state of each redox form of cytochrome c must be considered in order to explain differences in physicochemical properties (69, 80, 108, 109). The magnitude of the vibrational oscillations of ferricytochrome c is larger than that for ferrocytochrome c due to its comparative instability. Thus, the differences in physicochemical properties of ferri-ferrocytochrome c may be explained by a

change in the accessible dynamic states with change in oxidation state, rather than the time-averaged conformational difference determined by X-ray crystallography (110). Computer simulations of the dynamic structure of enzymes have led to the conclusion that some physiological reactions, such as the reversible binding of oxygen by myoglobin, would be impossible if the molecule had the rigid structure depicted by X-ray crystallography (108). The mechanism of enzyme activity should not be based on a static picture of the protein structure (109). The magnitude of the average atomic velocities is regulated by temperature. A computer simulation study of protein motion revealed that individual atomic fluctuations within globular enzymes are not independent of each other. Due to the tight packing of residues on the interior of the structure, one atom cannot move appreciably without a concurrent movement of its neighbors. Thus, collective motions that develop over periods of several picoseconds control the movement of individual interior atoms. These low-frequency collective motions can serve to provide the appropriate configuration for effective catalytic action. Movement of up to 2 Å is possible on the surface of a protein where packing is not as tight, while movement of atoms within the protein are restricted to approximately 1 Å. The dynamics of the structure of a protein are strongly affected by solvent (109). While the internal motions are not strongly affected by solvent, the movement of surface atoms has a diffusive character that is

dependent on the viscosity of the solvent. Thus, the rate at which a protein can alter its conformation is strongly dependent on solvent viscosity and therefore, temperature. The magnitude of the conformational fluctuations is controlled by the internal hydrogen bond and chemical bond structure of the protein. Since the motions of atoms throughout an enzyme are interconnected, individual events at one site, such as binding to a reaction partner or change in solvation, can affect rates of reaction at another site. An electro-mechano-chemical model (109) of dynamic enzyme interaction proposes that transition state active site conformation is coupled to low-frequency, collective vibrational modes of the protein. These low-frequency, concerted motions are much slower than individual atomic vibrations. Relatively long-term conformational states are assumed to be provided by large dipole oscillations of the protein.

A computer analysis (111) of the structural fluctuations of the atoms of tuna ferrocytochrome c revealed that movement becomes increasingly restricted toward the center of the protein. At radii of 6, 9, 12, 15, 18, and 21 Å, the average fluctuations are 0.66, 0.70, 0.73, 0.98, 1.05, and 1.64 Å. The heme atoms had the smallest fluctuations, i.e., 0.51 Å. Atoms on the met-80 side of the heme undergo larger fluctuations in position than those on the his-18 side, i.e., 0.71 Å versus 0.56 Å.

An enthalpy-entropy compensation mechanism has been thought to play a role in the dynamic nature of enzyme

catalysis (110). The thermodynamic parameters of free energy, pressure, and temperature are virtually constant in an enzymatic reaction. Changes in enthalpy, entropy, and volume are the critical thermodynamic parameters in enzyme catalysis. The central feature of this model is that a change in enthalpy at an active site required for a fluctuation of nuclear coordinates is compensated by an entropy change elsewhere in the polypeptide structure of the enzyme.

Electron transfer with cytochrome c is believed to occur via an outersphere mechanism (88, 112). An inherent step in this mechanism is the formation of an activated complex prior to electron transfer. The exposed heme edge of mammalian cytochrome c is surrounded by positively charged residues. Charge interactions appear to be responsible for the formation of precursor complexes. Strong binding of reactants prior to electron transfer has been observed in redox reactions of cytochrome c with small molecules (35). As mentioned earlier, cytochrome c is a highly charged molecule. Studies of anion binding (113), reactions with variously charged inorganic redox partners (114-117), and reactions with nonphysiological, biological (118-126), and physiological (120, 127-130) reaction partners have indicated that the driving force for the formation of the activated complexes is electrostatic. To determine the site of binding to its physiological redox partners, a series of studies of chemical modification of the charged residues on the surface of cytochrome c have been conducted (120, 127-

129, 131-134). The analysis of the interactions of a series of singly modified residues of cytochrome c with cytochrome c oxidase and cytochrome c reductase, as well as with non-physiological partners, led to the conclusion that cytochrome c has a common site for electron transfer, and it is centered in the ring of positively charged residues that surround the solvent-exposed heme edge. Modification with trifluoroacetate and trifluoromethylphenylcarbamate neutralized the positive charge of the lysine residues. The use of these two substituents demonstrated the effect of steric bulk and charge on binding. The lysine residues with the greatest effect on the rates are, in order of decreasing effect, at positions 13, 72, 25, 87, 8, 79, and 27 for oxidase and 13, 72, 79, 27, 87, 8, and 88 for reductase. Change in charge of a residue rather than the bulk of the chemical modifier proved to play the dominant role. Cytochrome c which was singly modified with 4-carboxyl-2,6-dinitrophenol (CDNP) was used to convert the positive charge of a lysine to a negative charge. The results obtained were similar to those described above, except that the effect on the rate of the reaction was more pronounced due to the increase in charge difference. The CDNP study determined that the lysines which most significantly affect reactivity are 13, 72, 86, 87, and 8 for oxidase and 13, 72, 86, 87, and 27 for reductase.

The chemical modification studies described above determined the effects of modification of active site resi-

dues. In contrast, an acetylation study was done on cytochrome c - reductase and - oxidase complexes that did not involve active site residues (120). This approach avoids the possible conformational effects of chemical modification of active site residues. Only those residues not involved in the bond between cytochrome c and either reductase or oxidase are susceptible to acetylation. This study indicated the same reaction site as with the surface residue, chemical modification studies. The lysine groups most protected from acetylation were, in order, 13, 86, 87, 8, 72, and 73 for the complex with oxidase and 86, 87, 13, 8, 79, and 5 with reductase. Residue 13 seems to play the most prominent role in binding.

It has been demonstrated that the outer groups surrounding the exposed heme edge are quite mobile (111). This reinforces the premise that cytochrome c is capable of interacting in a dynamic manner, through binding, with its redox partners to effect favorable positioning of the redox centers. It is also believed that binding serves to distort the substrate toward the transition state, thus using the energy of specific substrate binding interactions to lower the activation energy to product formation (136).

The reaction site for cytochrome c occupies a limited area on the surface of the protein of approximately 3% (137), yet reactions of cytochrome c with its physiological redox partners take place at nearly diffusion-controlled rates. Chemical modification studies of cytochrome c have

demonstrated that dipole moments of 325 and 308 debye exist for horse heart ferri- and ferrocytochrome c, respectively (138). The dipole moment thus serves to orient the enzyme within the electric field of its redox partners so that high electron transfer rates are achieved. Total protein charge dominates the electrostatic interactions at large reactant separations. The orienting effect of the dipole moment becomes stronger upon close approach of reactants. Reactions of cytochrome c with the nonphysiological enzymes plastocyanin and azurin (124) exhibited lower rates of electron transfer and were less affected by CDNP modification of lysine residues at the reaction site of cytochrome c. This indicates that the electric fields of the reactants do not orient cytochrome c with these nonphysiological enzymes as effectively as with its physiological redox partners. Also, there is not a precise molecular interaction domain between cytochrome c and the nonphysiological redox partners.

Margoliash and coworkers (116) reinforced the premise that the site for electron transfer is the solvent-exposed heme edge through a study of electron transfer kinetics for the reaction of CDNP singly modified cytochrome c with iron and cobalt complexes. They found that the center of the reaction site was the β-carbon of phe-82, and the reaction site included the solvent-exposed heme edge. Also, the size, nature, or charge of the reaction partner does not alter the reaction site. The preorienting effect of a dipole moment within cytochrome c for favorable positioning

for electron transfer was also supported by a study of electron transfer between flavodoxin and cytochrome c (122).

Cytochrome b_5 exists along the inner surface of the outer membrane of mitochondria, and may interact with cytochrome c (118). The crystal structures of both cytochrome c and cytochrome b_5 are known. Salemme (139) used a least-squares fitting process to propose a hypothetical structure for an intermolecular electron transfer complex of cytochrome c and cytochrome b_5. Cytochrome b_5 has a ring of negatively charged residues about its solvent-exposed heme edge that matches the corresponding ring of positively charged residues at the reaction site of cytochrome c. The computer-generated complex involved four complementary charge interactions between reaction site residues. The lysine residues 13, 27, 72, and 29 on cytochrome c interact with the cytochrome b_5 carboxyl groups of asp-48, glu-44, asp-60, and the exposed heme propionate, respectively. The structure of the complex indicates that water is excluded from the reaction site and that the heme groups are approximately coplanar with a heme edge-to-heme edge distance of 8.4 Å. The charge neutralization resulting from the surface residue interactions and the exclusion of water from the reaction site in the complex both serve to create a hydrophobic, low dielectric environment along the electron transfer path between the heme edges. An ionic strength study of the electron transfer reaction between surface residue chemically modified cytochrome c and cytochrome b_5 (118) and

an NMR study of the complex (123) supported the computer-generated model of the electron transfer complex between these two enzymes. Moore and Eley (123) reported that two of the lysine groups involved in binding, lys-13 and lys-79, are involved in maintaining the internal structure of cytochrome c. Binding to these groups leads to a weakening of the heme crevice and the Fe-S bond. They propose that the binding of cytochrome c to its reaction partners may lead to an alteration of the heme environment that activates the complex toward electron transfer. This theory is supported by a differential scanning calorimetry study (140) of the cytochrome c and cytochrome c_1 complex that illustrated that the thermodenaturation temperature of cytochrome c was reduced when complexed to cytochrome c_1, thus indicating a destabilization of cytochrome c. A spectroscopic analysis of the interaction between cytochrome c and cytochrome b_1 revealed that formation of the complex is largely entropic in origin, with a $\blacktriangle H°$ of 1 ± 3 kcal/mole and a $\blacktriangle S°$ of 33 ± 11 eu.

Since the crystal structures of cytochrome c's redox partners, cytochrome c reductase (or cytochrome bc_1) and cytochrome c oxidase (or cytochrome aa_3), are not known, determining the nature of their interaction with cytochrome c is difficult. As mentioned previously, cytochrome c oxidase is the terminal enzyme in the electron transport chain. It obtains electrons from ferrocytochrome c molecules and then reduces molecular oxygen. Although the cytochrome c

active site for electron transfer to cytochrome c oxidase has been determined (vide supra), the number of active sites and their positions on oxidase have not been determined. The bimolecular rate constant for the presteady-state reaction of cytochrome c with cytochrome c oxidase has been determined as a function of ionic strength (125). By extrapolating to zero ionic strength from a plot of ln k°' vs. $I^{1/2}$, a rate constant of 10^{11} $M^{-1}s^{-1}$ for the reaction was obtained. By using this value and one similarly obtained for a reaction rate at infinite ionic strength, an effective charge on beef cytochrome oxidase of -8 to -10.5 was calculated. Thus, it appears that there is an interaction of oppositely charged residues at the active sites of cytochrome c and oxidase, as is the case for the reactions of cytochrome c with cytochrome b_5 and cytochrome c peroxidase. The effect of variation in temperature for this reaction was also studied (125, 130). Below 20 °C, the enthalpy of activation was calculated to be ca. 16 kcal/mole. Above 25 °C, the enthalpy of activation is between 1 and 4 kcal/mole. This indicates that the reaction is not diffusion-controlled below 20 °C and is diffusion-controlled at temperatures above 20 °C. For diffusion-controlled reactions, an enthalpy of activation of ca. 3.5 kcal/mole is expected, due to the temperature dependence of the viscosity of the solvent. The enthalpy of activation was not affected by chemical modification of active site residues on cytochrome c (125) or by ionic strength (130). These results

led to the conclusion that the effect of chemical modification is purely electrostatic, without any steric effects. The fact that the rate constant vaired with ionic strength while the activation enthalpy remained constant, indicates that the kinetics are controlled by a smaller increase in activation entropy upon association at increasing ionic strength. A large, positive activation entropy of 30 eu was determined. Nonelectrostatic contributions to the activation entropy were determined to be 14 to 17 eu. Most of the active site on cytochrome c is composed of hydrophobic side chains about the solvent-exposed heme edge that are surrounded by the positively charged lysine groups. Thus, the formation of an electron transfer complex with cytochrome oxidase probably releases structured water into the bulk solution, resulting in a gain in entropy. The change in activation enthalpy that occurs at ca. 21 °C may be due to a variation of the interaction of cytochrome c with the phospholipid membrane.

Several studies have led to the conclusion that there are two binding sites for cytochrome c on cytochrome oxidase (141), a high affinity and a low affinity site, and that they may both be catalytically active. The complicated kinetic behavior observed from the interaction of cytochrome c with cytochrome oxidase with change in concentration of reactants has resulted in many different theories. Margoliash and coworkers (141) have recently reviewed the literature (most of it from Margoliash's lab), and they concluded

that there is a single catalytic site for electron transfer on cytochrome oxidase. Under conditions of low concentrations of ferrocytochrome c, the rate of dissociation of ferricytochrome c from cytochrome oxidase is much slower than the rate of electron transfer, and is the rate-limiting step. A slow, steady-state rate constant of 2 to 10 s^{-1} is observed. As the concentration of ferrocytochrome is increased, the rate constant increases. Previous studies had attributed this to electron transfer between ferrocytochrome c and a ferricytochrome c-cytochrome oxidase complex at a second catalytic site (142). The single catalytic site model attributes the increase in rate constant to the enhanced rate of dissociation of ferricytochrome c from the catalytic site caused by the repulsive electrostatic effect of nonproductive binding of ferrocytochrome c to the surrounding phospholipid membrane. This effect is attributed to the alteration of the electrostatic environment of the active site on oxidase due to the high concentration of strongly positive cytochrome c bound to the membrane in the immediate vicinity. Thus, complicated kinetic patterns are observed providing the rate of dissociation of product bound at the catalytic site is rate-limiting. The upper limit for electron transfer rates, as determined by this model, is reached when the bimolecular association constant for the binding of ferrocytochrome c to the active site becomes the rate-limiting step. Following this point, substrate inhibition is observed.

The reaction of cytochrome c with mitochondrial ubiquinol-cytochrome c reductase has also been investigated by Margoliash (143). The reductase complex (a.k.a. complex III or cytochrome bc_1 complex) was removed from the inner membrane of mitochondria and solubilized by detergent for this study. The quinol reductant and ferricytochrome c were found to react independently with the reductase complex. Thus, a ternary complex is not necessary, but also not precluded. Analysis of the effect of pH on this reaction revealed that optimum kinetics were observed at pH 8. At low concentrations of ferricytochrome c, simple Michaelis-Menton kinetics were observed. As the concentration of ferricytochrome c was increased, the rate constant for electron transfer increased less than expected. When the concentration was increased further, substrate inhibition was observed. Cytochrome reductase was found to preferentially bind ferricytochrome c over ferrocytochrome c. This is in contrast to the equivalent binding strengths of both forms of cytochrome c to cytochrome oxidase (141). At low ionic strength, considerable nonproductive binding of ferricytochrome c to the reductase complex and associated phospholipid membrane was observed. This nonproductive binding of positively charged substrate to the reductase complex in the vicinity of the active site alters the electron transfer rate through electrostatic effects. This model was also proposed for the reaction of ferrocytochrome c with cytochrome oxidase (141). However, the effect of variation of

ionic strength on the kinetics of the reaction of cytochrome c with its two physiological redox partners differs for each reaction due to the different substrate/product binding ratios for the two reactions. Ferrocytochrome c binds as strongly as ferricytochrome c to cytochrome oxidase. Thus, an increase in the rate of product dissociation caused by the electrostatic effect of nonproductive binding has a large effect of the overall rate constant. This process is also strongly affected by ionic strength. For a 25 mM to 100 mM range of ionic strengths (143), the strength of product binding to cytochrome reductase is much less than that of substrate binding. Above 100 mM ionic strength, substrate and product bind with equal strength. Accordingly, the reaction of cytochrome c with the reductase complex is much less affected by variation in ionic strength from 25 mM to 100 mM than the corresponding reaction with cytochrome oxidase. Substrate inhibition is observed for both systems at high substrate concentrations. This again is attributed to the concentration at which nonproductive substrate binding in the vicinity of the active site leads to a decrease in the rate of substrate binding to the active site.

D. Electron Transfer Theory

Oxidation-reduction reactions are generally classified as: inner sphere electron transfer, outer sphere electron transfer, or electron tunneling. Both outer sphere electron transfer and tunneling are remote attack reactions. It is widely accepted that electron transfer occurs at the exposed

heme edge of cytochrome c (1-3, 112); consequently, remote attack is implied. Reactions of cytochrome c with inorganic complexes (114, 144), have revealed that the rate of reaction depends strongly on the ability of the complex to delocalize its electrons through metal-to-ligand π-bonds and on the hydrophobicity of the ligands. Electrostatic interactions draw the reactants together, then the hydrophobicity of the ligands permits penetration of the protein surface, which allows effective orbital overlap with the π-orbitals of the heme group. Steric restraints of the iron atom placement within the interior of the enzyme preclude inner sphere electron transfer, which requires a metal-ligand-metal bridge. The low-spin electron state of cytochrome c favors outer sphere electron transfer due to the minimal inner sphere reorganizational energy required.

Outer sphere electron transfer represents the simplest class of electron transfer reactions in that no bonds are formed or broken. Electron transfer proceeds by a collision between reactants followed by the formation of a precursor complex. Dissociation of the reactant-product complex follows electron transfer. The observed rate constant for the reaction is the product of the equilibrium constant for the formation of the precursor complex and the rate of electron transfer within the precursor complex.

The distinction between outer sphere electron transfer and electron tunneling is not clear. Basically, the distance between the two reaction centers and the differences

between the reactant and product nuclear coordinates seem to be controlling factors, since both of these features contribute to the activation energy. Distances relate to the degree of orbital overlap (required for an outer sphere reaction, but not for electron tunneling). At large distances, the conductivity of the matter between the oxidant and reductant must be considered (145). If electron tunneling is occurring, the conductivity relates directly to tunneling probability. If one considers two potential energy curves as a function of reaction coordinate (Figure 4), one for the reactants and one for the products, an intersection is observed. This intersection relates to a point where the coordination spheres of the two metal ions are the same, i.e., the Franck-Condon restriction is met. According to the Franck-Condon principle, the nuclear velocities and the internuclear distances do not change during electron transfer. If the ions are close together, a relatively large gap develops at the intersection, and its magnitude is proportional to the magnitude of electronic coupling, i.e., orbital overlap, and the system will remain on the lower potential energy curve. The process is described as being adiabatic if the reaction goes to completion every time the intersection region is attained. However, if the ions are far apart or the difference in reactant and product nuclear coordinates is large, the energy gap at the crossover point becomes small. Thus, the probability of crossing from reactants to products depends on tunneling probability.

Figure 4. Electron transfer reaction diagrams. (a): No electronic interaction between the reactants. (b): Slight interaction. (c) Considerable interaction. R represents reactants plus environment and P represents products plus environment. (Adapted from Marcus, R. A. In "Tunneling in Biological Systems", Chance, B.; DeVault, D.; Frauenfelder, H.; Marcus, R. A.; Schrieffer, J. F.; Sutin, N., Eds.; Academic Press: New York, 1979; 109-127).

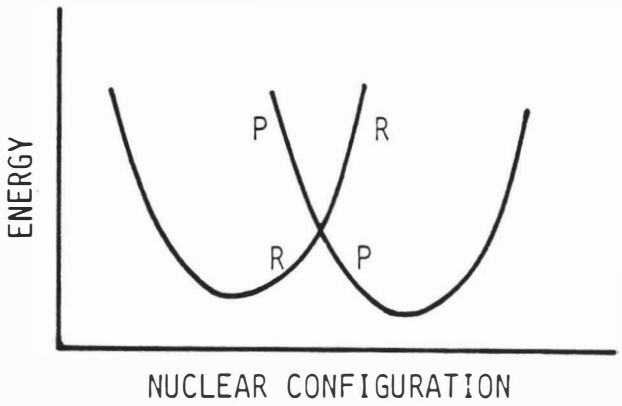
ENERGY
P
R
R
P
NUCLEAR CONFIGURATION

a

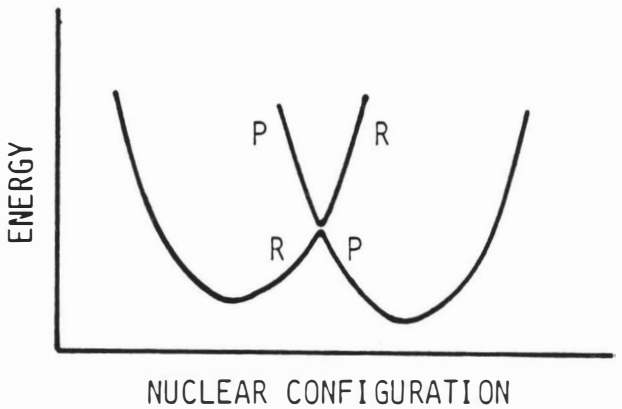
ENERGY
P
R
R
P
NUCLEAR CONFIGURATION

b

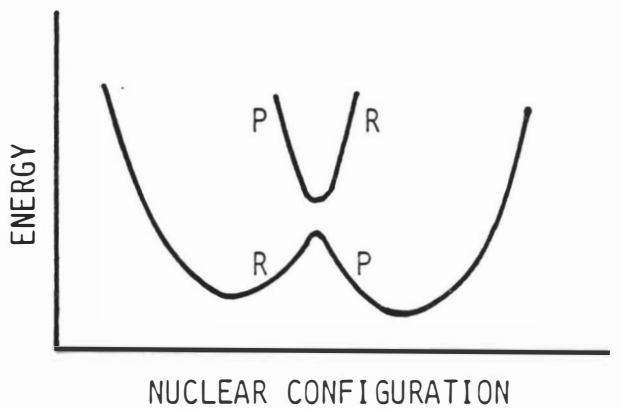
ENERGY
P
R
R
P
NUCLEAR CONFIGURATION

c

It would be convenient to consider outer sphere electron transfer as an adiabatic process and non-adiabatic processes as electron tunneling. However, this direct relationship does not have a sound theoretical basis. All that can be said is that non-adiabatic processes are affected by both the Franck-Condon principle and an electron transition probability. In adiabatic processes, either "classical" outer sphere electron transfer may be occurring or, if electron tunneling is occurring, its probability constant is large. Quantum mechanical tunneling considers the electron to have a finite probability of penetrating a potential energy barrier. The conventionally used expression for electron tunnelling probability does not contain a temperature dependence. Hopfield (146) invoked a temperature dependence in the probability of electron tunnelling by assuming coupling of thermally activated, molecular vibronic states to electronic states during tunnelling between statically oriented reactants. The heme edge-to-heme edge distance during the reaction of cytochrome c with its physiological reaction partners is longer than that expected for classical outer sphere electron transfer but is close to the estimated range of a thermally activated tunnelling process (112). Salemme (3) does not consider the distinction between these mechanisms to be critical, since they may be different mathematical descriptions of the same physical process.

Marcus theory (112, 147-150) is often used to evaluate outer sphere electron transfer reactions. For homogeneous

reactions, an expression is given which relates the cross reaction rate constant, k_{12}, between two reactants to the equilibrium constant, K, the self-exchange rates for each reactant, k_{11} and k_{22}, and a term, f, which is usually assumed to be unity for reactions with a small driving force:

$$k_{12} = (k_{11}k_{22}Kf)^{1/2}$$

For this relationship to hold, all reactions must be adiabatic or uniformly non-adiabatic. The rate constant is also related to the overall free energy barrier, $\blacktriangle G^*$, by the expression:

$$k = pZ\exp(-\blacktriangle G^*/RT)$$

p: Probability of electron transfer in the activated complex (equals one for adiabatic processes)

Z: Collision frequency (based on gas-phase collision model)

To reach the transition state, i.e., the intersection region of Figure 4, fluctuations of the vibrational coordinates must be considered when a reactant has different equilibrium bond lengths or bond angles than the product. Also, the fluctuations of the orientational coordinates of polar solvent molecules must be considered. Thus, the reorganizational energy required can be divided into inner sphere and outer sphere categories. Another contribution to the activation energy is the work required to bring the reactants or products together to form the activated complex. Proper orientation of the reactants must also be considered due to the nonspherical nature of π-orbitals and possible active

site considerations (such as with cytochrome c).

Extension of classical Marcus theory to biological systems is complicated primarily by a poorer understanding of the biological environment compared with the environment in solution studies. Other complications include the effect of interaction of reactants with biomembranes and differences in the relative free energy of substrate binding with change in oxidation state.

Marcus theory is often cited in discussions of the electron transfer behavior of cytochrome c. A basic attribute of Marcus theory is the use of self-exchange rate constants to predict cross reaction rate constants. An experimental self-exchange rate constant for cytochrome c at an ionic strength of 0.1 M and pH 7 is 1.2 X 10^3 $M^{-1}s^{-1}$ (151). Marcus and Sutin (112) used a combination of estimated and empirical data to calculate a self-exchange rate constant for cytochrome c which is in close agreement with the above experimental value. A heme edge separation of approximately 10 Å was used. The inner sphere reorganizational energy was assumed to be small (5 kJ/mole), which is consistent with the similarity of the equilibrium structures of the two oxidation states of cytochrome c. The outer sphere reorganizational energy was divided into two contributions: one for solvent and the other for reorientation of the protein dipoles. The outer sphere reorganizational energy was estimated to be 25 kJ/mole. This compares well with an experimental activation energy of ca. 29 kJ/mole (151).

The rate constant of heme-heme self-exchange is at least four orders of magnitude larger than that for cytochrome c. This difference is attributed to the greater reactant separation for cytochrome c due to the protein cage about the heme. The much greater reaction rate for cytochrome c with cytochrome b_5, cytochrome c peroxidase, and its physiological redox partners than with itself is attributed to differences in electrochemical driving forces and to enhanced precursor-complex stability due to appropriate active site charge interactions. Marcus and Sutin (112) state that the application of Marcus theory to the interaction of cytochrome c with ferri-ferrocyanide (an extensively studied reaction) is sometimes flawed since the self-exchange rate for ferri-ferrocyanide is strongly dependent on solution conditions.

Marcus maintains (147) that reactions at electrodes have many features in common with solution reactions. The electrode can be considered as a reactant with adjustable energy levels. Also, just as solution reactants can bind to each other, electroactive species can adsorb to the electrode. The heterogeneous electrode reaction rate constant can be related to the corresponding homogeneous reaction rate constant by a simple equation (152):

$$(k_{11}/Z_{hom})^{1/2} \geq k_{het}/Z_{het}$$

Z_{hom} and Z_{het} are the collision frequencies of the chemical and electrochemical reactions, respectively (10^{11} L/mole and 10^4 cm/sec). The homogeneous reaction rate is larger than

the heterogeneous reaction rate when the electroactive species-electrode distance is larger than one half of the homogeneous activated complex distance.

E. Heterogeneous Electrochemistry of Cytochrome c

The direct electron transfer behavior of cytochrome c with a variety of electrodes has been studied by many groups since 1970. This work has recently been thoroughly reviewed (45, 153). A brief summary of the important parameters that affect the heterogeneous electrochemistry of cytochrome c will be given here. Details of research relevant to the work presented in this dissertation are included in the results and discussion section.

As noted earlier, electron transfer between cytochrome c and its physiological redox partners occurs at membrane/solution interfaces. Clearly, there are significant differences between these interfaces and those of electrodes in electrolyte solutions. However, the interaction of cytochrome c with an electrode may model its physiological reaction. The primary characteristic which the systems have in common is the existence of a structured water layer, which contains specifically and nonspecifically adsorbed charge sites, at the interfacial region. Another common characteristic, depending on electrode material, is the presence of active sites for both adsorption of substrate and electron transfer.

It appears that the essential requirement for reversible electron transfer of cytochrome c with an electrode is

that it must be able to reversibly and rapidly bind to the electrode. The kinetics of the reaction of cytochrome c at various electrodes range from irreversible to reversible. Surface preparation or surface chemical modification have been found to play a large role in controlling the degree of reversibility. With mercury and platinum electrodes, large overpotentials are required to reduce ferricytochrome c. The principal reason cited for this irreversible electrochemical behavior is irreversible adsorption of reactant to the electrode surface. Reversible heterogeneous electron transfer has been observed at chemically modified (18, 27, 30, 32, 34-36, 41, 42, 49-52), metal oxide semiconductor (15, 29, 37, 38, 45, 46, 55, 56), graphite (47), and carbon fiber (58) electrodes. The availability of appropriate sites for reversible binding of cytochrome c is proposed to facilitate electron transfer in each case. Albery et al., (30) has proposed that the free energy of adsorption is used to overcome the activation energy required for reaction.

A critical criterion for reversible heterogeneous electron transfer between any electrode and cytochrome c is sample purity (38, 56). It was found that initial reversible behavior at tin-doped indium oxide electrodes quickly deteriorated with time when commercial horse heart cytochrome c preparations were used as received from Sigma Chemical Company. However, when the sample was purified by cation exchange chromatography, long-term reversible behavior was observed. The interfering impurities are deamidated

and oligomeric forms of cytochrome c.

The interaction of cytochrome c with an electrode is believed to be similar to that with its physiological reaction partners. Electrostatic interaction with an electrode will orient cytochrome c for effective electron transfer. Favorable electrostatic interaction depends on the excess charge density at the electrode/solution interface, which is affected by electrode potential, electrode material, and electrolyte composition. Adsorption of the positively charged residues at the active site of cytochrome c to the electrode surface then occurs, probably through hydrogen bonding. The type of electrode material will determine the availability of binding sites and the strength of binding. Close approach of cytochrome c to the electrode occurs through a structured water environment. The degree of solvent structuring is strongest immediately adjacent to the electrode surface. Binding interactions should serve to overcome the energy required to penetrate this ordered environment. Electron transfer then occurs. The distance between electrode and heme edge has been estimated to be approximately 10 Å (45). This is close to the 8 Å distance proposed for the heme edge-to-heme edge separation of cytochrome c with cytochrome b_5 (118, 139). Cytochrome c then disengages from the electrode and diffuses into bulk solution.

CHAPTER II - EXPERIMENTAL

Horse heart cytochrome c, type VI, Sigma Chemical Co., was purified by chromatography on carboxymethylcellulose (CM-52, Whatman) according to a published procedure (154). The purified cytochrome c was then lyophilized and stored at -4 °C. Due to the long time required for a temperature study (several hours), very pure cytochrome c was necessary. The process of lyophilizing denatures some ferricytochrome c, and not all of the sample returns to its native form when dissolved in water. This was determined from the observation that purified, lyophilized cytochrome c showed band separation when repurified, whereas purified, nonlyophilized cytochrome c passed through the column as a single band. Therefore, a small portion of the lyophilized, purified cytochrome c was repurified and stored in solvent prior to experimental use. The maintance of electrochemical reversibility for up to 12 hours was a very sensitive indication of sample purity. The cytochrome c was used as collected from the column in the 0.2 M ionic strength phosphate buffer eluent for the experiments in phosphate buffer. To obtain cytochrome c in Tris/cacodylic acid buffer, the phosphate ions were removed by repeated dilutions followed by concen-

trations using a stirred ultrafiltration cell (Amicon Model 52) with a YM5 filter. Tris(hydroxymethyl)aminomethane was used as received from Sigma Chemical Co. (Trizma Base, reagent grade). Cacodylic acid (hydroxydimethylarsine oxide, Sigma Chemical Co., 98% pure), was recrystallized twice from 2-propanol. Water used in this work was purified with a Milli RO-4/Milli-Q system (Millipore Corp.) and exhibited a resistivity of 18 MΩ on delivery. Cytochrome c concentrations were determined by the reduced minus oxidized difference molar absorptivity, $\Delta\varepsilon$ = 21,100 $M^{-1}cm^{-1}$ at 550 nm (155), on a Beckmann Acta MVII spectrophotometer. Ferricytochrome c was reduced by dithionite. All other chemicals used in this work were ACS reagent grade. Buffers were prepared by mixing the acid and base components to achieve the desired pH. Concentrations were adjusted to achieve an ionic strength of 0.2 M. The ratio of each of the ionic species to the analytical concentration was calculated for a given pH. These relative concentrations were then used to calculate the analytical concentration required to establish an ionic strength of 0.2 M. Standard acid-base equations were used to determine the proportional concentration of each of the ionic species (156).

A nonisothermal electrochemical cell was used for the cyclic voltammetry and potential step chronocoulometry temperature studies (23, 157). The half-cell containing the working electrode and the liquid junction of the reference electrode were encased in a water jacket. The Ag/AgCl (1.00

M KCl) reference electrode was physically isolated from the thermostated region of the cell by small-diameter glass tubing, and remained at room temperature. The tip of the reference electrode was within a few mm of the working electrode to minimize uncompensated resistance. Solution volume was approximately 1 mL, and a platinum auxiliary electrode was used. Reference 158 is an excellent source of information for the proper design and use of electrochemical cells.

The time required to bring the test solution to a desired temperature was determined by placing a YSI 44203 thermistor in the test solution adjacent to the working electrode. The internal solution temperature rapidly adjusted to the circulator bath temperature. At least 10 minutes equilibration time was allowed following a temperature change. Tin doped indium oxide OTE materials were obtained from PPG Industries. The OTE electrodes were cleaned by successive 5 minute sonications in Alconox solution, in 95% ethanol and twice in purified water (159). The working electrode was attached to the bottom of the cell by a retainer plate and an O-ring seal. Each working electrode was only used for one experiment.

Reference 160 is an excellent source for a general discussion of potential step and sweep methods. Potential step chronocoulometry experiments were performed by stepping 400 mV negative from an initial potential of 522 mV vs. NHE. The experiments were conducted in 0.2 M ionic strength, pH 7.0, Tris/cacodylic acid buffer. Data were acquired at 10

points/s by an integrating analog/digital 16-bit converter interfaced to a UNC microcomputer (161). Specific details for the operation of this data acquisition system and program examples are contained in reference 162. Base line data were acquired for 1 s prior to the potential step, and their average was subtracted from all subsequent points. Background electrolyte data were acquired for each experiment with the working electrode used for that experiment and subtracted from the total coulometric response. The computer-recorded current was then digitally summed to yield charge. An in-house constructed potentiostat of conventional design was used for most electrochemical work. A PAR 174 polarographic analyzer was also used for cyclic voltammetry. The triangle wave generator that was used to perform cyclic voltammetric experiments was triggered by the computer. Cyclic voltammetric data were acquired at a rate calculated to obtain 2 data points/mV. A 20-μs conversion time, 12 bit, fast Datel ADC-HX12B analog/digital converter-based interface card was used to acquire cyclic voltammetric data. Data showed 60-Hz noise, and were digitally smoothed by a 12-point polynomial smoothing routine (163). Slow potential scan rate experiments were also smoothed by an analog fourth-order Butterworth filter with a cutoff frequency of ca. 50 Hz. Successive fast potential scan rate cyclic voltammograms were averaged until a smooth response was obtained. Formal potentials were determined from the average of the peak potential values from reversible cyclic

voltammograms acquired at low potential scan rates. The difference in the computer-acquired background (electrolyte alone) and total (electroactive species present) cyclic voltammograms was used in these determinations. A program then determined the potential at which the maximum cathodic and anodic currents occurred from each digitally stored cyclic voltammogram, providing precise values for formal potentials. The standard deviations for cathodic peak potentials, anodic peak potentials, and formal potentials were typically less than 1 mV.

An optically transparent nonisothermal electrochemical cell was used for derivative cyclic voltabsorptommetry (164) and potential step chronoabsorptometry (165) experiments. Reference 166 gives an overall description of spectroelectrochemical techniques at optically transparent electrodes. This cell is similar in construction to the cell described above. The solution path length was determined by the distance between the working electrode and the end of a quartz light pipe, and was approximately 1mm. The path length was varied to ensure that semi-infinite diffusion existed. The optical path was perpendicular to the working electrode surface.

Initially, the cell was arranged in the spectrophotometer so that the working electrode was vertical. Considerable time was spent investigating what appeared to be a homogeneous chemical reaction that followed electron transfer at elevated temperatures and very slow scan rates. The

cause of this behavior was the vertical orientation of the electrode. A horizontal working electrode orientation eliminated the strange behavior at slow scan rates (Figure 5). This reinforces the standard electrochemical practice of using a horizontally mounted working electrode whenever possible. Vertical electrodes are subject to convection, resulting from the development of density gradients, during slow potential scan rate experiments (167).

A single beam UV/VIS spectrophotometer was used. It consisted of a quartz-halogen source, Heath monochromator, a photomultiplier tube, and a Heath photomultiplier module. The spectrophotometer was constructed by Henry Blount at the University of Delaware. An operational amplifier current-to-voltage converter was used to change the photomultiplier tube current to voltage. The initial signal from the system, prior to the beginning of an experiment, is P_o. The output of the spectrophotometer after initiation of an electrochemical experiment is P. Absorbance was calculated from the relationship: Absorbance = $-\log(P/P_o)$. The 416 nm radiation ($\blacktriangle\varepsilon$ = 57,000 $M^{-1}cm^{-1}$) (155) was used to monitor the concentration of ferrocytochrome c. A wide slit width (largest setting) was used to increase the signal. This caused the apparent molar absorptivity to decrease. Narrowing the slit width resulted in an absorbance appropriate for the concentration of cytochrome c. The system molar absorptivity coefficient, at wide slit widths, was determined from a diffusion-controlled response for cytochrome c.

Figure 5. Cyclic voltammetry of $K_3Fe(CN)_6$ demonstrating the effect of working electrode orientation at slow scan rates. Scan rate = 1 mV/s, temperature = 45 °C, (a): working electrode in vertical position, (b): working electrode in horizontal position.

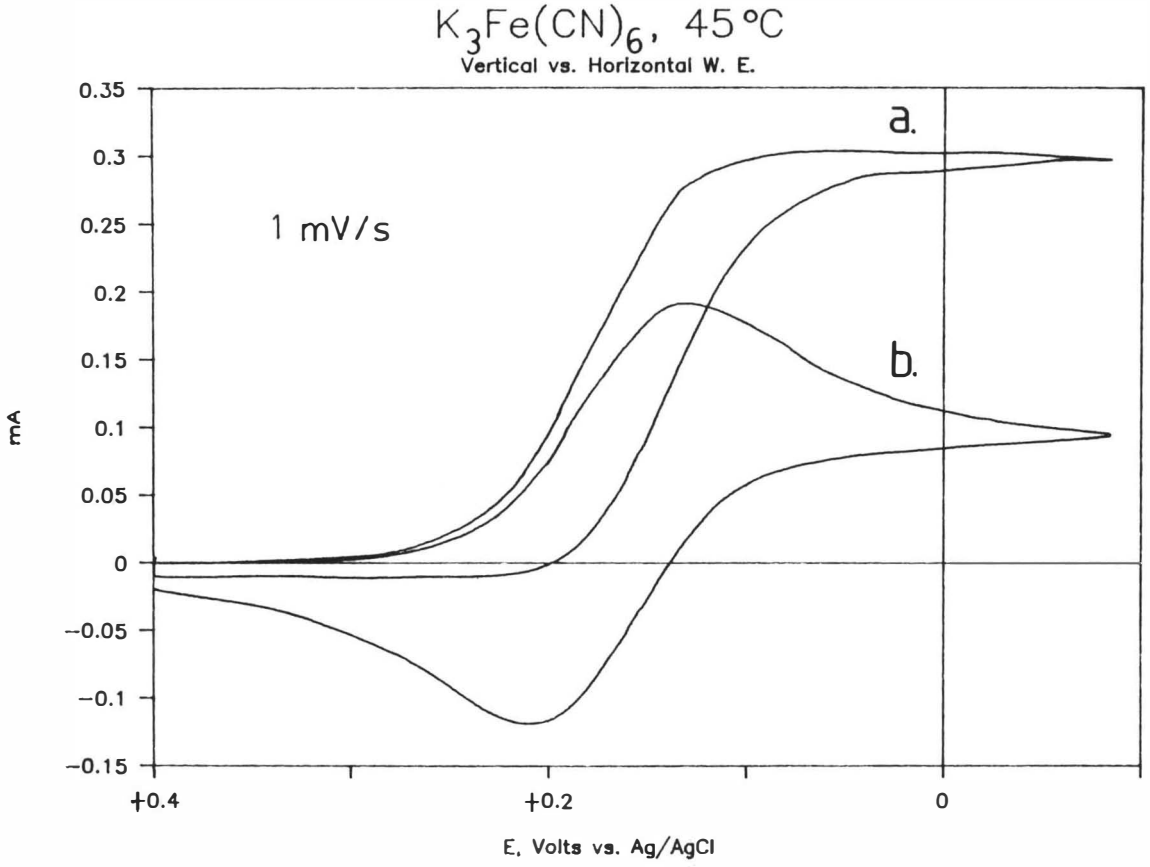
$K_3Fe(CN)_6$, 45 °C
Vertical vs. Horizontal W. E.
1 mV/s
a.
b.
mA
0.35
0.3
0.25
0.2
0.15
0.1
0.05
0
−0.05
−0.1
−0.15
+0.4
+0.2
0
E, Volts vs. Ag/AgCl

An IBM PC AT microcomputer system, containing a 12-bit Data Translations DT2801A analog-to-digital and digital-to-analog board, was used to control and collect data for the spectroelectrochemical experiments. The board was programmed by a commercial software package, DT/Notebook, from Data Translation, 100 Locke Drive, Marlborough, Mass., 01752. Lotus 123 (software from Lotus Development Corporation, 55 Cambridge Parkway, Cambridge, MA, 02142) and the fast Fourier transform function of DT/Notebook were used for data analysis. A Lotus 123 worksheet was created to generate the working curves required to analyze potential step chronoabsorptometry results. The error function contained within the equation that describes the working curve was approximated by equation 7.1.26 in reference 168. The absorbance response attributed to adsorbed species was calculated by a modified Beer's law equation: Absorbance = ε' X Concentration, where concentration has the units of mole/cm^2 and ε' = ε X 1000 cm^3. Noise from the spectrophotometer output was partially removed by using a capacitor in parallel with the feedback resistor of a voltage multiplier. The noise was increasingly reduced as the time constant (resistance times capacitance) increased. A very smooth signal can be obtained by using a large time constant; however, the magnitude of the signal was significantly decreased as a consequence of the large time constant, and the data collected did not accurately represent the actual experimental output. Small time constants, in combination with signal averaging,

were used to collect the potential step results.

A fourth-order Butterworth filter was used to reduce the signal noise from the spectrophotometer for the derivative cyclic voltabsorptommetry work. The magnitude of the absorbance in the DCVA experiments was much larger than the magnitude of the signal from the potential step experiments. Consequently, an excellent signal-to-noise ratio was obtained. However, creation of a derivative cyclic voltabsorptammogram requires the derivative of the absorbance profile with respect to time. This process degrades the signal-to-noise ratio. Fast Fourier transform smoothing of the absorbance prior to taking the derivative proved to be the best method for improving the signal-to-noise ratio without artificially affecting the response through the smoothing process. The procedures outlined by Smith (169, 170) were followed for the use of Fourier smoothing of electrochemical data. Reference 128 gives an overview of the application of transform techniques to chemistry. A Fourier transform of the data was obtained. The absorbance profile was rotated so that the first and last points of the data array were zero. This process avoided the problem of "ringing," i.e., low frequency oscillations that occur throughout the waveform when a transform of data with different starting and end points is obtained. The high frequency noise components were removed prior to an inverse transform. The frequency cutoff point determines the signal-to-noise ratio. It is important to leave enough frequency information to accu-

rately describe the waveform. A digitally simulated, reversible, integrated cyclic voltammogram was used as a test to determine the frequency cutoff point where the best smoothing occurred without increasing the peak separation. Signal noise is probably the most serious limitation in the use of analog-to-digital converters. Care must be taken so that excessive filtering does not degrade the response in short time experiments.

The following method was used to convert the derivative of absorbance with respect to potential, dA/dE, of derivative cyclic voltabsorptometry to its current analog, i, of cyclic voltammetry. The absorbance, A, observed is related to the charge consumed, Q, by the expression (164): $A = \varepsilon Q1000/nF(\text{Electrode Area})$ (164). This relationship is used to convert dA/dE to dQ/dE. The difference in potential between each computer-acquired point divided by the time between points is used as dE/dt. Multiplying dQ/dE by dE/dt gives dQ/dt. Current is the derivative of charge with respect to time, i.e., dQ/dt = i. Hence, the potential-dependent function, dA/dE, of derivative cyclic voltabsorptometry is converted to a corresponding current that represents only the faradaic portion of a simultaneously acquired total current that contains both faradaic and nonfaradaic contributions.

CHAPTER III - RESULTS AND DISCUSSION

A. Separation of Faradaic and Nonfaradaic Response.

The formal reduction potential of cytochrome c was determined from the midpoint potential of reversible and quasi-reversible cyclic voltammograms, i.e., those with peak separations of 60 to 80 mV. As with all of the research presented here where current is the observed experimental result, background responses obtained for electrolyte alone were subtracted from the total electrochemical response obtained for cytochrome c. The subtraction of background was necessary due to the nonideal nonfaradaic current response of the tin-doped indium oxide electrodes used. The degree of nonideal behavior depended on the type of electrolyte used, the pH of the solution, temperature, and scan rate.

A solution forms a structured, immobilized layer at the surface of an electrode which behaves essentially as a capacitor to variations of electrode potential. The charging of the double layer at the electrode/solution interface causes a nonfaradaic current to flow during any voltammetric experiment. The magnitude of the nonfaradaic current is affected by experimental factors such as electrode material,

solvent, electrolyte, pH, specific adsorption of anions, and the time frame of the potential perturbation. At high analyte concentrations, the nonfaradaic current is small compared to the faradaic current which results from electron transfer to the electroactive species. However, at low analyte concentrations, the nonfaradaic current becomes the major component of the total recorded current.

The electrochemical behavior of the electrolyte solutions in the absence of electroactive species will be discussed prior to presenting the electrochemistry of cytochrome c. This nonfaradaic, or background, behavior must be separated from that of cytochrome c. The ability to accurately differentiate between the faradaic response from cytochrome c and the nonfaradaic response of the electrochemical cell is a determining factor in the reliability of this electrochemical investigation.

The effect of temperature on the background cyclic voltammograms obtained in pH 5.3 Tris/cacodylic acid buffer is shown in Figure 6. The irregular behavior increases with elevation in temperature. It is noteworthy that an ideal nonfaradaic current response to a linear potential sweep is rectangular in shape, with current depending only on scan direction and rate, and it is independent of potential. The deviation from nonideal behavior also depends on scan rate. Nonfaradaic current is directly proportional to scan rate. Figure 7 shows the scan rate dependence of background cyclic voltammograms in pH 5.3 Tris/cacodylic acid buffer. Each

Figure 6. Cyclic voltammetry of pH 5.3 Tris/cacodylic acid electrolyte alone at various temperatures. Scan rate is 20 mV/s. (a): 5° C, (b): 25 °C, (c): 45 °C, (d): 65 °C, (e): 75 °C.

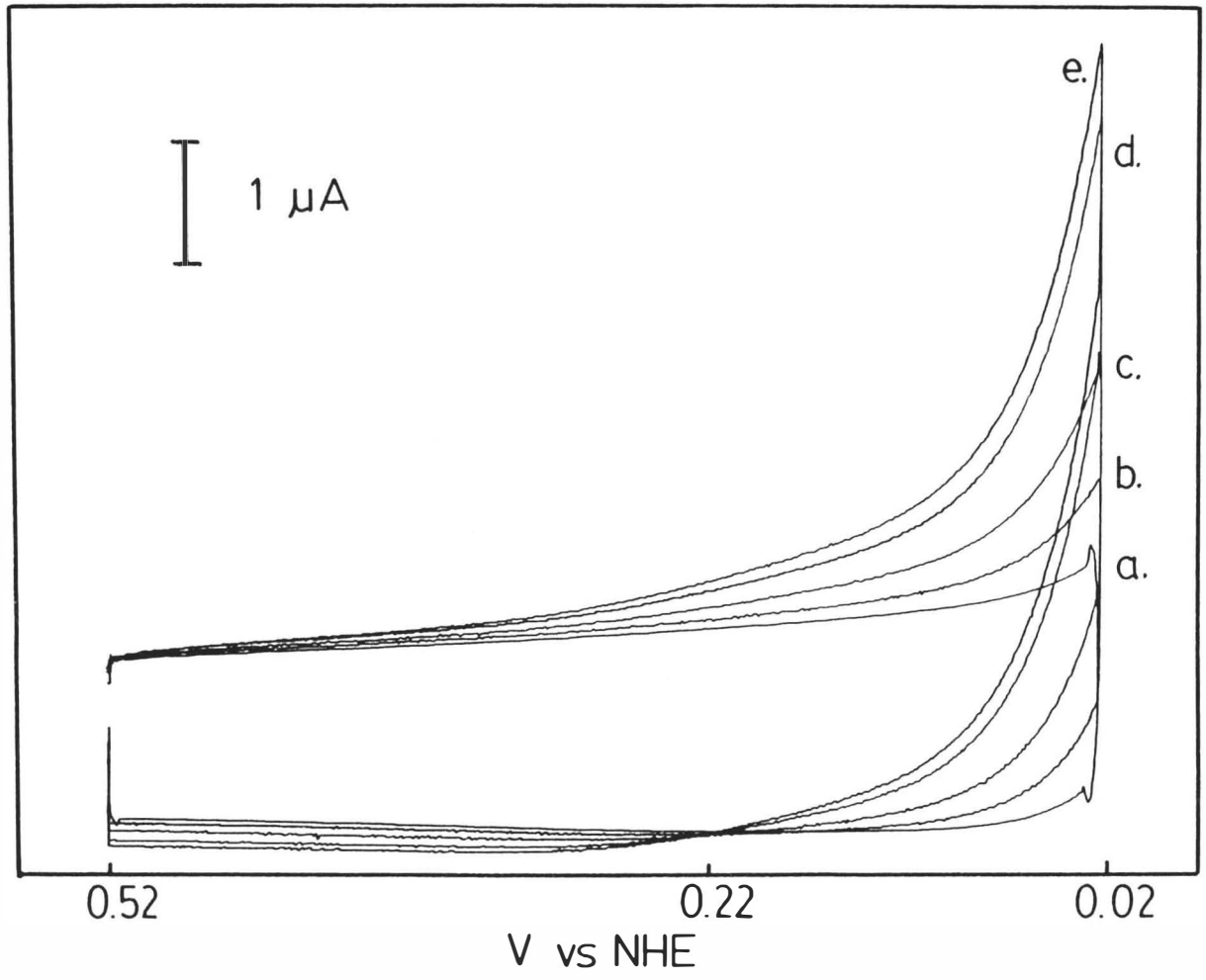
e.
d.
c.
b.
a.
1 μA
0.52
0.22
0.02
V vs NHE

Figure 7. Cyclic voltammetry of pH 5.3 Tris/cacodylic acid electrolyte alone at various scan rates. Temperature is 55 °C. (a): 20 mV/s, (b): 511 mV/s. Faster scan rates have the same morphology as (b).

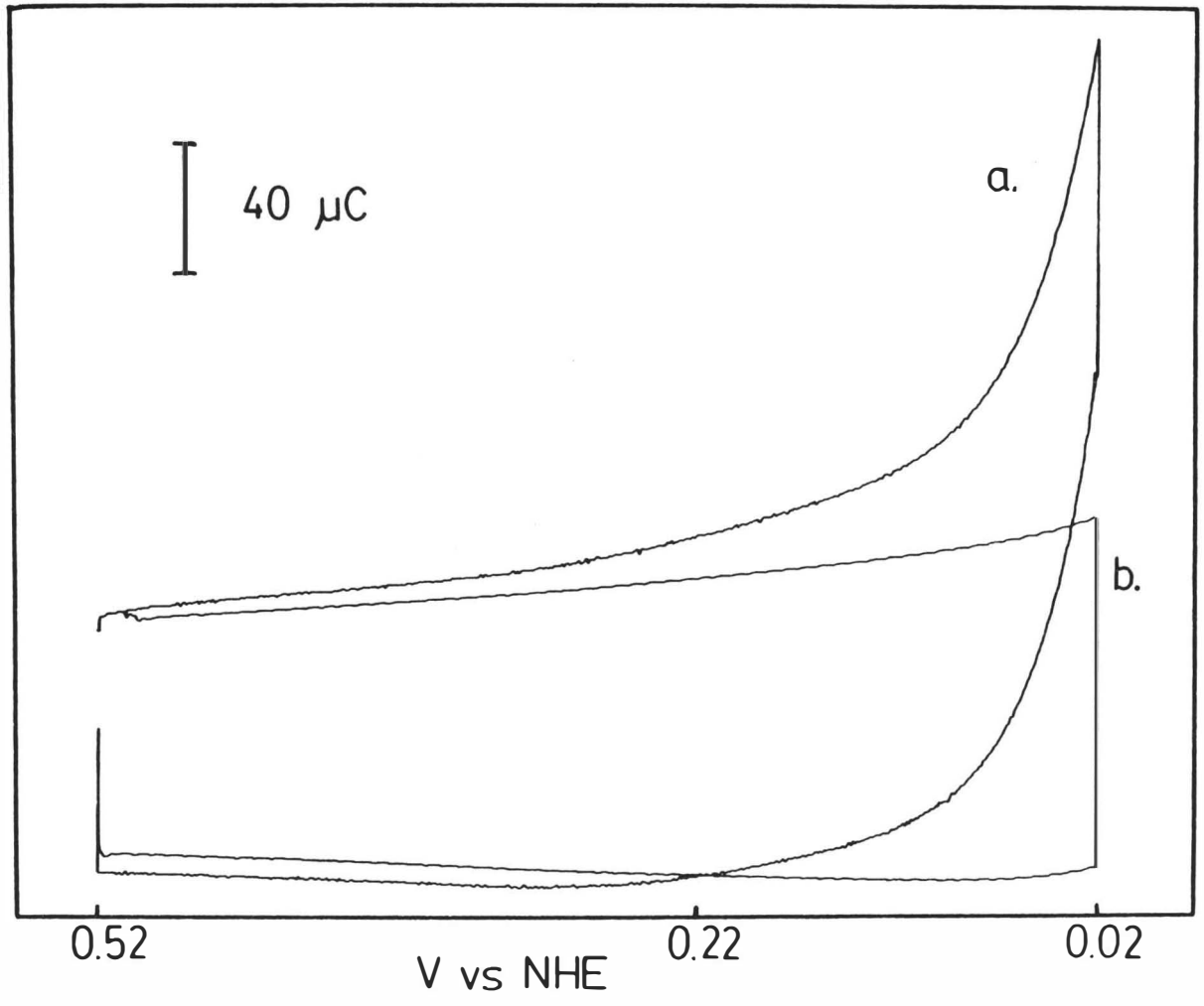
40 µC
a.
b.
0.52
0.22
0.02
V vs NHE

has been divided by its scan rate so that the relative shapes can be compared. (Current divided by scan rate yields capacitance.) As can be seen, the irregularity is more pronounced at lower scan rates. This suggests that the nonfaradaic current observed at negative potentials is at least partially due to a rate-limited process. This may be due to a diffusion-limited ionic movement within the gel layer at the electrode surface and/or to kinetic-limited electrochemical processes within the electrode material. As mentioned previously, this nonideal behavior increases with temperature for any particular scan rate. Increase in temperature enhances both diffusion and kinetic rates. Variation in pH also affects the nonfaradaic response of the indium oxide electrode. Figure 8 demonstrates this for a series of constant ionic strength phosphate buffers.

Temperature, pH, and electrolyte composition affect the electrochemical behavior of the indium oxide electrode used to evaluate the heterogeneous electron transfer characteristics of cytochrome c. In some cases, the nonfaradaic response to temperature and/or pH prevented the observation of a faradaic response from cytochrome c. Background electrochemical responses become increasingly less prominent as the concentration of electroactive species increases. Unfortunately, the electrochemical reversibility of cytochrome c at solid electrodes decreases with increase in concentration. Thus, a compromise between the proportion of faradaic to nonfaradaic response and electrochemically

Figure 8. Cyclic voltammetry of phosphate buffer at pH 5.0, 7.0, 9.0, and 11.0. All CV's were obtained at 20 mV/s and at room temperature. Each buffer had an μ of 0.2 M.

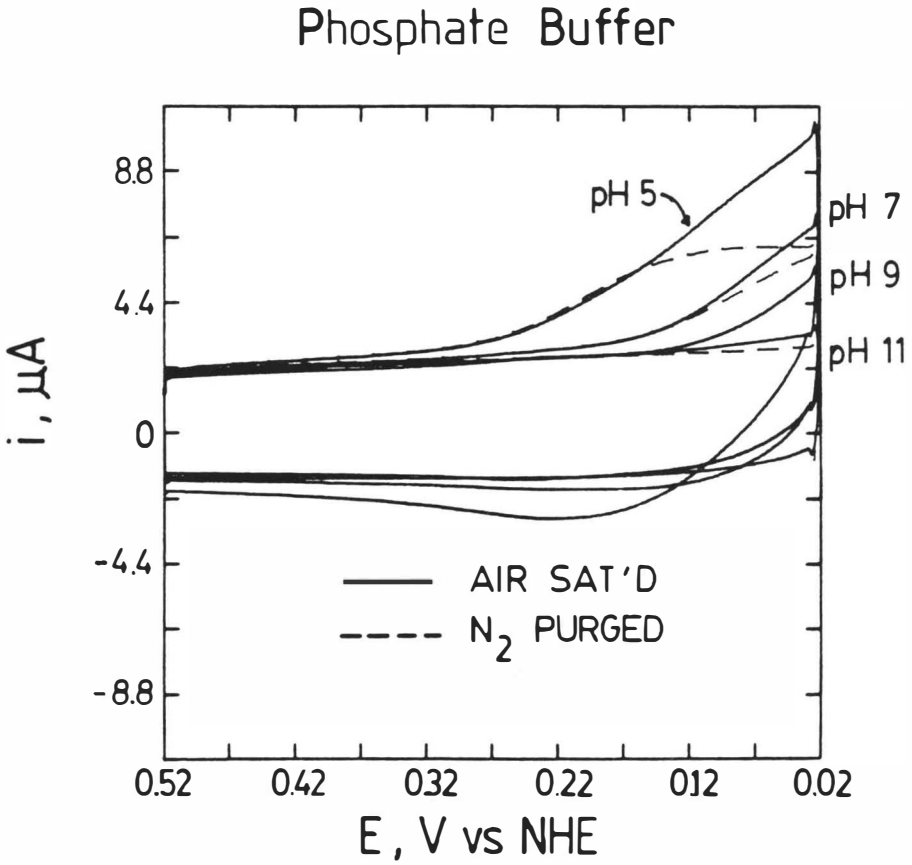
Phosphate Buffer
8.8
4.4
0
-4.4
-8.8
i, μA
pH 5
pH 7
pH 9
pH 11
AIR SAT'D
N2 PURGED
0.52
0.42
0.32
0.22
0.12
0.02
E, V vs NHE

reversible behavior must be reached.

Tin-doped indium oxide electrodes were used for all of the work presented here. The electrode/solution interface of a metal oxide is strongly affected by solution pH (171). Prior to immersion in water the electrode surface will be hydroxylated by water vapor. Hydroxyl groups adsorb to cationic sites, and H^+ groups adsorb to the oxygen atoms. The result is that the surface of the metal ion is covered with hydroxyl groups. When the electrode is placed in water, the following reactions can occur:

$$H^+(\text{surface}) + OH^-(\text{soln}) = H_2O$$

$$OH^-(\text{surface}) + H^+(\text{soln}) = H_2O$$

The metal oxide surface becomes hydrated by a highly structured monolayer of water molecules. The acid-base properties of the metal oxide and the pH of the solution will determine whether the electrode surface will carry a net negative or positive charge. The pH at which the number of surface hydronium ions equals the number of surface hydroxyl ions is known as the point of zero charge (pzc). The metal oxide will act as either a solid base or solid acid.

The pzc of an electrode is an important criterion for effective electrostatic interaction with strongly cationic cytochrome c. This electrostatic effect has been used to explain the difference in reversibility of cytochrome c with various metal oxide electrodes. For example, cytochrome c is less electrochemically reversible at fluoride-doped tin oxide electrodes than at the tin-doped indium oxide elec-

trodes used in this work (45). This was proposed to be due to the positive charge at the surface of the tin oxide electrodes at the reduction potential of cytochrome c in the neutral pH buffer used. The indium oxide electrode has at least a less positive charge, if not a negative charge, on the electrode surface in the same potential region. This model of electrostatic effects was reinforced by ionic strength and pH variation effects on the interaction of cytochrome c with the tin oxide electrode. An increase in ionic strength improved the reversibility. This is due to a lessening of the repulsive effect between the positive charge on the electrode surface and the positive charge at the active site for electron transfer of cytochrome c. Increasing the pH of the solution, at constant ionic strength, to effect alkaline conditions improved the kinetics, whereas a change to acidic conditions had the opposite effect. This variation of kinetics with change in pH has also been reported at ruthenium dioxide electrodes (46). The pH dependence was attributed to the charge on the metal oxide surface becoming more positive in acidic solutions.

Adsorption of electrolyte ions on a metal oxide electrode also affects the net charge at the electrode surface. Preferential adsorption of anions will shift the charge in a negative direction, and the opposite will occur in response to the preferential adsorption of cations. The pH at which there is no net charge on the electrode surface in the presence of adsorbed electrolyte ions is known as the point of

zero zeta potential (pzzp) or the isoelectric point (iep). This is not the same as the pzc mentioned earlier which refers to the case of equal adsorption of H^+ and OH^- ions. Thus, the electrolyte used will affect the charge on the electrode.

The thermodynamic and kinetic behavior of cytochrome c at indium oxide electrodes were probed in two buffer systems, phosphate and Tris/cacodylic acid, and at three pH values, 5.3, 7.0, and 8.0. The two buffer systems were chosen as extremes in interactive behavior with cytochrome c. Phosphate anions have been shown to bind strongly to positively charged surface lysine residues of cytochrome c, whereas Tris/cacodylic acid buffer does not interact with cytochrome c (172, 173). This same tendency to bind to cytochrome c appears to hold for interaction with the indium oxide electrode surface. The nonideal background behavior was more pronounced in phosphate buffers at each pH investigated. As mentioned earlier, the degree of positive charge on a metal oxide electrode increases with decrease in pH. This causes a corresponding increase in the attraction of electrolyte anions to the electrode surface. Hydroxide ions and electrolyte anions will compete for the cationic surface sites. The greater nonideal nonfaradaic behavior exhibited in phosphate buffer probably reflects the stronger tendency of phosphate anions to bind to the electrode surface than cacodylate anions. Figures 6-8 show that the nonideal behavior becomes more pronounced at negative potentials. An

explanation for this behavior is that the nonideal, nonfaradaic current is due to ion migration in the gel layer in the interfacial region. Initially, scanning the potential in a negative direction has no effect on the nonfaradaic current. This current arises from the charging of the double layer, i.e., reflects the capacitance of the electrical double layer at the electrode surface. The constant nonfaradaic current in the positive region of the potential scan indicates that the interface structure is not being affected by change in potential. As the electrode potential becomes increasingly negative, the adsorbed electrolyte anions begin to dissociate from their cationic binding sites. The movement of these ions in the interfacial region gives rise to a current from ion migration. As the potential becomes increasingly negative, the rate of ion migration increases, and a larger current is observed. However, this current begins to level off and then drops. This is probably due to depletion of adsorbed ions. This model is supported by the increase in nonideal behavior with decrease in pH in that there are more specifically adsorbed electrolyte anions present under acidic conditions due to an increased number of cationic binding sites on the electrode. The difference between phosphate and Tris/cacodylic acid buffers at any pH is due to their respective strengths of binding to the electrode. The decrease in nonideal behavior with increase in scan rate can be attributed to the diffusion rate of ion migration.

Another model for this nonideal behavior has been presented by Kuwana et al.(159). They investigated the effect of potential variation on indium oxide electrodes in 1N H_2SO_4, and reported the same electrochemical behavior observed in this work. The nonideal behavior at negative potentials was attributed to reduction of the surface oxide. Auger and ESCA analyses confirmed that a stoichiometry change had occurred. If a stoichiometry change is occurring in the pH range used for the research described here, the electrolyte dependence of the nonideal behavior may be due to a difference in the strength of specific adsorption of phosphate and cacodylate anions. The temperature and scan rate dependence of the irregular behavior would agree with this model if the kinetics of this process are being affected. It is noteworthy that the reduction of the electrode material itself would be an interfering faradaic process rather than nonfaradaic. A major difference between this model and the ion migration model discussed above is that cacodylate anion binding to the electrode should be stronger than that of phosphate anions. Stronger binding would cause a larger cathodic potential shift for the reduction of the metal oxide.

At each pH studied, cytochrome c behaved less reversibly in phosphate buffer than in Tris/cacodylic acid buffer. This difference was most pronounced in the pH 5.3 solutions. Reversible behavior was observed over a wide temperature range in pH 5.3 Tris/cacodylic acid buffer, and remained

stable for a day at room temperature. A temporary electrochemical response for cytochrome c in pH 5.3 phosphate buffer was observed when the solution was first added to a water equilibrated electrode. This response completely disappeared within an hour (Figure 9). The same effect was observed when a Tris/cacodylic acid buffer-cytochrome c solution was titrated with a phosphate buffer-cytochrome c solution. The degree of irreversibility was proportional to the amount of phosphate buffer solution added to the cell. A difference in electrochemical kinetics for cytochrome c in the two buffer systems is probably at least partially due to phosphate anion binding to surface residues in the vicinity of the active site of the enzyme. However, the time dependence of the response is difficult to explain if phosphate anion binding to the surface residues is the only factor. If the indium oxide electrode is first equilibrated with pH 5.3 phosphate buffer, no electrochemical response is observed. The difference between the two systems appears to be the incorporation of phosphate anions in the electrode/solution interface. An initial, reversible response is obtained with the water equilibrated electrode. The response gradually disappears as the phosphate anions interact with the electrode. This model is reinforced by the absence of any response when the electrode has been equilibrated with the phosphate buffer prior to introduction of the sample solution. Consequently, it seems that the presence of phosphate anions in the interfacial region

Figure 9. Cyclic voltammetry of cytochrome c in pH 5.3 phosphate buffer. All CV's were obtained at 20 mV/s and at room temperature. The CV with the largest peak current was obtained immediately after addition to the electrochemical cell. Subsequent CV's were obtained at approximately 10 minute intervals and are in order of decreasing response. The working electrode was equilibrated in pure water by overnight soaking prior to addition of the cytochrome c solution.

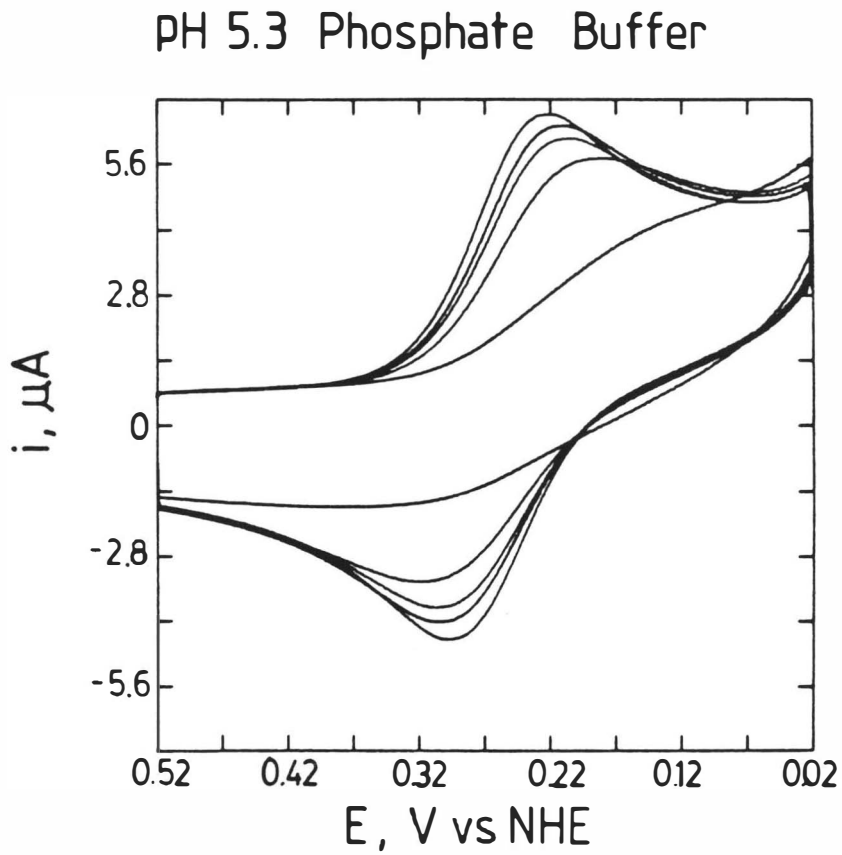
pH 5.3 Phosphate Buffer
i, μA
5.6
2.8
0
-2.8
-5.6
0.52
0.42
0.32
0.22
0.12
0.02
E, V vs NHE

interferes with the heterogeneous electrochemical behavior of cytochrome c. This may be due to anion-anion repulsion between those specifically adsorbed on the electrode and those bound to the active site for electron transfer on cytochrome c. If the electrode is first equilibrated in pH 5.3 Tris/cacodylic acid buffer, the same result is obtained as in the case when a water-equilibrated electrode is used, i.e., transitory electrochemical response. Accordingly, the premise that phosphate anions interact more strongly with the indium oxide surface is supported. The cytochrome c in the phosphate buffer sample solution that is added to the cell with the Tris/cacodylic acid buffer equilibrated electrode can not be affected by the small amount of Tris/cacodylic acid buffer remaining on the electrode. The only possible alteration of the system is the incorporation of phosphate anions into the interfacial region displacing any cacodylate anions that may be there. Similar experiments were performed with pH 7.0 phosphate and Tris/cacodylic acid buffers with the same results, although differences were less profound due to smaller differences in electrochemical reversibility at pH 7.0.

The electrochemical reversibility of ferricyanide at indium oxide electrodes is strongly diminished by changing from Tris/cacodylic acid buffer to phosphate buffer, as indicated by an increase in peak separation from 59 mV to 134 mV at a scan rate of 5 mV/s. The cathodic peak shifted 58 mV in a negative direction, and the anodic peak shifted

17 mV positive. Ferricyanide and ferrocyanide have negative charges of -3 and -4, respectively. It is highly unlikely that phosphate anions bind ferricyanide. Electron transfer between an electrode and ferri-ferrocyanide would be more difficult if phosphate anions were specifically adsorbed to the electrode due to electrostatic repulsion. The asymmetry of the peak potentials about the formal potential for ferri-ferrocyanide in phosphate buffer under quasi-reversible conditions indicates that the electrochemical transfer coefficient, α, is less than the 0.5 value determined in Tris/cacodylic acid buffer by a symmetrical spread of peak potentials under quasi-reversible conditions. An α of less than 0.5 indicates that the energy barrier for oxidation is less than that for reduction. The -4 charge of ferrocyanide would have a stronger electrostatic repulsion from specifically adsorbed phosphate anions than the -3 charge on ferricyanide. This observed kinetic dependence upon buffer strengthens the proposal that phosphate anions interact more strongly than cacodylate anions with the indium oxide electrode surface.

It is clear that the electrochemical behavior of the indium oxide electrode is affected by variation of temperature, pH, and electrolyte. To separate the nonfaradaic and possible interfering faradaic current from the total response given by cytochrome c, the current from background experiments in electrolyte alone was subtracted from the cytochrome c response. In order for this subtraction method

to be valid, the nonfaradaic behavior of the electrochemical cell must be the same in the presence and absence of cytochrome c. A spectroelectrochemical technique was used to isolate the nonfaradaic component under mixed faradaic/nonfaradaic conditions.

Due to the species selectivity of the optical probe, the spectroelectrochemical technique, derivative cyclic voltabsorptommetry (DCVA) (164), provides a response which is free from interfering faradaic and nonfaradaic currents. The nonfaradaic component of the current obtained under mixed faradaic/nonfaradaic conditions can be isolated by simultaneously recording absorbance and current from a spectroelectrochemical cell. The derivative of the absorbance of one half of the redox couple with respect to potential (dA/dE) plotted versus potential has the same morphology as the current versus potential plot of a cyclic voltammogram (CV). The absorbance of an electrochemically produced species is equivalent to the faradaic charge (Q) consumed by the electroactive species. The derivative of charge with respect to time is current. The absorbance of an electrochemically produced species can be converted to charge (164). By converting dA/dE to its analogous current and subtracting this from the experimentally recorded current, a CV of the nonfaradaic component is obtained. Thus, a background CV is extracted under actual experimental conditions.

This method of isolating the nonfaradaic current under mixed faradaic-nonfaradaic conditions was applied to a temp-

erature study of cytochrome c in pH 7.0 phosphate and Tris/cacodylic acid buffers. Figure 10 shows an example of simultaneously obtained CV and DCVA data. The difference in current at any particular potential is the nonfaradaic component of the CV. The figure also shows the difference plot obtained from the CV and DCVA data. The significant experimental finding is that the background CV's obtained in electrolyte alone corresponded well with those obtained by the difference spectroelectrochemical technique. Consequently, the background subtraction technique used for a significant portion of the research presented here is a valid method. The similarity of the background responses in the presence and absence of cytochrome c indicates that the protein does not significantly alter the electrode/solution interface structure. Further experimental results (to be discussed in a latter section) indicated that cytochrome c does adsorb to the electrode surface. Clearly, the adsorption is weak in that strong adsorption would alter the double layer structure at the electrode surface. As pointed out in Chapter I, reversible, rapid adsorption of cytochrome c to an electrode surface is a criterion for reversible electrochemical behavior. Strong, irreversible adsorption results in irreversible electrochemistry.

B. Temperature, Electrolyte, and pH Dependence of the Formal Potential of Cytochrome c

1. In pH 7.0 Buffer

A series of control experiments were performed to

Figure 10. Derivative cyclic voltammetry and cyclic voltammetry of cytochrome c. (a): CV, (b): DCVA, (c): DCVA subtracted from CV. 10 mV/s scan rate obtained at 40 °C.

CV — DCVA

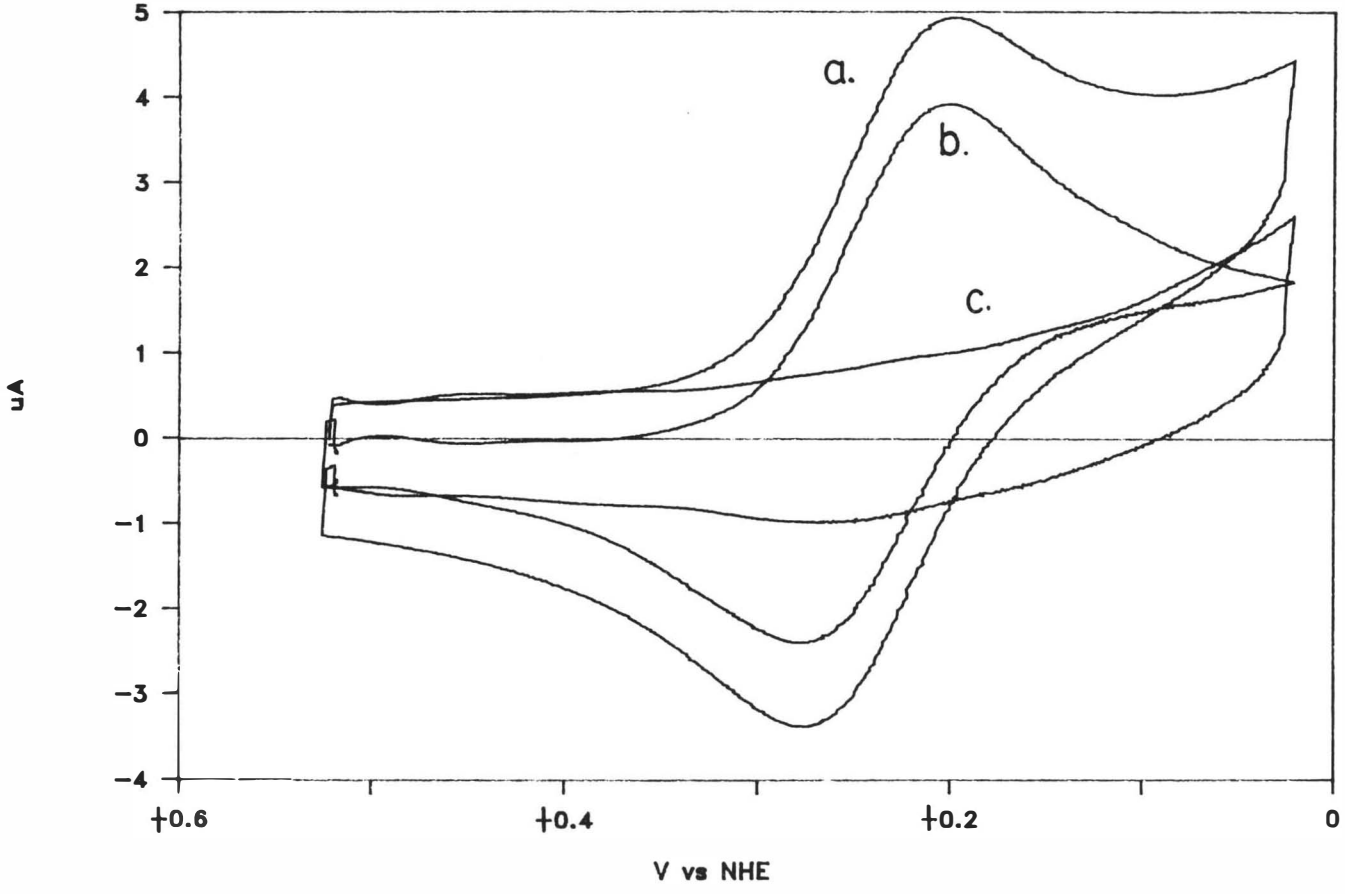

confirm that the cell being used in this work behaved in a nonisothermal manner (157). In a nonisothermal cell, the temperature of the reference electrode is held constant, in this case, at ambient temperature (22 ± 1 °C), while the temperature of the redox couple of interest is varied. Under such conditions, the reaction center entropy change, is given by:

$$\blacktriangle S_{rc}^{\circ} = nF(dE^{\circ\prime}/dT) = S_{red} - S_{ox} \qquad (1)$$

where n is the number of electrons transferred, F is the Faraday constant, E°' is the formal potential, and T is the temperature of the redox couple of interest. The liquid junction potential difference between the two electrolyte media used in this work, Tris/cacodylic acid buffer and phosphate buffer in the presence and absence of NaCl, was determined to be less than 1 mV by measuring the potential of the silver/silver chloride reference electrode versus a saturated calomel reference electrode in each medium. The uncertainty in the determination of $\blacktriangle S_{rc}^{\circ}$ by this procedure is ±1 eu (157).

The model system chosen for the evaluation of the non-isothermal behavior of the cell used in this work was $K_3Fe(CN)_6$. The temperature dependence of both the formal potential and the formal heterogeneous electron-transfer rate constant, k°', for this redox couple is shown in Figure 11. A reaction center entropy change of -37 eu was obtained by using Equation 1 from the potential data shown in this figure. Lin and Breck (174) extrapolated to zero ionic

strength and reported a reaction center entropy change of -43 eu. Evaluation of their data at 0.2 M ionic strength yielded a matching value of -37 eu. Moreover, a formal potential for $K_3Fe(CN)_6$ at 25 °C determined from potentiometric redox titrations has been reported that agrees with the value determined in the present work from cyclic voltammetric results, namely, 424 mV vs. NHE (175). These results establish that the cell configuration used in this work is nonisothermal.

Using pure cytochrome c proved to be the essential requirement for successfully conducting the research presented here. The evaluation of the temperature dependence of the electrochemical behavior of cytochrome c required long-term electrochemical stability of the system. Bowden and Hawkridge reported (38) that purification, by ion exchange chromatography, of type VI cytochrome c from Sigma Chemical Company resulted in long-term stable, heterogeneous electrochemistry at indium oxide electrodes. Cytochrome c, used as received, showed a rapid loss of electrochemical response with time. Purification, followed by lyophilization, gave a sample with long-term, stable electrochemical response. For this work, the lyophilized sample was not pure enough. Repurification of the purified, lyophilized cytochrome c revealed that the freeze drying process irreversibly denatured some of the sample. Addition of the impurities collected during the repurification to native cytochrome c caused a rapid loss of electrochemical

Figure 11. Temperature dependence of the E°' and k°' of $K_3Fe(CN)_6$. Results shown are the averages of three separate experiments at three different indium oxide electrodes. All solutions contained 1.0 mM $K_3Fe(CN)_6$ and were pH 7.0 and 0.20 M ionic strength. Two solutions only contained Tris/-cacodylate buffer, and the third solution also contained 0.10 M NaCl. Temperatures (°C), formal potentials (mV vs. NHE), and formal heterogeneous electron-transfer rate constants ($X10^3$, cm/s): 5, 451.4 (±0.9), 5.5 (±1.4); 15, 438.7 (±0.2), 7.2 (±1.6); 25, 423.8 (±0.6), 9.4 (±2.0); 35, 410.3 (±1.0), 11.5 (±2.5); 45, 393.2 (±0.6), 13.3 (±2.6); 55, 377.4 (±0.4), 15.1 (±2.6); 65, 361.2 (±0.4), 17.2 (±3.4); and 75, 347.1 (±2.1), 18.7 (±4.2). Parentheses contain standard deviations.

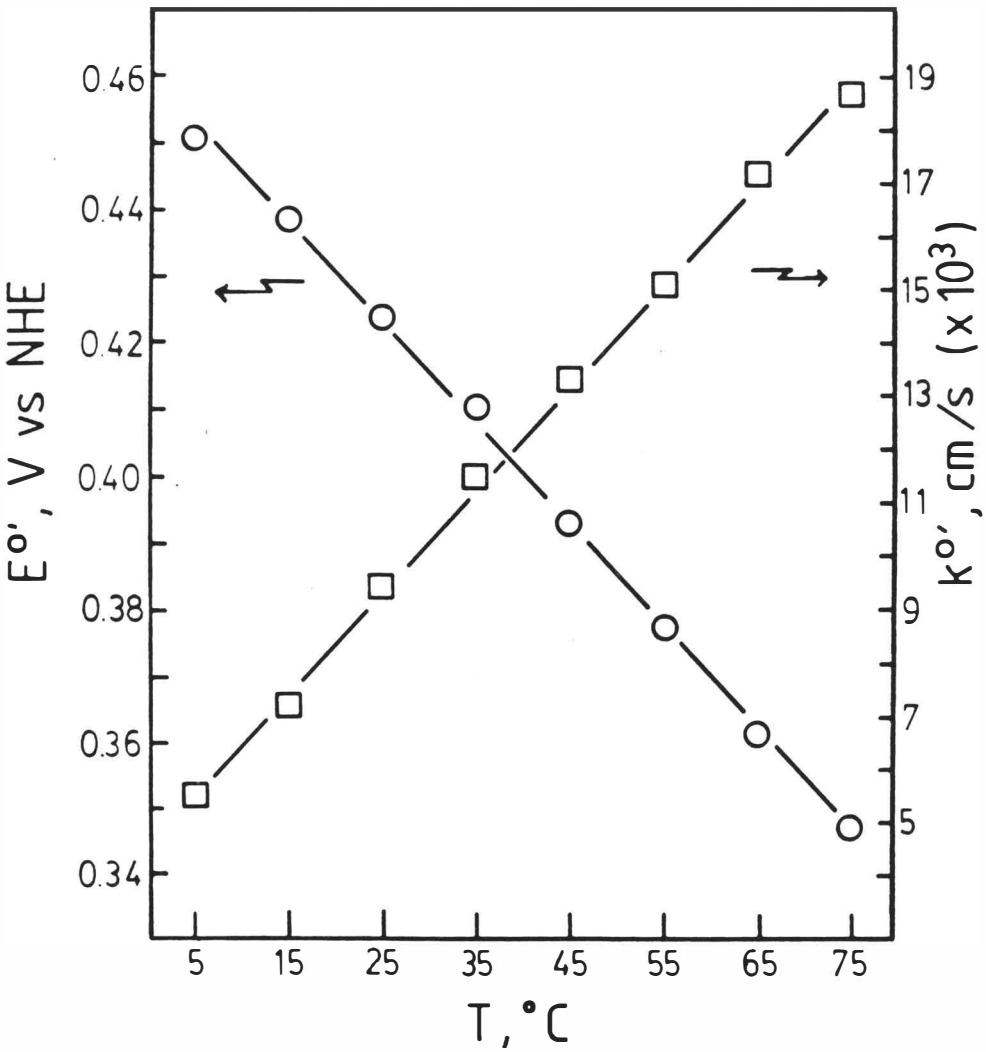
0.46
0.44
0.42
0.40
0.38
0.36
0.34
E°', V vs NHE
19
17
15
13
11
9
7
5
k°', cm/s (x 10³)
5
15
25
35
45
55
65
75
T, °C

reversibility. The leading band impurity was electrochemically reversible, and demonstrated behavior that indicated that some of the response was due to adsorbed material. The peak separation was ca. 50 mV at 20 mV/s scan rates and ca. 40 mV at 100 mV/s scan rate. A peak separation of 58 mV is expected for a reversible cyclic voltammogram of diffusing electroactive species. A reversible cyclic voltammogram of adsorbed material shows no peak separation. When both adsorbed and solution-resident electroactive species are present, the current due to adsorbed material becomes more pronounced at faster scan rates than that due to diffusing species, and this is reflected by the morphology of the cyclic voltammogram. Cyclic voltammograms were collected over a four hour period and no change in behavior was observed. At this point, some of the following band cytochrome c material was added to the electrochemical cell which caused a rapid loss in electrochemical response. The leading band material is described as deamidated forms of cytochrome c, and the following impurity bands are oligomers of cytochrome c (154). The deamidated forms are electroactive, and show stronger adsorption to indium oxide electrodes than native cytochrome c. The oligomers cause a loss of electroactivity to occur when added to a solution of native or mixed native and deamidated cytochrome c. The deactivation process probably occurs through the formation of an insulating layer of strongly adsorbed, electroinactive oligomers to the electrode surface.

The temperature dependence of the formal potential of cytochrome c was determined in the two buffer solutions used in this work at pH 7.0. Both phosphate and Tris/cacodylic acid buffers were prepared to be pH 7.0 at 22 °C and 0.20 M in ionic strength. The pH of the phosphate buffer varied with temperature in a manner that was similar to that previously reported for 0.025 M phosphate buffer (176), with pH values of 7.09 at 5 °C and 6.88 at 55 °C. The pH of Tris/cacodylic acid buffer was 7.22 at 5 °C and 6.55 at 55 °C, exhibiting a larger temperature dependence than the phosphate buffer but not as large as for Tris/HCl buffers (176). Both ferricytochrome c (177) and ferrocytochrome c (77) remain conformationally stable between the pH values given above.

Figure 12 shows the dependence of the formal potential on temperature for cytochrome c in phosphate buffer. The formal potential at 25 °C is ca. 256 mV vs. NHE. Linearity is observed from 5 to 55 °C, and $dE^{\circ\prime}/dT = -5.5 \times 10^{-4}$ V/deg. This slope yields a $\blacktriangle S_{rc}^{\circ}$ of -12.7 eu, which compares well with the value of -12.9 eu reported by Taniguchi et al. (23) for the mediated reduction of cytochrome c in pH 7.0 phosphate buffer. Another group used a method similar to this work, i.e., reversible cyclic voltammetry, at a chemically modified gold electrode, and obtained a $\blacktriangle S_{rc}^{\circ}$ of -11.8 ± 1.1 eu (51). The fact that similar results were obtained at two different solid electrodes and in a homogeneous study indicate that the variation of the formal

Figure 12. Temperature dependence of the E°' of cytochrome c in pH 7.0 phosphate and Tris/cacodylic acid buffers. (squares) Phosphate buffer, pH 7.0, 0.20 M ionic strength. $dE°'/dT = -5.5 \times 10^{-4}$ V/°C (5-55 °C), $\blacktriangle S_{rc}° = -12.7$ eu, r = -0.9993. Results shown are the averages of six separate experiments. Three experiments were in phosphate buffer only and three experiments were in phosphate buffer that also contained 0.1 M NaCl. Temperatures (°C) and formal potentials (mV vs. NHE): 5, 267 (±2.0); 15, 262 (±1.2); 25, 256 (±1.0); 30, 254 (±0.6); 35, 251 (±1.0); 40, 248 (±1.0); 45, 245 (±1.3); 50, 242 (±1.1); 55, 240 (±0.5). (circles) Tris/cacodylic acid buffer, pH 7.0, 0.20 M ionic strength. $dE°/dT = -5.8 \times 10^{-4}$ V/°C (5-65 °C), $\blacktriangle S_{rc}° = -13.4$ eu, r = -0.9989. Each value is the average of three separate experiments. Temperature (°C) and formal potential (mV vs. NHE): 5, 275 (±0.6); 15, 269 (±0.8); 25, 264 (±0.8); 35, 259 (±1.0); 40, 255 (±1.2); 45, 252 (±0.8); 50, 249 (±0.5); 55, 247 (±0.9); 60, 244 (±0.5); 65, 240 (±0.8).

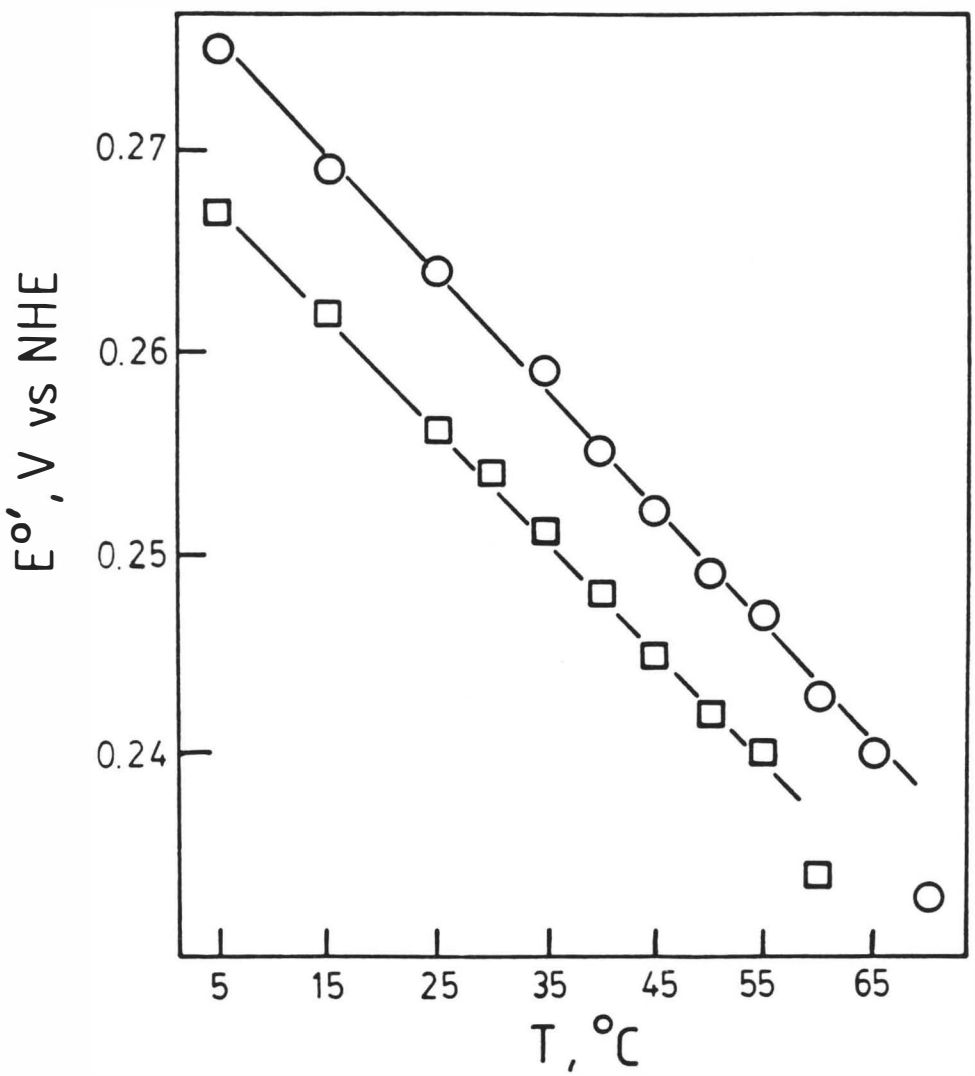
E°', V vs NHE
0.27
0.26
0.25
0.24
5
15
25
35
45
55
65
T, °C

potential of cytochrome c with change in temperature, as determined by heterogenous methods, reflects the thermodynamic behavior of cytochrome c rather than an artifact of the experimental method. The formal potential for cytochrome c in Tris/cacodylic acid buffer is ca. 8 mV anodic of formal potential in phosphate at any particular temperature, with a formal reduction potential of 264 mV vs. NHE at 25 °C. The $\blacktriangle S_{rc}°$ of -13.4 eu is experimentally indistinguishable from the -12.7 eu value in phosphate buffer. One significant difference between the results in the two buffers is that a linear relationship between formal potential and temperature was maintained to 65 °C in Tris/cacodylic acid buffer. This is 10 °C higher than in phosphate buffer. The formal potentials were determined every 5 °C. It was possible only to obtain one formal potential (at 60 °C in phosphate and 70 °C in Tris/cacodylic acid buffer) after the break in linear behavior due to the onset of irreversible electrochemistry. The formal potential of cytochrome c is 240 mV vs. NHE in both phosphate buffer at 55 °C and in Tris/cacodylic acid buffer at 65 °C, i.e., irreversible behavior begins at approximately the same formal potential. This indicates that the formal potential is an excellent indicator of the conformation of ferricytochrome c.

Cooling the pH 7.0 phosphate buffer-cytochrome c solution that had been heated to 55 °C did not restore reversible behavior. The cell was thoroughly rinsed and then allowed to soak overnight in water. A fresh, cytochrome c

solution added to the cell yielded irreversible behavior. The electrode was removed from the cell, cleaned, and then returned to the electrochemical cell. Reversible behavior for cytochrome c was obtained at the cleaned electrode. This indicates that cytochrome c exposed to 55 °C, in pH 7.0 phosphate buffer, irreversibly adsorbs to the electrode surface and blocks electron transfer to solution-resident species.

The 695 nm absorption band of ferricytochrome c, in pH 7.0 phosphate buffer, was monitored from 21 to 66 °C. The intensity of the band diminished with increase in temperature, indicating a weakening of the Fe-S bond. Cooling the solution to room temperature caused the intensity of the 695 nm band to return to its original level, indicating a reversible temperature effect on cytochrome c. Thus, electron transfer at indium oxide electrodes at temperatures above ca. 50 °C, in pH 7.0 phosphate buffer, causes an irreversible change to occur in cytochrome c which cannot be attributed to the effects of temperature alone. Irreversible adsorption to the electrode and loss of electroactivity accompanies this irreversible change.

Several attempts were made to evaluate the temperature dependence of the formal potential of cytochrome c by thin-layer spectroelectrochemistry. The redox ratio of cytochrome c was set by the electrode potential and determined by monitoring the 550 nm absorption band of ferricytochrome c. Room temperature evaluations gave reproducible results

that agreed with those determined by cyclic voltammetry. Condensation of water vapor on the optically transparent working electrode at low temperatures and bubble formation at elevated temperatures caused severe baseline drift to occur. Variation of temperature from 25 to 45 °C in both pH 7.0 phosphate and Tris/cacodylic acid buffers yielded a negative shift in formal potential. However, the results were not precise. The determination of formal potentials by cyclic voltammetry at temperatures above and below room temperature was much more precise, accurate, and rapid than by thin-layer spectroelectrochemistry, and the latter technique was not used further.

The differences observed in the formal potential of cytochrome c reacting at indium oxide electrodes in the two buffers used in this study are attributed to anion binding in the case of phosphate buffer. Phosphate anions bind to the positively charged lysine residues surrounding the solvent exposed heme edge (172). The anions may electrostatically reduce charge repulsion between the positively charged heme group of ferricytochrome c and the positively charged lysine residues, thus stabilizing the oxidized form of cytochrome c. This is reflected by the relatively negative formal potentials for cytochrome c in phosphate buffer as compared to those in Tris/cacodylic acid buffer. There is experimental evidence (79, 85, 123, 173) that binding to the lysine residues in the active site region destabilizes the structure of ferricytochrome c. Hence, the binding of

phosphate anion to cytochrome c may cause an increase in solvent exposure of the heme group. This would also result in an increased stabilization of the oxidized form relative to the structure present in the absence of anion binding and a corresponding negative shift in reduction potential.

The electrostatic and conformational explanations of the different formal potentials of cytochrome c in the two buffer systems have different conformational implications. Both models propose that the negative shift of formal potential in phosphate buffer, relative to that in Tris/cacodylic acid buffer, is due to phosphate anion binding which causes a stabilization of the positively charged heme group in ferricytochrome c. If a purely electrostatic effect from the interaction of phosphate anions and the heme group causes the shift in formal potential, the conformation of ferricytochrome c in both buffer systems is the same at the same temperature. However, if phosphate anion binding shifts the conformation of ferricytochrome c to that with an increased solvent exposure of the heme group, the conformation of the oxidized form is different in the two buffer systems at any one temperature. An increase in temperature causes an opening of the crevice about the solvent exposed heme edge in both buffers. A conformational shift due to phosphate anion-ferricytochrome c interaction would have a constant additive effect on the opening of the crevice throughout the temperature range studied. Consequently, ferricytochrome c may have the same conformation in the two

buffer systems when the formal potential is the same. This occurs at different temperatures in the two buffers used. Recall that the linear range of the formal potential versus temperature relationship extends to different temperatures in the two buffers but ends at approximately the same formal potential. If anion binding has this conformational effect, it should be reflected by a lowering of the temperature of denaturation and the pK of alkaline isomerization. This has been reported for the alkaline isomerization of ferricytochrome c in the presence perchlorate anions (178). The shift in pK was attributed to the preferential binding of perchlorate to the alkaline form of ferricytochrome c (state IV) over the neutral form (state III). However, chloride and phosphate anions do not cause a shift in pK (178). Both phosphate and chloride anions bind to ferricytochrome c with approximately the same strength (179). Osheroff et al. (172) found that phosphate anions bind to both oxidation states of ferricytochrome c, while chloride anions only bind to ferricytochrome c. Other groups report that chloride anions do bind to ferrocytochrome c (179, 180). Clearly, there are differences of opinion on change of anion binding strength with change in oxidation state. Most studies indicate that binding is stronger to the oxidized form (7). The binding sites are in the region of the solvent-exposed heme edge (7, 178-180) of ferricytochrome c. The solvent exposure of the heme group decreases significantly (82) on reduction. The dependence of binding strength on oxidation

state of cytochrome c supports the view that there is an electrostatic interaction between the anions and the solvent-exposed heme edge. The electrostatic model is also supported by the $\blacktriangle S_{rc}°$ for cytochrome c, which is the same (within experimental error) in both the binding and nonbinding buffers. However, a conformational perturbation induced by anion binding may increase the extent of solvent exposure of the heme group sufficiently to cause the observed 8 mV shift in formal potential without making a noticeable difference in $\blacktriangle S_{rc}°$. A change of enthalpy of $\blacktriangle H°$ = -9.5 Kcal/mole has been reported for the reduction of cytochrome c (40). The formal potentials of cytochrome c at 25 °C in phosphate and Tris/cacodylic acid buffers correspond to a change in free energy of $\blacktriangle G°$ = -5.90 kcal/mole and $\blacktriangle G°$ = -6.09 kcal/mole, respectively. The change in $\blacktriangle G°$ with buffer corresponds to a difference of 0.7 eu in $\blacktriangle S_{rc}°$ ($\blacktriangle H°$ held constant and $\blacktriangle G° = \blacktriangle H° - T\blacktriangle S°$). The accuracy of the $\blacktriangle S_{rc}°$ values reported here is ± 1 eu (157) while the accuracy of the formal potentials is ± 1 mV. Thus, a change in formal potential due to a conformation change resulting from anion binding can be easily determined while the corresponding difference in $\blacktriangle S_{rc}°$ is not experimentally observable. The phosphate and chloride anion binding study (179) also revealed that there is a difference in the dynamics of the active site region between the two oxidation states. The average structures of ferri- and ferrocytochrome c are almost identical. It is the large difference in the

dynamics of the protein structures of the two oxidation states that accounts for the difference in physicochemical properties. The complexity of enzyme dynamics makes it difficult to clearly define anion binding effects. Probably, there are both electrostatic interactions with the heme and residue vibrational effects resulting from anion binding. In either case, it does seem reasonable that the cathodic shift in formal potential of cytochrome c observed in the presence of phosphate anions is due to a stabilization of the positively charged heme in ferricytochrome c.

As mentioned previously, the reduced form of cytochrome c is very stable, and undergoes mild conformational changes throughout the temperature range used for this study (63, 77, 79). The oxidized form is less stable, and undergoes larger conformational changes. The formal potential indicates the relative stability of the oxidized and reduced forms. As the temperature is increased, the crevice around the solvent-exposed heme edge opens, and allows greater solvent exposure of the heme, thus stabilizing the positively charged heme group of ferricytochrome c. Previous studies have indicated that in ferricytochrome c, the Fe-S bond gradually and continuously weakens with the increase in temperature (76, 83, 88). The residues adjacent to the met-80 group are also flexible (76, 181). The conformational change on reduction is primarily a closing of the crevice about the solvent-exposed heme edge (82). The difference in conformation is associated with a change in the Fe-S bond

length which affects conformational changes by a "pull-push" mechanism (76). Similarly, the temperature dependent Fe-S bond length may play a role in controlling the crevice about the heme within each redox state as a function of temperature. The $\blacktriangle S_{rc}°$ values for cytochrome c determined in both buffer media used in this work are small in magnitude, negative in sign, and, within experimental error, the same, i.e., -13 ± 1 eu. The sign and magnitude of this reaction center entropy change are consistent with a small conformational change to a more compact structure in the environment about the heme on reduction (23). Charge-induced outer sphere solvent reorganization can only be a small factor in this entropy change since the heme is largely shielded from the solvent. Moreover, a positive contribution to $\blacktriangle S_{rc}°$ would be expected for a +1 to a neutral charge change (157).

The negative entropy change for the reduction of cytochrome c has also been attributed to the decrease in size of cytochrome c when reduced, followed by water filling the void, with subsequent water structure formation through hydrogen bonding (14, 17, 24). This model is based on the biphasic behavior of the temperature dependence of the formal potential of cytochrome c in the presence of chloride anions (0.1 M). The break occurred at 42 °C. Below 42 °C a $\blacktriangle S_{rc}°$ of -10.2 eu was observed, while above 42 °C a value of -75.0 eu was obtained. This effect should be strongly dependent on chloride concentration, but concentration studies were not reported.

Three of the experiments in phosphate buffer were conducted in the presence of 0.1 M NaCl. No chloride entropy effect was observed. A similar study of the temperature dependence of the formal potential of cytochrome c, in pH 7.0 phosphate buffer, in the presence of NaCl, as determined by heterogeneous electron transfer at a chemically modified gold electrode (52) also failed to reveal the chloride effect. This difference in results for temperatures above 42 °C may be due to several factors. The previous work employed spectropotentiostatic experiments using optically transparent thin-layer electrode (OTTLE) cells and a mediator to couple the redox state of cytochrome c to the potential applied to the gold minigrid working electrode. Therefore, the OTTLE results are based on optical measurements that probe redox states in bulk solution. The results presented here are based on cyclic voltammetry responses, and are therefore dependent on the flux of electroactive species at the electrode/solution interface and bulk solution conditions. The dimension of the diffuse double layer under the present experimential conditions, i.e., 0.20 M ionic strength, is less than 5 Å (182), and cytochrome c has a diameter of ca. 25-30 Å, not including the solvation sheath (61). These factors suggest that cytochrome c molecules undergoing electron transfer reactions in these experiments exhibit characteristics that are largely due to the bulk solvent properties. However, if the physiological binding domain of cytochrome c is indeed facing the

electrode surface during electron transfer, chloride anions may be excluded form this region, preventing the observation of the chloride-dependent behavior observed by the OTTLE technique above 42 °C.

The OTTLE work employed 1 mM solutions of cytochrome c, whereas the heterogeneous technique described here used concentrations ranging from 60 to 100 μM. An attempt to use a pH 7.0 phosphate buffer, 1 mM cytochrome c, 0.1 M NaCl solution failed due to the concentration dependence of the electrochemical reversibility of cytochrome c. Cyclic voltammograms acquired at 10 mV/s showed peak separations of at least 165 mV at 25 °C. Table 1 lists the peak separation and midpoint potentials for this concentration. In order for the average of peak potentials to be used in determining formal potentials, the peak separation should be close to 60 mV, i.e., reversible behavior must exist. Given this caveat, it is still worth noting that the chloride-induced break at 40 °C did not occur. A linear regression analysis of the data provided a change in reaction center entropy of ca. -9.2 eu, which is reasonably close to the -12.7 eu determined for lower protein concentration, reversible cyclic voltammograms.

The effect of chloride anions on the formal potential temperature dependence of cytochrome c in Tris/cacodylic acid buffer was examined by the combined DCVA-CV technique. The effect of the chloride anions in the nonbinding buffer was to shift the thermodynamic behavior of cytochrome c to

TABLE 1

Temperature, ° C	$\blacktriangle E_p$, mV	E_{mp}, mV vs NHE
5	217[a.]	258
15	192	256
25	164	253
30	154	251
35	150	249
40	144	247
45	142	244
50	139	241
55	140	239

a. Peak separation from 10 mV/s scan rate cyclic voltammograms.

close to that observed in phosphate buffer. The formal potential was shifted ca. 6 mV cathodic of that in the absence of chloride anions. This was determined by repeatedly alternating between two Tris/cacodylic acid cytochrome c solutions, one with and one without 0.1 M NaCl, in the same electrochemical cell. The formal potential varied linearly from 25 to 55 °C with a $\blacktriangle S_{rc}°$ of ca. -17 eu. This result is from the average of three DCVA's and three background-subtracted CV's obtained in one experimental run. The DCVA results were not as precise (± 3 mV) as the background-subtracted CV (± 1 mV) results. The temperature dependence of the formal potential of cytochrome c in pH 7.0 phosphate and Tris/cacodylic acid buffers was also evaluated by DCVA, and gave the same results as with the background-subtracted CV experiments. Again, the DCVA experiments were not as precise as the CV experiments. This is probably due to the degradation of the signal-to-noise ratio resulting from taking the derivative of the absorbance signal.

Tris/cacodylic acid is a nonbinding buffer, whereas chloride and phosphate anions bind to ferricytochrome c. The cathodic shift in formal potential on addition of chloride anions to Tris/cacodylic acid buffer reinforces the model that anion binding affects the heme environment of ferricytochrome c. The absence of a change in formal potential of cytochrome c in phosphate buffer on addition of chloride anions indicates that chloride anions do not displace phosphate anions bound to ferricytochrome c. The

binding strength of phosphate anions to ferricytochrome c is slightly larger than that of chloride anions (172). The $\blacktriangle S_{rc}°$ value of -17 eu for cytochrome c in Tris/cacodylic acid buffer that was 0.1 M in NaCl indicates that the interaction of chloride anions with cytochrome c differs from that of phosphate anions (-13 eu). The more negative $\blacktriangle S_{rc}°$ observed in the presence of chloride anions relative to that observed in phosphate buffer is probably not due to a larger conformational or electrostatic interaction, induced by chloride anions, as the change in formal potential is not as pronounced for chloride as for phosphate anion binding. Osheroff et al. (172) reported that phosphate anions bind to both oxidation states of cytochrome c, whereas chloride anions bind only to ferricytochrome c. The release of chloride anions contingent on reduction of the protein may explain the larger, more negative $\blacktriangle S_{rc}°$ value observed in the presence of chloride anions. The $\blacktriangle S_{rc}°$ of cytochrome c is the same (± 1 eu) in phosphate and Tris/cacodylic acid buffers. This reinforces the view that phosphate anions bind to both oxidation states and that the formal potential difference in the two buffers is due to the additional conformational weakening of the heme crevice induced by anion binding.

Background CV's were obtained for pH 7.0 Tris/cacodylic acid buffer both with and without added NaCl. The addition of NaCl had no effect on their morphology. This is in contrast to the previously noted difference in background CV's

between phosphate and Tris/cacodylic acid buffers, and indicates that chloride anions do not interact as strongly with the surface of the indium oxide electrode as phosphate anions. A possible reason for this is that phosphate anions adsorb to the electrode through hydrogen bonding. Chloride anions do not hydrogen bond, and are probably expelled from the negatively charged indium oxide electrode surface. This idea reinforces the explanation given above for the difference in the temperature dependence of the formal potential of cytochrome c in neutral 0.1 M NaCl solutions, as determined by homogeneous (14, 17, 24) and heterogeneous (52, and this work (56)) methods, i.e., that the chloride anions are excluded from the heterogeneous electron transfer reaction site.

The model system of ferri-/ferrocyanide was also evaluated in the presence of 0.1 M NaCl. Direct addition of NaCl to the 0.2 M ionic strength Tris/cacodylic acid solution changed the $\blacktriangle S_{rc}°$ considerably due to the ionic strength dependence of the reduction of this very negative anion (change of -3 to -4). However, the temperature dependence of the formal potential about 42 °C was still linear. Adjustment of the Tris/cacodylic acid concentration so that 0.2 M ionic strength conditions were maintained in the presence of 0.1 M NaCl resulted in no difference in thermodynamic behavior between 25 and 75 °C from that observed in the absence of NaCl. Any bulk water structure effects of adding 0.1 M NaCl should have been observed in this reaction

due to the large outer sphere, i.e., solvent reorganization change accompanying the reduction of ferricyanide.

2. In pH 5.3 Buffer

A shift in solution pH from 7.0 to 5.3 causes an increase in the thermal stability of ferricytochrome c (88). This was determined by monitoring the 695 nm absorption band of ferricytochrome c which arises from a charge transfer from the axially bound sulfur of the met-80 to the heme iron. In addition, Moore's (76) NMR study of the effect of temperature on ferricytochrome c was conducted at a pH of 5.3. An increase in pH or temperature lead to the denaturation of ferricytochrome c. For these reasons, the temperature dependence of the formal potential of cytochrome c in pH 5.3 Tris/cacodylic acid and phosphate buffers was investigated.

The irreversible electrochemical behavior of cytochrome c in pH 5.3 phosphate buffer has already been discussed. This was partially attributed to the large concentration of specifically adsorbed anions present at the electrode/ solution interface. The relative ratio of monobasic and dibasic phosphate anions changes with pH. The differences in interaction of monobasic and dibasic phosphate with the electrode interface and in binding to ferricytochrome c are not known.

The variation of formal potential with temperature in pH 5.3 Tris/cacodylic acid buffer (Figure 13) was linear from 5 to 75 °C with a $\blacktriangle S_{rc}°$ of -12.0 eu. The formal poten-

tial was 268 mV vs. NHE at 25 °C. Irreversible electrochemistry was observed at 80 °C. The linear range extends 20 °C beyond that observed for cytochrome c in pH 7.0 phosphate buffer and 10 °C beyond that in pH 7.0 Tris/cacodylic acid buffer. The formal potential is 239 mV vs. NHE at 75 °C in pH 5.3 Tris/cacodylic acid buffer. Thus, the loss of linear formal potential versus temperature behavior occurs at approximately the same formal potential in pH 5.3 Tris/cacodylic acid buffer and in both pH 7.0 buffer systems but at a higher temperature. This indicates that the acidic pH stabilizes the conformation of ferricytochrome to thermal denaturation. Moore (76) reported that ferricytochrome c remains in its native conformation to 77 °C at pH 5.3. This strongly supports the view that the formal potential of cytochrome c will vary linearly with temperature in neutral and acidic media as long as ferricytochrome c remains in its native form. Again, the conformation of ferrocytochrome c is largely unaffected over the temperature ranges discussed here. It remains in its native conformation to 97 °C at pH 7.0 (77).

The formal potential of cytochrome c shifts ca. 4 mV in the anodic direction with decrease in pH of 7.0 to 5.3 in Tris/cacodylic acid buffer at the same temperature. This empirical result supports the view that the degree of solvent exposure of the positively charged heme in ferricytochrome c contributes to determining the reduction potential of cytochrome c. Under acidic conditions, the positively

Figure 13. Temperature dependence of the E°' of cytochrome c in pH 5.3 Tris/cacodylic acid buffer and pH 8.0 phosphate and Tris/cacodylic acid buffers. Each value is the average from three experiments. (squares) pH 5.3 Tris/cacodylic acid buffer. $dE°'/dt = -5.5 \times 10^{-4}$ V/°C (5 to 75 °C), $\blacktriangle S_{rc}°$ = -12.6 eu, r = -0.9974. Temperatures (°C) and formal potentials (mV vs. NHE): 5, 278; 15, 273; 25, 268; 35, 263; 45, 257; 55, 253; 60, 249; 65, 247; 70, 242; 75, 239. (x) pH 8.0, Tris/cacodylic acid buffer. $dE°'/dt = -5.5 \times 10^{-4}$ V/°C (5 to 40 °C), $\blacktriangle S_{rc}°$ = -12.7 eu, r = -0.9959. $dE°'/dT = -1.04 \times 10^{-3}$ V/°C (45 to 60 °C), $\blacktriangle S_{rc}°$ = - 24.0 eu, r = -.9989. Temperatures (°C) and formal potentials (mV vs. NHE): 5, 274; 15, 269; 25, 264; 30, 261; 35, 257; 40, 254; 45, 249; 50, 244; 55, 239; 60, 233. (diamonds) pH 8.0 phosphate buffer. $dE°'/dT = -6.1 \times 10^{-4}$ V/°C (5 to 40 °C), $\blacktriangle S_{rc}°$ = -14.2 eu, r = -0.9959. $dE°'/dT = -1.40 \times 10^{-3}$ V/°C (45 to 55 °C), $\blacktriangle S_{rc}°$ = -32.3 eu, r = -0.9966. Temperatures (°C) and formal potentials (mV vs. NHE): 5, 267; 15, 261; 25, 256; 30, 252; 35, 248; 40, 245; 45, 240; 50, 234; 55, 226.

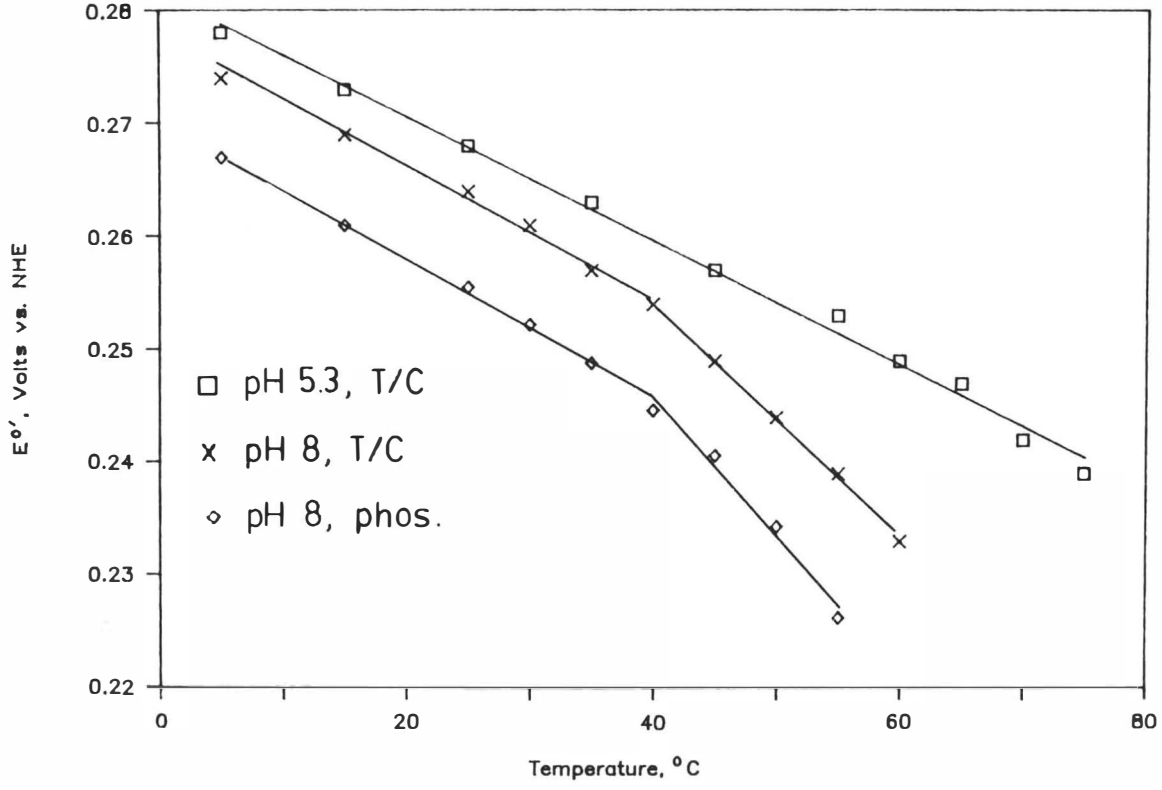
E°′ vs. Temperature
0.28
0.27
0.26
0.25
0.24
0.23
0.22
E°′, Volts vs. NHE
pH 5.3, T/C
pH 8, T/C
pH 8, phos.
0
20
40
60
80
Temperature, °C

charged heme, located in a largely hydrophobic environment, is less exposed to solvent and therefore, is not as resis-- tant to reduction as in neutral or basic solutions.

3. In pH 8.0 Buffer

The formal potential of cytochrome c in alkaline phosphate and Tris/cacodylic acid buffers showed a clear biphasic temperature dependence (Figure 13), with the change in slope occurring at ca. 40 °C in both systems. From 5 to 40 °C, there was no difference in formal potential from that observed in pH 7.0 buffers. From 40 to 55 °C, the formal potential at pH 8.0 became increasingly negative relative to that observed at pH 7.0. This higher temperature region is also linear. In pH 8.0 phosphate buffer, a $\blacktriangle S_{rc}°$ of -32 eu was found for the temperature range of 40 to 55 °C. The $\blacktriangle S_{rc}°$ of cytochrome c in pH 8.0, from 40 to 60 °C, was -24 eu. The $\blacktriangle S_{rc}°$ was approximately -13 eu in both buffers from 5 to 40 °C. The pH of the phosphate buffer prepared as pH 8.0 at room temperature was invariant from 5 to 55 °C. However, the pH 8.0 Tris/cacodylic acid buffer changed with temperature. A solution prepared as pH 8.0 at room temperature had a pH of 8.5 at 5 °C, 7.6 at 40 °C, and 7.3 at 55 °C. This temperature dependence was more pronounced than that for the pH 7.0 Tris/cacodylic acid buffer due to the higher concentration of Tris in the alkaline solution. Tris buffers are known to be very susceptible to temperature effects (176). The pH 5.3 Tris/cacodylic acid buffer was found to be virtually temperature independent. The tempera-

ture dependence of the pH 8.0 Tris/cacodylic acid buffer is the probable cause of the difference in the $\blacktriangle S_{rc}°$ values obtained for cytochrome c above 40 °C in the two buffers. While the phosphate buffer remained at pH 8.0 above 40 °C, the Tris/cacodylic acid buffer became increasingly acidic. It has already been demonstrated that changing from neutral to acidic conditions stabilizes cytochrome c to the effects of temperature.

The change in $\blacktriangle S_{rc}°$ at 40 °C is probably due to a distinct conformational change in ferricytochrome c to a form which is less structured than that existing below 40 °C. The larger conformational change then required on reduction to the largely pH and temperature independent conformation of ferrocytochrome c is reflected by the more negative $\blacktriangle S_{rc}°$. An interesting point is that the discontinuity in the formal potential versus temperature relationship occurs at the same temperature, but at different formal potentials, in the two buffers. The formal potential at which the break occurs in the pH 8.0 phosphate buffer is 245 mV versus NHE, and 254 mV vs. NHE in pH 8.0 Tris/cacodylic acid buffer. It has been suggested here that the formal potential of cytochrome c is a sensitive indicator of the conformation of ferricytochrome c. This should be true at least in the vicinity of the heme group in that conformational changes would change the degree of solvent exposure of the positively charged heme and the hydrophobicity of its environment. The finding at pH 8.0 that the temperature at which

the break occurs is independent of buffer and formal potential suggests that the cause of biphasic behavior is not in the vicinity of the solvent-exposed heme edge.

Taniguchi et al. (51) have also investigated the formal potential temperature dependence of cytochrome c at pH 8.0 by the same technique used for this work. They report the same biphasic behavior, with the break occurring at 40 °C. The $\blacktriangle S_{rc}°$ below 40 °C was -10.3 eu and was -41.1 eu from 40 to 55 °C. The phosphate buffer used contained 0.1 M sodium perchlorate. The difference in $\blacktriangle S_{rc}°$ in their work (-41 eu) and this work (-30 eu in phosphate buffer) is probably due to the effect of perchlorate anion binding to ferricytochrome c. Perchlorate anions have been shown to interact differently with ferricytochrome c than phosphate or chloride anions (178). Taniguchi (51) points out that no remarkable changes occurred in the Raman spectrum of ferricytochrome c in pH 8.0 buffer from 0 to 55 °C, and concludes that a change in the heme environment is unlikely. He attributes the biphasic behavior in alkaline solution to a change in the structure of the protein moiety of cytochrome c that occurs in a more pronounced fashion above 40 °C. The protein is still in its native conformation between 40 and 55 °C in the alkaline solution. This supports the view presented here that the biphasic behavior observed at pH 8.0 is caused by a conformational event distinct from that which causes the onset of irreversible electrochemistry that corresponds to a formal potential of 240 mV vs. NHE observed in

the neutral and acidic buffers. Myer (73) reported that an intermediate state IIIb exists between the native state III and the alkaline state IV. The transition from state III to state IIIb produces a conformational change in ferricytochrome c which does not affect the ligation to the heme or the hydrophobicity of the heme environment. The transition from state IIIb to state IV involves both a change in the iron coordination and the hydrophobicity of the heme environment. The break in the formal potential vs temperature plot at 40 °C in pH 8.0 media is probably due to a state III to state IIIb transition. State IIIb is electroactive, but has different adsorption characteristics than state III. This will be discussed further in the next section.

C. Kinetic and Adsorption Behavior of Cytochrome c

The primary technique used to investigate the heterogeneous electron transfer kinetics of cytochrome c at indium oxide electrodes was cyclic voltammetry. An advantage of cyclic voltammetry is that both thermodynamic and kinetic parameters can be determined for many electroactive species. Slow scan rate, reversible cyclic voltammograms are used to determine reduction potentials. The redox ratio of the analyte instantaneously, i.e., reversibly, adjusts to the free energy of the electrode as described by the Nernst equation. The current is limited only by mass transport of the analyte to the electrode. Experimental conditions limit the mode of transport to diffusion. The current is then a function of the concentration gradient of the electroactive

species at the electrode surface. The current increases with scan rate due to the increased rate at which the analyte is consumed which causes a concomitant stepping of the concentration gradient. A peak is observed at an electrode potential which forces the redox ratio to a point where the concentration of the species being reduced (or oxidized) is essentially zero. The concentration gradient can not be increased further, and the current begins to decrease due to depletion effects. The peak separation of reversible cyclic voltammograms is independent of scan rate. This significant feature arises from the thermodynamic dependence of the redox ratio on the electrode potential. The potential difference between a peak and the formal potential of the redox couple is therefore constant. A cyclic voltammogram contains both a cathodic and an anodic peak. Thus, the midpoint between these two peaks is the formal potential of the system when reversible behavior is observed. Fast scan rate, quasi-reversible cyclic voltammograms provide heterogeneous electron transfer rate constants, and also reflect the type and strength of adsorption of an electroactive species to the electrode surface. The electron transfer kinetics are calculated from the increase in peak separation from that of a reversible system. The increase in peak separation is caused by the inability of the redox potential to adjust to the potential of the electrode in the time allowed by the scan rate of the experiment. A more robust electrode potential, i.e., an overpo-

tential, is then required to force the redox ratio to the point where a peak is observed. The current is also affected by electron transfer kinetics since the redox ratio does not strictly follow the rate of electrode potential variation. The amount of material electrolyzed is less than that for the reversible case, and smaller currents are obtained. Figure 14 shows a series of reversible and quasi-reversible cyclic voltammograms obtained from the same solution in an electrochemical cell. The reversible, 20 mV/s scan rate, cyclic voltammograms have a linear variation of the peak potentials with change in temperature that reflects the linear temperature dependence of the formal potential. The larger current at higher temperature is caused by an increase in the diffusion rate produced by a decrease in solvent viscosity with increase in temperature. The quasi-reversible, 500 mV/s scan rate, cyclic voltammograms demonstrate a nonlinear variation of peak potential with change in temperature, indicating that the current is limited by both diffusion and electron transfer kinetics. The heterogeneous electron transfer rate constant was determined from the cyclic voltammetric peak separation by the method of Nicholson (183).

1. In pH 7.0 Buffer

In order to evaluate the heterogeneous rate constant, k°', by the peak separation method, the diffusion coefficient of the electroactive species must be known. The temperature dependence of the diffusion coefficient of

Figure 14. Reversible (20 mV/s scan rate) and quasi-reversible (509 mV/s scan rate) cyclic voltammetry of cytochrome c in pH 5.3 Tris/cacodylic acid buffer. Temperatures (°C), 5, 15, 25, 35, 45, 55, 65.

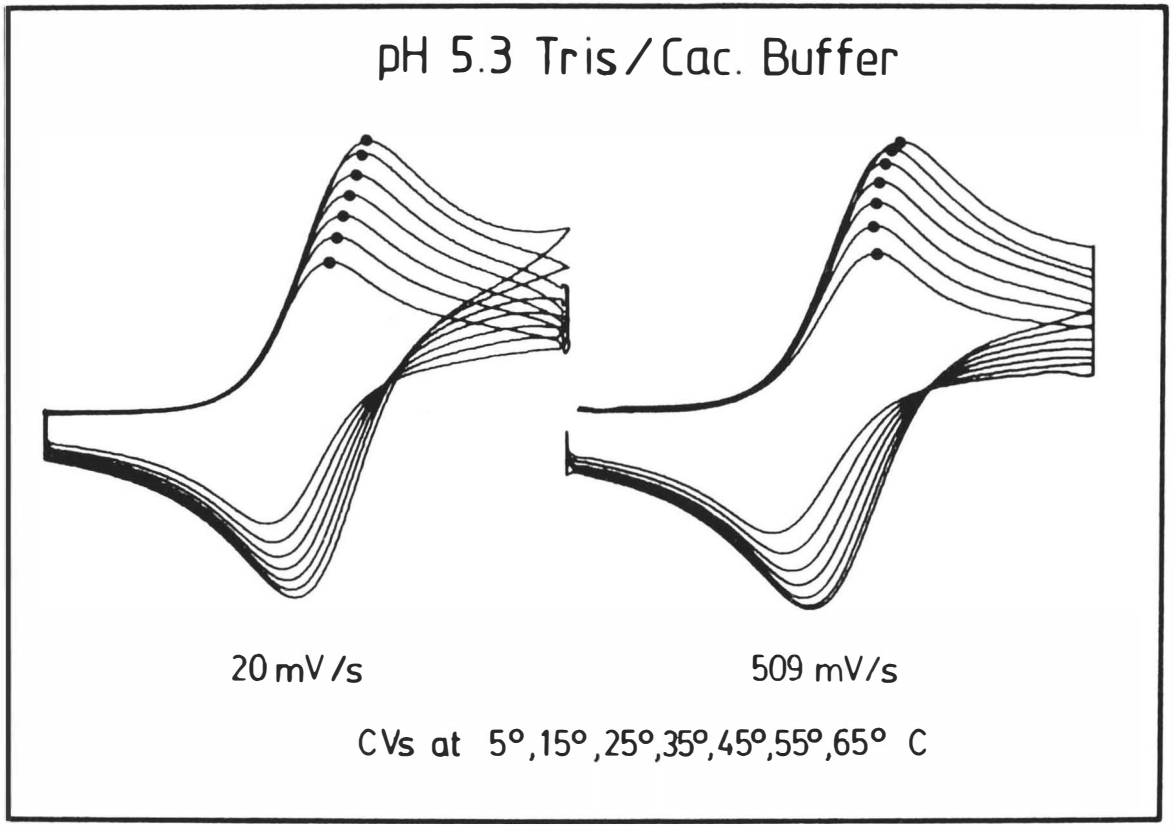
pH 5.3 Tris / Cac. Buffer
20 mV/s
509 mV/s
CVs at 5°, 15°, 25°, 35°, 45°, 55°, 65° C

cytochrome c was determined by potential step chronocoulometry (Figure 15), assuming a value of 1.16 X 10^{-6} cm^2/s at 25 °C(104). This diffusion coefficient was used in conjunction with the slopes of the Q vs. $t^{1/2}$ plots to obtain corresponding diffusion coefficients at the respective temperatures (Figure 16). Diffusion coefficients are directly proportional to temperature divided by the viscosity of the medium (188). Various equations differ by the parameters used to predict the proportionality constant. Theoretical D values reported in this work are based on a proportionality constant calculated by using the literature D value of cytochrome c and the viscosity of pure water at 25 °C. Deviations of experimental values from theoretical values are less than 10% over the temperature range studied and may be explained by the fact that experimental results were obtained in 0.2 M ionic strength buffer whereas, theoretical values are based on the viscosity of pure water.

While the reduction potential for cytochrome c varied linearly with temperature from 5 to 55 °C in pH 7.0 phosphate buffer, the heterogeneous electron transfer rate constant showed a sharp break in behavior at approximately 41 °C. The corresponding reduction potential for the maximum rate constant is 247 mV vs. NHE. Figure 16 shows the results from one experiment. This behavior was observed in each of the experiments; however, the values of the heterogeneous electron transfer rate constant at any temperature varied up to approximately ± 50 % between experiments.

Figure 15. Temperature dependence of the diffusion coefficient of cytochrome c. Experiment results obtained from the average of six experiments (open circles). Calculated values (dashed line). Temperatures (°C) and values of experimental diffusion coefficients (X 10^6, cm^2/s): 5, 0.72; 15, 0.93; 25, 1.15; 35, 1.40; 45, 1.72; 55, 2.06; 65, 2.5. Solution conditions: Tris/cacodylic acid buffer, pH 7.0, cytochrome c concentrations form 51 to 78 μM.

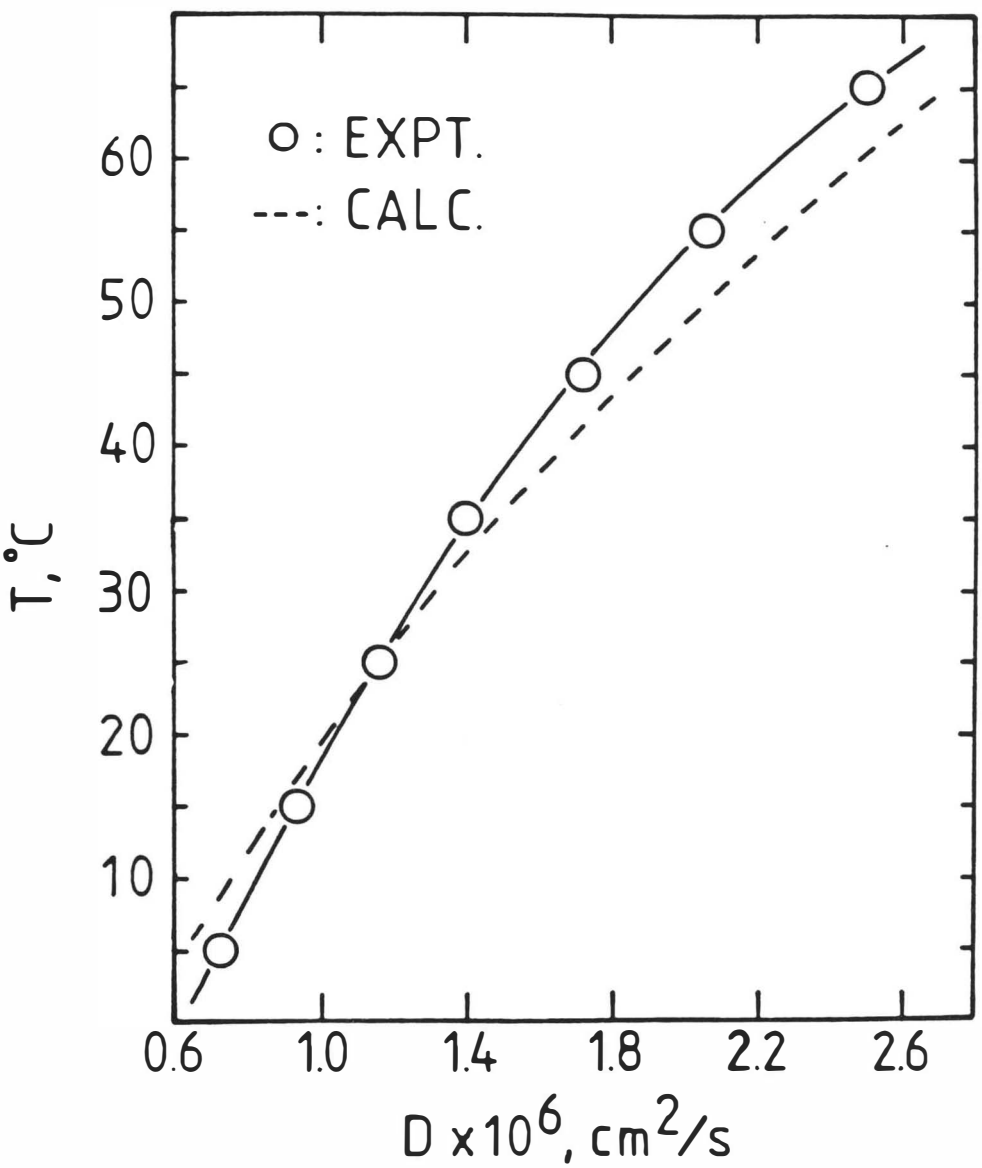
o : EXPT.
---: CALC.
T, °C
60
50
40
30
20
10
0.6
1.0
1.4
1.8
2.2
2.6
D x10^6, cm^2/s

The electrochemical response for cytochrome c in Tris/cacodylic acid buffer, at the same pH and ionic strength, was evaluated. Figure 16 shows the effect of temperature on the heterogeneous rate constant for cytochrome c in Tris/cacodylic acid buffer from 5 to 65 °C. Two differences in behavior were noted: the rate constant is larger in Tris/cacodylic acid than in phosphate buffer, and the break in kinetic behavior with temperature occurs at approximately 55 °C in Tris/cacodylic acid buffer, as opposed to 41 °C in phosphate buffer. The reduction potential for cytochrome c in Tris/cacodylic acid buffer at 55 °C is 246 mV vs. NHE. The reproducibility of the effect of temperature on the heterogeneous electron transfer rate constant is demonstrated in Figure 17, which shows the kinetic results from three individual experiments in Tris/cacodylic acid buffer and their average. The break in kinetic behavior is further illustrated in Figure 18 by observing the dependence of the cathodic peak potential on temperature. This behavior is scan rate dependent. The kinetic effect on the peak current is more pronounced at faster scan rates.

The heterogeneous electron transfer rate constant for the ferri-/ferrocyanide model system used in this study was determined from 5 to 75 °C, and it was found to vary linearly with temperature (Figure 11). This indicates that the biphasic kinetic behavior of cytochrome c is due to a property of cytochrome c rather than a characteristic of the electrochemical cell.

Figure 16. Temperature dependence of the k°' of cytochrome c in pH 7.0 phosphate (squares)and Tris/cacodylic acid buffers (circles) and in pH 5.3 Tris/cacodylic acid buffer (triangles). Results shown for each case were obtained on one cytochrome c solution.

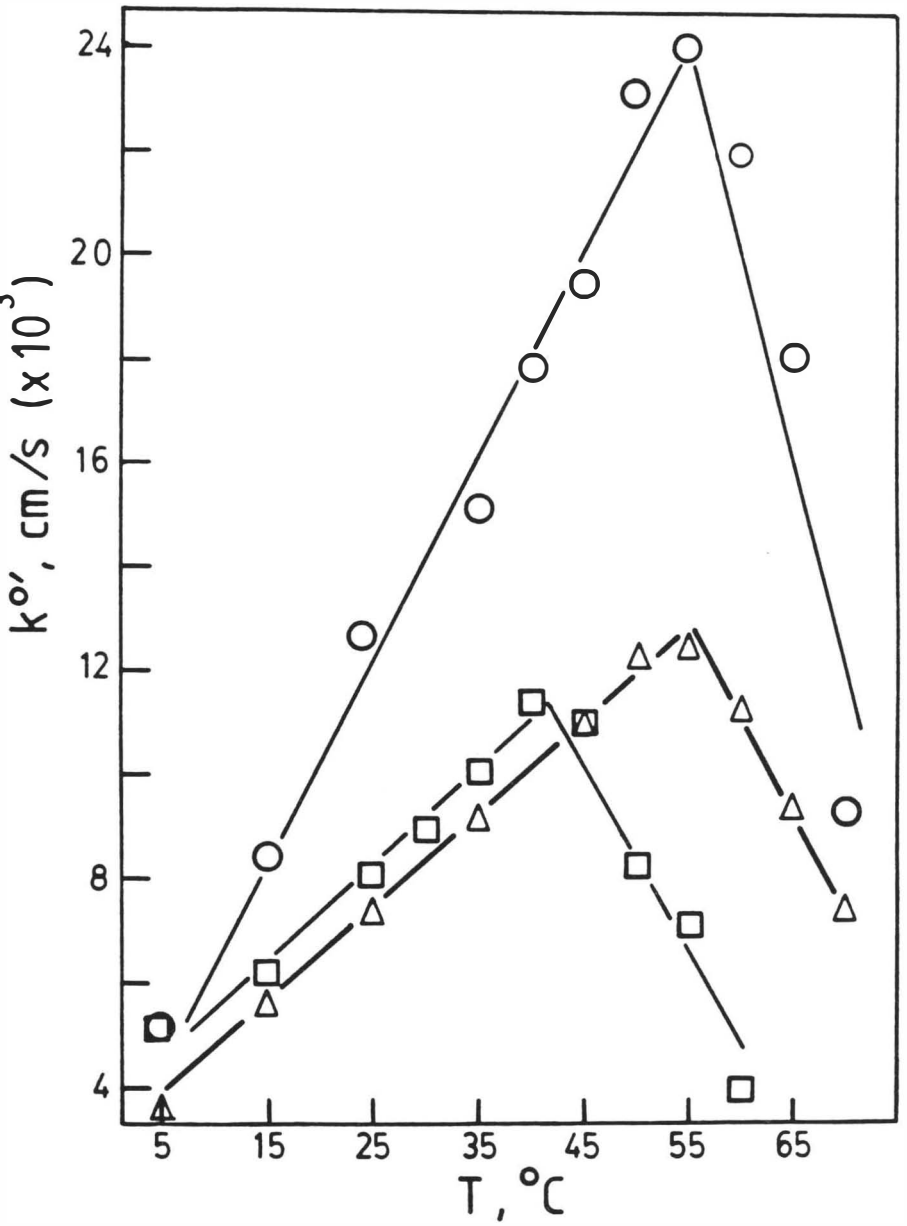
24
20
16
12
8
4
k°', cm/s (x10³)
5
15
25
35
45
55
65
T, °C

Figure 17. Temperature dependence of k°'(X 10^3, cm/s) of cytochrome c in pH 7.0 Tris/cacodylic acid buffer from three experiments. Squares, diamonds, and plus signs each represent data from one cytochrome c solution at different In_2O_3 electrodes.

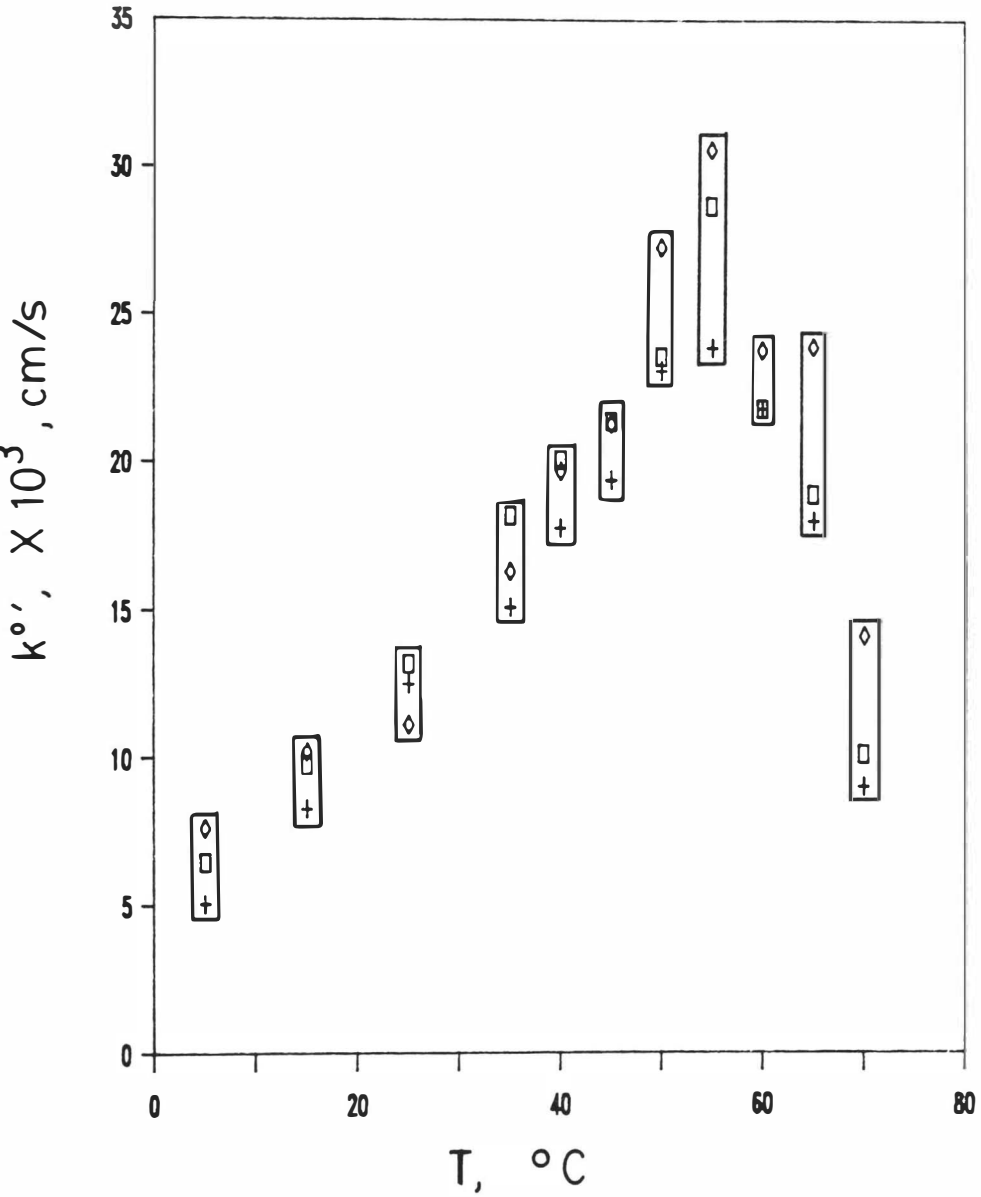
k°', X 10^3, cm/s
T, °C
0
5
10
15
20
25
30
35
0
20
40
60
80

Figure 18. Temperature dependence of the $i_{p,c}$ of quasi-reversible cyclic voltammograms (all 509 mV/s scan rate) of cytochrome c in pH 5.3 (squares), 7.0 (plus signs), and 8.0 Tris/cacodylic acid buffers (diamonds). The peak currents are all normalized to the peak current obtained at 5 °C.

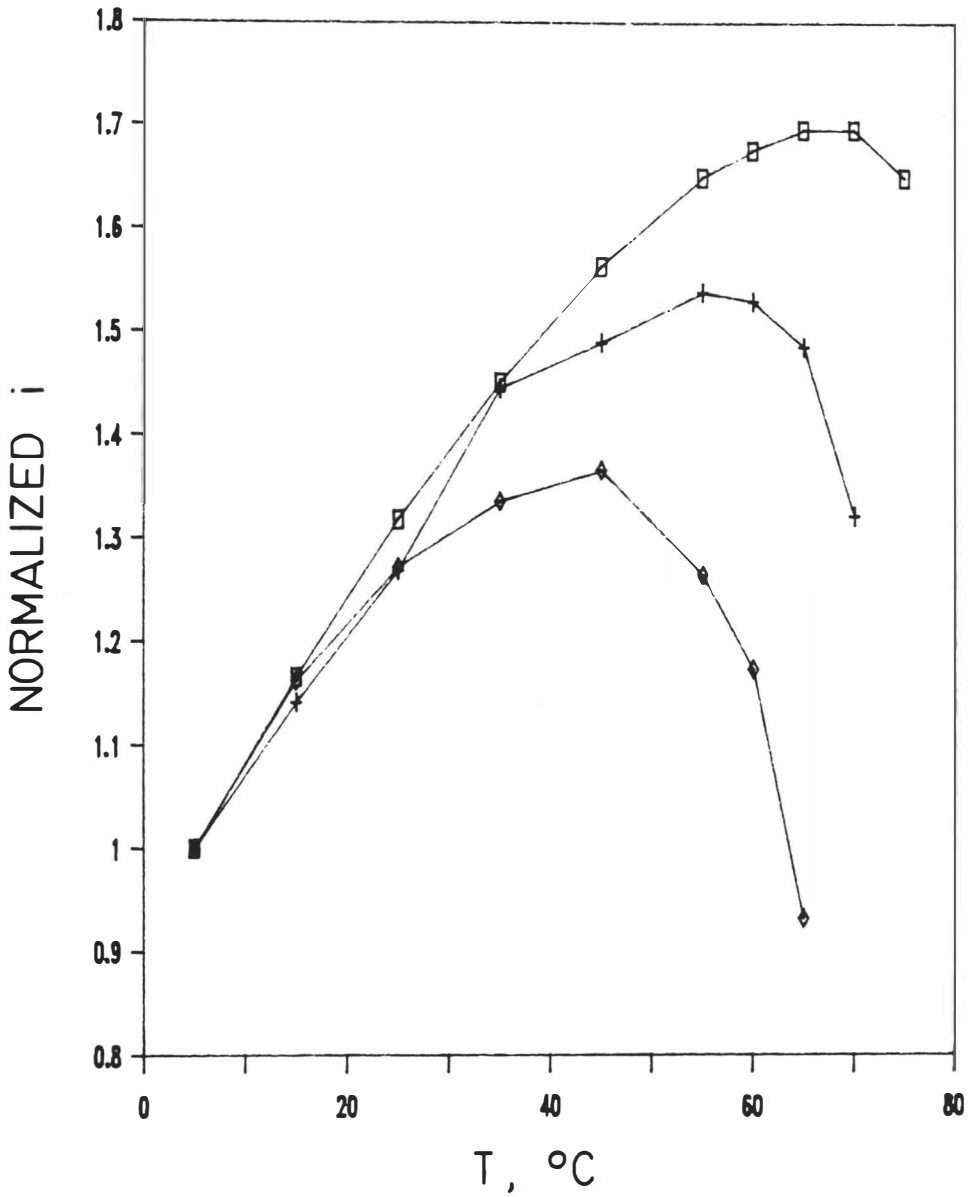
NORMALIZED i
1.8
1.7
1.6
1.5
1.4
1.3
1.2
1.1
1
0.9
0.8
0
20
40
60
80
T, °C

The maximum $k^{\circ'}$ for the reaction of cytochrome c occurs at the same formal potential in the two buffer systems. This suggests that there is the same relative difference in conformation between ferri- and ferrocytochrome c at the peak $k^{\circ'}$ in both the buffers, even though the temperature at this point is 14 °C lower in phosphate buffer than in Tris/cacodylic acid buffer. In both buffer systems, an increase in temperature allows greater solvent exposure to the positively charged heme group in ferricytochrome c, thus electrostatically stabilizing the oxidized form. In phosphate buffer, anion binding to the lysine residues about the solvent-exposed heme edge causes additional solvent exposure through conformational effects (123, 173). Thus, the conformation at which a maximum $k^{\circ'}$ is observed occurs at a lower temperature in phosphate buffer than in the noninteractive Tris/cacodylic acid buffer. A reasonable assumption is that the controlling factor which accounts for the break in kinetic behavior with change in temperature is the conformation of ferricytochrome c with respect to the conformation of the electron transfer transition state. Accordingly, the ease of electron transfer may increase with temperature, due to the above reasons, to the point where the fluctuation of the nuclear coordinates to the transition state becomes difficult. This may occur at a point where high spin character begins to develop. Moore and Williams (76) have reported that ferricytochrome c is 12% high spin at 67 °C in pH 5.25 buffer. Also, the position of the aromatic

ring on the phe-82 residue relative to the heme may pass through an optimum for effective orbital overlap, resulting in an increase in the probability of electron transfer This argument would require that the electron transfer process be nonadiabatic. Moore and Williams also reported (76) that the temperature-dependent NMR shifts of cytochrome c residues which are caused by changes in conformation were biphasic, with the break occurring at ca. 65 °C. Their work was conducted at pH 5.25. Previous work (88) has indicated that the Fe-S bond is less perturbed by temperature at pH 5.25 than at pH 7. Thus, the biphasic behavior of the NMR shifts with change in temperature may be related to the biphasic kinetic behavior reported in this dissertation. Electrolyte and pH affect the change of the Fe-S bond length with temperature. Optimum electron transfer kinetics are then observed for a specific Fe-S bond length and position of adjacent residues, which are reflected by a corresponding formal potential. The solvent environment of the ferricytochrome c affects the temperature at which this optimum conformation occurs.

It is interesting to note that the variation in intramolecular electron transfer rate constant with temperature has been reported for ruthenium complex modified cytochrome c. Isied et al. noticed an increase in rate constant with temperature from 3 to 44 °C (184). This was observed in pH 7.0 phosphate buffer, for which a maximum rate of heterogeneous electron transfer at 41 °C is reported here. However,

no results were reported for temperatures above 44 °C in the work that is cited above (184). Gray and co-workers (185) studied the same Ru modified cytochrome c system, and reported no significant change in kinetic behavior over the temperature region of 0 to 80 °C. However, a graph showing intramolecular electron transfer rate constants for this complex versus temperature in pH 7.0 phosphate buffer shows evidence of a peak at approximately 40 °C.

Another potential contribution to the temperature-dependent break in kinetics is the variation of the surface excess (the moles of adsorbed reactant per unit electrode area) of ferricytochrome c that was observed in this work. Experimentally determined values of E°', D, k°', cytochrome c concentration, and electrode area were used to digitally simulate cyclic voltammograms (Appendix A). The simulation algorithm is based on Butler-Volmer theory. A discrepancy was noted between theoretical and experimental currents, which varied with scan rate and temperature (Figure 19). The difference was largest at fast scan rates and between 35 and 40 °C in both buffer systems. The cathodic peak current showed the largest difference. This type of behavior indicates that ferricytochrome c is weakly adsorbed at the electrode surface (186). The strength of adsorption is described as being weak since the peak potentials are not significantly shifted relative to that expected in the absence of adsorption. The simulated cyclic voltammograms were based on heterogeneous electron transfer rate constants determined

by peak separation of the cyclic voltammograms. When faster scan rates are used, the contribution of adsorbed species to the total current becomes more important since the charge consumed by adsorbed reactant remains constant while the charge consumed by solution-resident reactant decreases. Differences between calculated and experimental peak currents were used to determine the surface excess of adsorbed ferricytochrome c on the electrode (187). At faster cyclic voltammetric scan rates, the total number of cytochrome c molecules reduced is smaller than at slower scan rates, although the measured peak current is larger. The current consumed by a fixed number of adsorbed cytochrome c molecules therefore becomes a larger fraction of the total current observed at faster scan rates. This trend is indeed observed, as shown in Figure 19. It should be recognized that at slow scan rates, where formal potential values were determined, the effect of adsorption on the recorded cyclic voltammograms is not discernable.

A maximum surface excess was observed around 40 °C for both buffer systems, as determined by the difference in peak current method. Table 2 lists surface excess values for various scan rates, temperatures, and buffers. An important point must be addressed here. At temperatures below 40 °C, the above method used to determine surface excess values was not as accurate as for the higher temperatures. The error in the amount determined increased with decrease in temperatures. The strength of reactant adsorption was strongest at

Figure 19. Real and simulated cyclic voltammograms of cytochrome c that demonstrate the presence of reactant adsorption. Experimental conditions: Tris/cacodylic acid buffer, pH 7.0, 0.20 M ionic strength, 96 μM cytochorme c, electrode area = 1.25 cm^2, T = 40 °C, Scan rates given on figure. Formal potential = 255 mV vs NHE, k°' = 2.01 X 10^{-2} cm/s, D = 1.56 X 10^{-6} cm^2/s. Experimental results (solid lines) and simulated results (dashed lines).

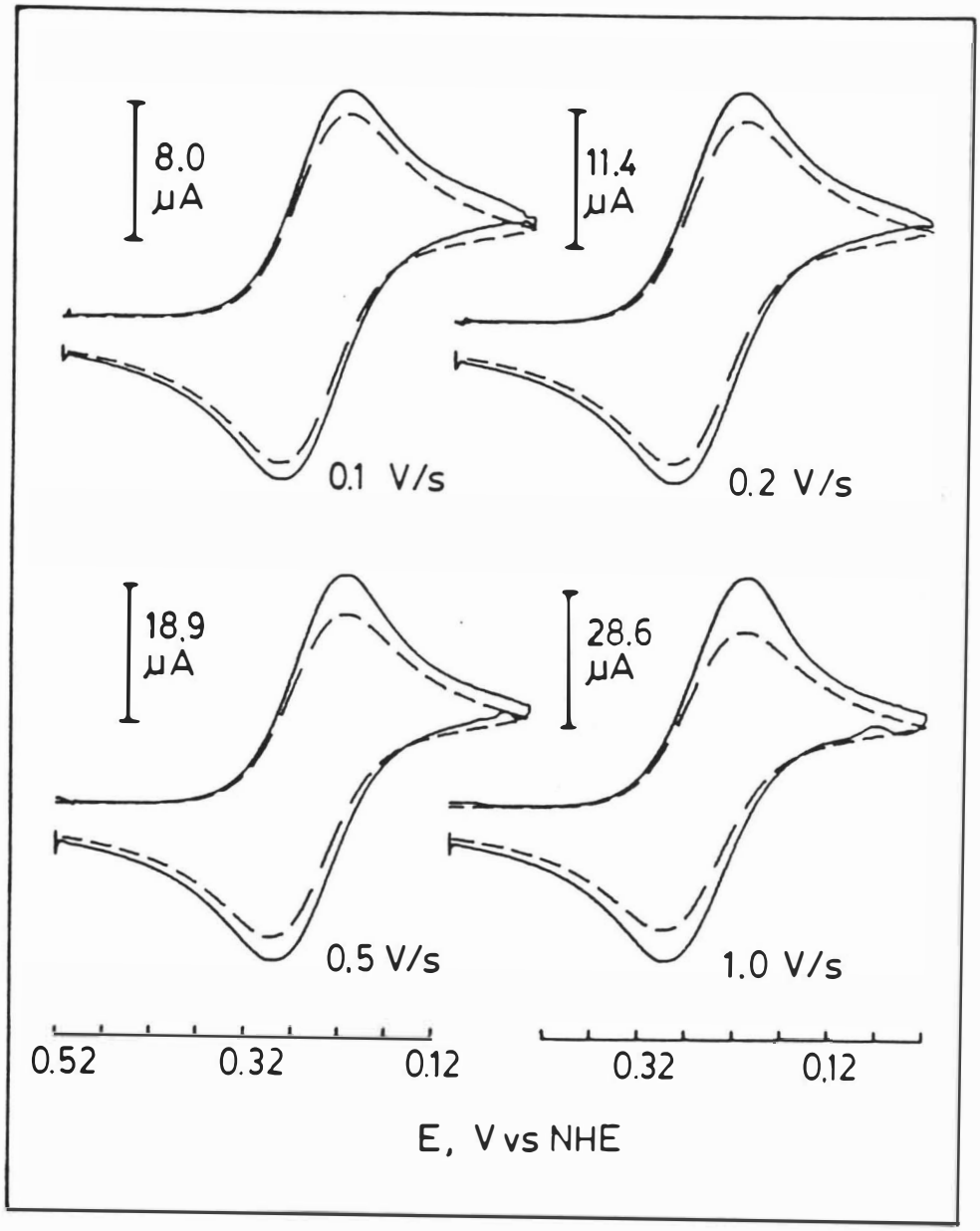
8.0
μA
0.1 V/s
11.4
μA
0.2 V/s
18.9
μA
0.5 V/s
28.6
μA
1.0 V/s
0.52
0.32
0.12
0.32
0.12
E, V vs NHE

TABLE 2

Surface Excess of Cytochrome c vs. Temperature

temp, °C	$\Gamma \times 10^{12}$, mole/cm^2 Tris/cacodylic acid	phosphate
5	5.8[a]	4.4[b]
15	7.3	6.3
25	8.4	6.8
30		7.6
35	9.5	7.6
40	9.9	8.1
45	9.8	8.0
50	9.3	7.9
55	7.8	7.7
60	5.9	6.2
65	1.7	

a. Surface excesses calculated from the difference in the calculated and experimental cathodic peak currents at a scan rate of 0.5 V/s. b. As in (a) but at a scan rate of 0.2 V/s.

the lowest temperature studied and steadily decreased with increase in temperature. A decrease in strength of adsorp--tion is expected as the temperature is raised since increased thermal motion weakens the adsorption interaction. At temperatures above 35 °C, the strength of reactant adsorption was sufficiently weak to have no effect on peak potentials. Therefore, the difference between the experimental cathodic peak current and a simulated (adsorption effects not considered) cathodic peak current yielded reliable estimates of the surface excess. At temperatures of 35 °C and below, the strength of reactant adsorption was sufficient to cause a small shift in the cathodic peak potential. The degree of peak potential shift caused by adsorption was greatest at 5 °C. Thus, the potential of maximum current for the adsorbed material and diffusing material is different, and the method based on peak current difference underestimated the surface excess at lower temperatures. The electron transfer rate constant is slower at the lower temperatures. The equation used to calculate the surface excess is applicable only to a reversible system. If the adsorbed material has a slower electron transfer rate constant at the lower temperatures, then this peak separation method would cause the amount of surface excess calculated to be less than the actual amount. In the lower temperature region, the peak separation exhibited by the cyclic voltammogram results from a complicated mixture of both kinetic and adsorption effects. The Nicholson method of

determining heterogeneous electron transfer rate constants does not consider adsorption. Therefore, the rate constants determined at temperatures below 40 °C are probably larger than those calculated by the peak separation method since reactant adsorption caused a larger peak separation. The difference in peak separation caused by reactant adsorption at pH 7.0 is slight and was not realized until the effect of stronger adsorption at pH 8.0 (vide infra) on fast scan rate cyclic voltammograms was noticed. At the lower temperatures, the electron transfer rate constant calculated by peak separation is scan rate dependent. Faster scan rates yielded smaller rate constants. Evaluation of the system with ferri-ferrocyanide indicated that this was not due to uncompensated current resistance in the electrochemical cell. The scan rate dependence of the rate constant decreased with increase in temperature. This behavior is again due to adsorption effects. The ratio of current from adsorbed material to that from diffusing species increases with scan rate. The scan rate dependent enhancement of peak separation from reactant adsorption at lower temperatures caused the scan rate dependence of the apparent electron transfer rate constant. These effects are subtle in pH 7.0 buffers and do not significantly affect the peak separation temperature dependence of the cyclic voltammograms. A small, negative shift in the cathodic peak potential caused by reactant adsorption is accompanied by a smaller negative shift in the anodic peak. This partially compensates for

the effect of adsorption on the peak separation of a quasi-reversible cyclic voltammogram.

The possible effect of reactant adsorption on the temperature dependence of the kinetics of cytochrome c was evaluated at 5 °C, where the peak asymmetry about the formal potential was the largest. A typical series of results from an analysis of cytochrome c in pH 7.0 Tris/cacodylic acid buffer is as follows. The 20 mV/s scan rate cyclic voltammogram was reversible with a 62 mV peak separation that was symmetrical about the formal potential. The peak separation increased to 70 mV, 82 mV, and 102 mV at scan rates of 200, 500, and 1000 mV/s, respectively. The asymmetry about the formal potential increased with scan rate. The cathodic peak was displaced from the formal potential by 57 mV, and the anodic peak by 45 mV, at the 1000 mV/s scan rate. The 102 mV peak separation corresponds to a heterogeneous electron transfer rate constant of 5.3×10^{-3} cm/s. Twice the difference between the anodic peak potential and the formal potential is 90 mV. This yields a rate constant of 7.7×10^{-3} cm/s, a difference of approximately 45 %. This represents an extreme in that the anodic peak potential separation from the formal potential is slightly reduced by reactant adsorption. The rate constant at 500 mV/s is 7.6×10^{-3} cm/s. The slower scan rate cyclic voltammogram is less affected by reactant adsorption. Again, at temperatures above 35 °C, simulated and experimental peak potentials agreed, indicating that reactant adsorption was not shifting

the peak potentials. The maximum kinetic behavior was observed at 55 °C, with a rate constant of 2.83 X 10^{-3} cm/s calculated at the 1 V/s scan rate and a 2.90 X 10^{-3} cm/s rate constant at the 500 mV/s scan rate. The quasi-reversible cyclic voltammograms are symmetrical about the formal potential and k°' is independent of scan rate. The main point is that the maximum electron transfer rate constant is approximately 3.5 times larger than the adsorption-adjusted rate constant at 5 °C. Consequently, the electron transfer rate constants in the pH 7.0 buffers determined by the peak separation method are valid and only partially affected by reactant adsorption.

A surface coverage of 8.3 X 10^{-12} mole/cm^2 corresponds to a monolayer of adsorbed cytochrome c when a value of 2000 $Å^2$/adsorbed cytochrome c molecule is used (8) (Table 2 provides surface coverage values at temperatures ≥ 40 °C). The 2000 $Å^2$ surface area coverage was found for ferricytochrome c at a mercury electrode in a pH 7.0 buffer solution. This value is approximately three times larger than that calculated for a close packed arrangement of cytochrome c based on X-ray crystal structure size. It is twice the surface area, if each cytochrome c molecule is assumed to occupy a rectangle which just fits the crystal structure diameter. The large surface area occupied by ferricytochrome c on mercury was attributed to a denatured, flattened conformation for mercury adsorbed cytochrome c. The irreversible electrochemical behavior of cytochrome c at mercury elec-

trodes has been attributed to strong, irreversible adsorption to mercury. The facile electron transfer kinetics of cytochrome c at indium oxide electrodes indicates that it is not denatured or flattened by adsorption to the electrode surface. Therefore, the moles per square centimeter for a monolayer of surface excess at indium oxide electrodes is probably larger than that determined for mercury. This premise is reinforced by the morphology of the cyclic voltammograms of cytochrome c at indium oxide electrodes where adsorption effects are observed. That is, the peak potentials are not strongly shifted from those expected in the absence of adsorbed electroactive reactant. Figure 20 shows a series of simulated cyclic voltammograms that demonstrate the effect of strength of adsorption of reactant at fast scan rates. A Langmuir isotherm is assumed, but the same general behavior would occur for other adsorption isotherms. Weak adsorption is indicated by peak current enhancement without peak potential shift. Strong adsorption causes two peaks to occur: one for diffusing species and the other for adsorbed species. The peak separation is due to the enhanced stability of a strongly adsorbed species. Intermediate adsorption strength results in cyclic voltammogram morphology which is between these two extremes.

The digital simulation of cyclic voltammograms that included adsorption effects proved to be a valuable tool for the analysis of these data. The important adsorption parameters are the limiting surface coverage, the strength of

Figure 20. Simulated cyclic voltammograms that demonstrate the effect of variation of reactant and product adsorption strength. All scans are based on reversible behavior. Scan rate = 1 V/s, electrode area = 1 cm^2, D = 1 X 10^{-6} cm^2/s, C = 100 μM, T = 25 °C, limiting surface coverage = 2 X 10^{-11} $mole/cm^2$. (a): Reactant adsorption, the products of the reactant adsorption equilibrium constant, K, and the bulk concentration, C, are: 1., 0; 2., 2; 3., 100; 4., 1000. (b): Product adsorption, same as a., except K represents product adsorption equilibrium constant.

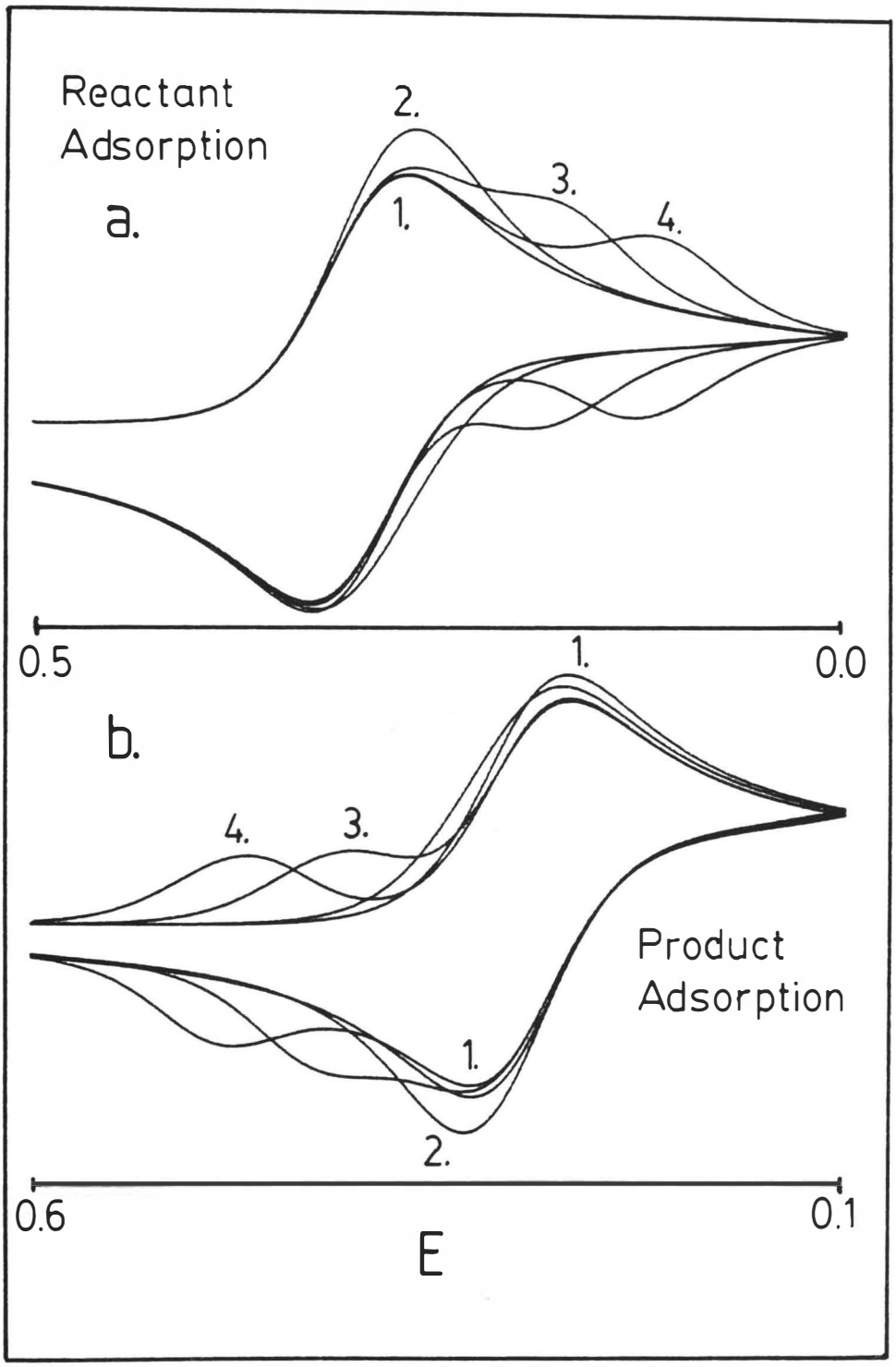
Reactant
Adsorption
a.
2.
1.
3.
4.
0.5
0.0
1.
b.
4.
3.
Product
Adsorption
1.
2.
0.6
0.1
E

adsorption as expressed by an equilibrium constant, and the bulk concentration of the adsorbate. The adjustment of these parameters affects peak currents and potentials. Weak adsorption has been classified as occurring when the product of the adsorption equilibrium constant and the bulk concentration of the adsorbate is less than 2 (186). Strong adsorption behavior occurs when this product is larger than 100 (186). Weak adsorption is characterized by a small negative shift in the cathodic and anodic peak potentials, as well as an enhancement of current. The current enhancement can be easily simulated for small adsorption equilibrium constants by increasing the limiting coverage. The peak potential shift can be increased by increasing the adsorption equilibrium constant and/or decreasing the limiting coverage. Matching experimental current and peak potential adsorption effects indicates that both the adsorption equilibrium constant and the limiting coverage have been at least qualitatively determined. Limiting the maximum surface coverage to that reported for ferricytochrome c on mercury resulted in an excessive peak potential shift when the strength of adsorption was increased to a level required to force the peak current to that experimentally observed. Good agreement with experimental results, at the three pH conditions investigated, was obtained with a limiting surface coverage of 2×10^{-11} mole/cm^2. This corresponds to a surface coverage of ca. 830 Å^2 per cytochrome c and a diameter of ca. 29 Å. This value is approximately the crystal

structure size of cytochrome c. The Stokes-Einstein diffusion equation (188) was used to estimate the effective diameter of solvated cytochrome c:

$$D = RT/6\pi r\eta N$$

r: radius of solute molecule

η: viscosity of solvent

N: Avogadro's number

A diffusion coefficient of 1.16×10^{-6} cm^2/sec and the viscosity of pure water at 25 °C gave an effective diameter of 42 Å. This value is slightly less than the 45 Å diameter for ferricytochrome c adsorbed on mercury. The calculated solvated diameter of cytochrome c is qualitative, but it is clearly larger than the crystal structure diameter of approximately 30 Å and indicates that it is surrounded by more than one structured water layer. This highly solvated structure and correspondingly large diameter suggests that ferricytochrome c may not be as flattened and denatured on mercury as proposed (8-11). Strong adsorption is required to force a full monolayer, i.e., a limiting surface coverage of the electrode. To achieve a close packed arrangement based on the dimensions of the crystal structure, a strength of adsorption sufficient to cause the removal of the solvation sheath of cytochrome c would be required. This does not occur. Simulation of 5 and 40 °C, 1 V/s scan rate cyclic voltammograms of cytochrome c in pH 7.0 Tris/cacodylic acid buffer provided a reactant adsorption equilibrium constant of 1 to 1.3×10^7 L/mole. There was no indication

of adsorption by 65 °C. Strongest reactant adsorption occurred at 5 °C. This was indicated by a ca. 7 mV negative shift of the midpoint potential from that of a reversible cyclic voltammogram. The product of the reactant equilibrium constant and the bulk reactant concentration is 1 to 1.3, which is in the range of weak adsorption. The simulation limiting surface coverage, reactant equilibrium constant, and bulk reactant concentration correspond to a surface coverage of ca. 1 to 1.5 X 10^{-11} mole/cm^2. These values indicated that ferricytochrome c is adsorbed to ca. one monolayer of coverage based on solvated dimensions. A free energy of adsorption at 25 °C of ca. 40 to 43 kJ/mole (9.5 to 10.2 kcal/mole) was calculated. The simulations written for this work determine the effects of either reactant or product adsorption, but do not consider mixed reactant-product adsorption. Discrepancies between simulated and experimental cyclic voltammograms revealed that the experimental anodic peak potentials were slightly larger (less than 10 %) than simulations based only on reactant adsorption. This indicates that product adsorption is also affecting the experimental results. Product adsorption decreases the current of the cathodic peak, and causes a positive shift in peak potential while enhancing the anodic peak potential. The overall effect of reactant adsorption clearly dominates, however.

Eddowes and Hill (30, 35) determined a surface excess of cytochrome c of 1.2 X 10^{-10} mole/cm^2. This clearly

represents more than a monolayer, although it is stated as representing monolayer coverage. For a monolayer of cytochrome c represented by 1.2 X 10^{-10} mole/cm^2, a surface area of ca. 140 $Å^2$ per molecule and a diameter of ca. 12 Å is required. This diameter is less than half of the crystal structure diameter. The use of this empirical limiting surface excess in the digital simulator results in very large current enhancement occurring prior to peak potential variation. Eddowes and Hill (30, 35) report a free energy of adsorption of 30 kJ/mole for cytochrome c at 4,4'-bipyridyl modified gold electrode at room temperature. The strength of adsorption corresponding to this free energy of adsorption is very weak (K•C of ca. 0.01), and would not perturb the cyclic voltammograms at the scan rates used in this work. It is difficult to reconcile this low strength of adsorption with their reported surface coverage that is ca. 10 times larger than that determined in this work. However, the conditions of their work are quite different from the work reported here. A gold electrode was used with a solution that contained a high concentration of surfactant. The formation of several monolayers of cytochrome c at an electrode surface may occur due to its large dipole moment. It has a cluster of positively charged residues at the active site and a cluster of negatively charged groups at the opposite side of the protein. The large positive charge on cytochrome c may be less electrostatically important than the dipole moment due to the high ionic strength

of the electrolyte solution and the size of the molecule. The adsorption of several monolayers of cytochrome c at a solid electrode may explain the concentration dependence of the heterogeneous electron transfer rate constant. At low concentrations (less than 100 μM), only a monolayer is formed. At higher concentrations, several layers form. A much slower diffusion coefficient would exist for the protein at these higher concentrations. A 1 mM solution of cytochrome c was examined at room temperature. A 160 mV peak separation was observed at 10 mV/s (Table 1). The concentration dependence may also be due to the amount of impurities contained in the cytochrome c solution. An important point is that the 1 mM solution did not show a decrease in electron transfer rate constant above 40 °C, an event which always occurred for pH 7.0 phosphate buffer solutions of lower cytochrome c concentration. Also, the electron transfer rate constant at any temperature is much lower in the 1 mM solution. The difference may be due to a higher contamination of the electrode surface from impurities in the higher concentration solution. As the temperature is increased, the impurities desorb from the electrode, allowing greater rates of electron transfer. If multiple adsorbed layers of cytochrome c are formed in the higher concentration solution, the enhanced rate with increase in temperature may be due to thermally induced loosening of the adsorbed layers resulting in greater rates of diffusion through the adsorbed material. It is clear that different processes are control-

ling the kinetics in the 1 mM solution as compared to the 60 to 100 μM solutions that were used for most of this work. Although the break in kinetics does not occur in the 5 to 55 °C temperature range for the 1 mM solution, the rate constant at 55 °C is much slower in the more concentrated solution than at the same temperature in the less concentrated solutions. Ten mV/sec scan rate cyclic voltammograms of the low concentration solutions are reversible from 5 to 55 °C. Also, the bulk solvent properties of the 1 mM solution are probably much different than the 100 μM solutions. The Stokes-Einstein equation predicts a specific volume of 1.92 g/cm^3 of cytochrome c. This corresponds to a saturated cytochrome c solution having a concentration of 0.022 M. The solution also contains 0.1 M NaCl and 0.09 M phosphate buffer. Thus, the viscosity of the solvent may be affected, and the diffusion coefficient of cytochrome c may be quite a bit slower than in the concentrated solution. This was checked by simulating the cyclic voltammogram of 1 mM cytochrome c at 25 °C. A heterogeneous electron transfer rate constant of 2.1×10^{-4} cm/s provided the correct peak separation. The literature diffusion coefficient of 1.16×10^{-6} cm^2/s provided a simulated cyclic voltammogram that precisely matched the experimental results, strongly indicating that the viscosity of the 1mM protein solution is the same as in the protein solutions of lower concentration. However, both the electron transfer rate constant and diffusion coefficient are unknown for this simmulation and the above

conclusion may therefore be incorrect. The slow scan rate cyclic voltammograms of the 1 mM solution are not affected by adsorption. There is a possibility that the temperature at which the break in kinetics appears to occur, as determined by cyclic voltammetry, is affected by adsorption. Again, the influence of adsorbed material on the morphology of a cyclic voltammogram is more pronounced at faster scan rates and at lower electroactive species concentrations.

Bowden, et al. detected cytochrome c irreversibly adsorbed to an electrode by conducting film transfer experiments (45). The cytochrome c solution was removed from the electrochemical cell, which was then lightly rinsed and filled with electrolyte. The presence of adsorbed material was clearly indicated by cyclic voltammograms with no peak separation. The reduction potential was shifted 15 mV negative of that for diffusing cytochrome c. A surface excess of 0.1 monolayer was calculated. These experiments were repeated, and the same behavior was observed with purified, lyophilized cytochrome c. Peak separations of 15 to 40 mV were observed at a 100 mV/sec scan rate. The peak currents did not change with variation of temperature from 25 to 55 °C. The temperature studies reported here required long-term stability of the electrochemical response of cytochrome c. It was found that freshly purified sample which had not been lyophilized was required (see Experimental section) to achieve long-term stability, i.e., on the order of 8 to 12 hours. The background cyclic voltammograms of electrolyte

alone were obtained after the cytochrome c experimental work. Moderate rinsing of the cell (approximately 10 rinses) left no indication of adsorbed cytochrome c. The irreversibly adsorbed cytochrome c observed following voltammetry of lyophilized cytochrome c may accordingly be attributed to denatured forms of cytochrome c that arise from the lyophilization process, e.g., oligomers of cytochrome c. The removal of any adsorbed ferricytochrome c by moderate rinsing reinforces the argument that its adsorption is weak in the two pH 7.0 buffers.

Eddowes and Hill (35) have suggested that reversible adsorption is necessary for facile electron transfer between cytochrome c and electrodes. Other groups have indicated that irreversible adsorption of cytochrome c at many electrode surfaces results in irreversible electrochemical behavior (43). Eddowes and Hill describe the adsorption process of their system as hydrogen bonding between the lysine residue adjacent to the solvent-exposed heme edge and the 4,4'-bipyridyl molecules of the chemically modified gold electrode used in their work. For the indium oxide electrode used in this study, the lysine residues may hydrogen bond to the oxide groups of the electrode surface. This view is supported by the pH dependence of the strength of adsorption of cytochrome c to the indium oxide electrodes. The strength of adsorption is strongest at pH 8.0 and weakest at pH 5.3.

Another kinetic parameter of heterogeneous electron

transfer is the electrochemical transfer coefficient, α, that reflects the symmetry of the activation energy about the transition state and varies between 0 and 1. An α of 0.5 reflects a symmetrical approach to the transition state from either product or reactant. A low α indicates that oxidation is favored, and a high α corresponds to a relative ease of reduction as compared to oxidation. Figure 21 shows the effect of α on cyclic voltammograms exhibiting quasi-reversible electrochemistry. Neither α nor $k^{\circ'}$ have any effect on a slow scan rate, reversible cyclic voltammogram. The peak separation of quasi-reversible cyclic voltammograms is relatively insensitive to variations of α from 0.3 to 0.7.

Single potential step chronoabsorptometry (165) experiments were used to determine α and $k^{\circ'}$ for cytochrome c in both pH 7.0 phosphate and Tris/cacodylic acid buffers. Potential steps of various magnitude, i.e., overpotential, were applied to ferricytochrome c from an initial potential where no electrochemistry occurred. A forward heterogeneous rate constant, k_f, was determined for each overpotential. The formal heterogeneous rate constant, $k^{\circ'}$, is calculated from the intercept of a plot of log k_f versus overpotential. The slope of this plot provides α.

Two methods were used to determine k_f: the use of a working curve in conjunction with normalized absorbance values (165), and a method based on the slope and intercept of an absorbance versus the square root of time plot (189).

Figure 21. Simulated quasi-reversible cyclic voltammograms that demonstrate the effect of variation of α. Scan rate = 1 V/s, electrode area = 1 cm^2, D = 1 X 10^{-6} cm^2/s, C = 100 μM, T = 25 °C, $k^{\circ\prime}$ = 0.01 cm/s. (a): α = 0.7 and 0.3, $\blacktriangle E_p$ = 84 mV for both α values. (b): same as (a), except $k^{\circ\prime}$ = 0.005, $\blacktriangle E_p$ = 104 mV for α = 0.7, and $\blacktriangle E_p$ = 110 mV for α = 0.3.

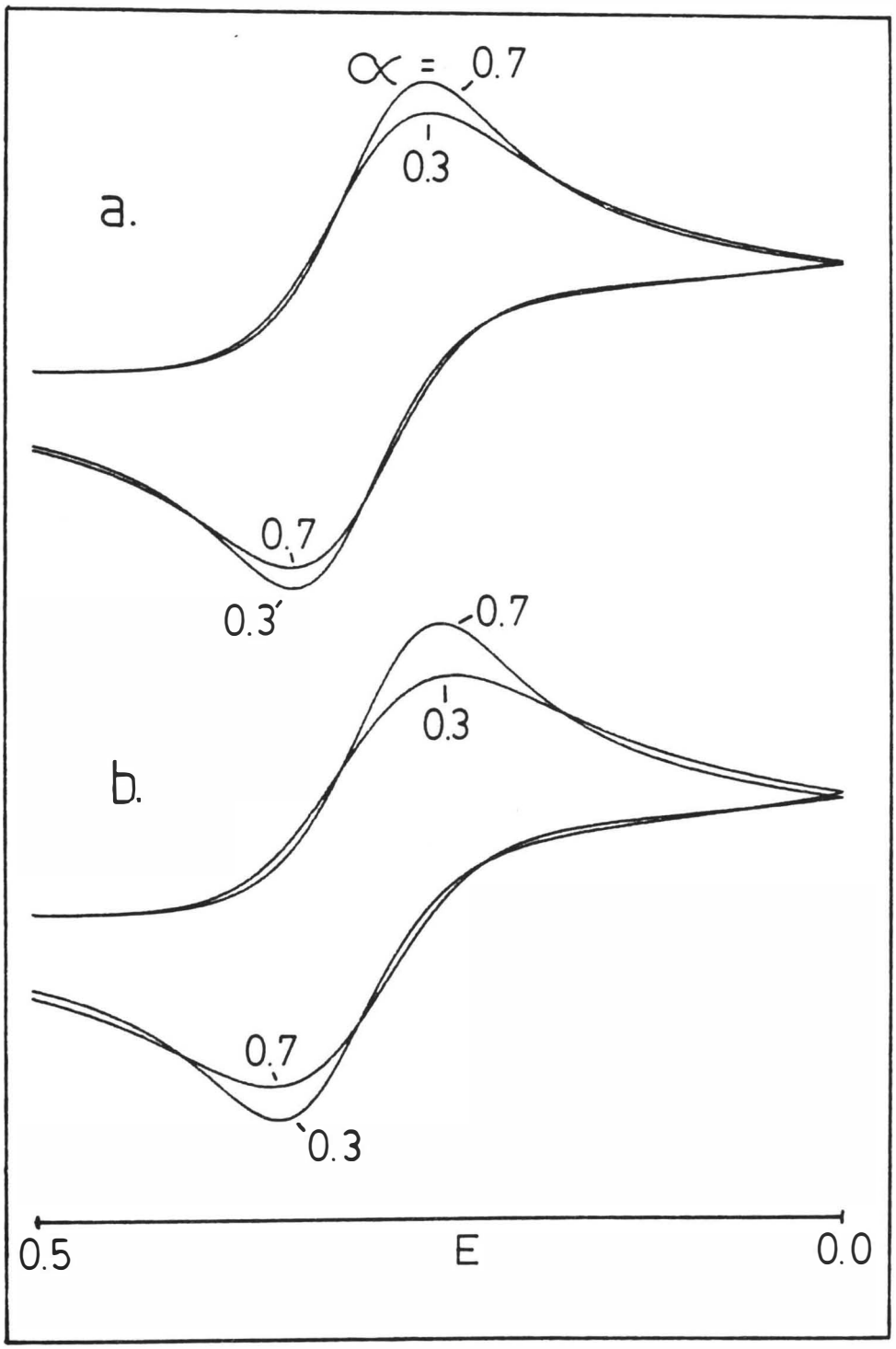
α = 0.7
0.3
a.
0.7
0.3
0.7
0.3
b.
0.7
0.3
0.5
E
0.0

The advantage of the first method is that it is mathematically precise, i.e., it does not include approximations. The second method proved to be more applicable to this system since a diffusion-controlled, i.e., large overpotential step, was not required. Application of large potential steps to the indium oxide electrode in contact with a cytochrome c solution has the unfortunate effect of causing a decrease in electrochemical reversibility. The experiments which began with the diffusion-controlled step yielded much lower k_f values and correspondingly unreliable α values, as compared to those that began with the smaller steps. In order to evaluate the effect of temperature on the kinetic parameters of cytochrome c, a diffusion-controlled step is required at each temperature. A subsequent kinetic evaluation at a different temperature then reflected the consequences of the experimental technique rather than the effect of temperature. One other important note on this technique is that the response from adsorbed material must be removed from the total response. This can easily be overlooked since the logarithm of the response to both adsorbed and diffusing material varies linearly with overpotential. The correction for adsorption increases with larger overpotential steps. This leads to an artificially large slope, resulting in a higher calculated α and, to a lesser degree, larger $k^{\circ'}$ than really exists. The amount of adsorbed material can only be determined from a diffusion-controlled step, so even the second mathematical treatment of the data

that does not require normalization to a diffusion-controlled step does not negate the requirement of obtaining this large overpotential step. Consequently, potential step experiments were not as informative as hoped.

The potential step experiments were all started at 25 °C. Diffusion-controlled steps revealed the presence of an adsorbed layer of ferricytochrome c at the indium oxide electrode surface. A surface excess of ca. 1.0×10^{-11} mole/cm^2 was determined from the positive intercept of the slope of absorbance versus the square root of time plot of a diffusion-controlled step. This is the same amount as determined by cyclic voltammetry. Step experiments were performed at 5 °C intervals. The surface excess diminished with increase in temperature. At 40 °C, no surface excess was indicated. Cyclic voltammetry clearly indicated that there is adsorbed reactant at this temperature. This anomalous behavior is due to the effect of repeated, large potential steps on the kinetics of the system. When the cell was heated to 40 °C prior to any electrochemistry, a surface excess of approximately a monolayer (based on 2000 Å^2) was detected with the first diffusion-controlled step. This surface excess then diminished with each subsequent step to the point where negative A vs. $t^{1/2}$ intercepts were observed, i.e., the steps were no longer diffusion-controlled. The negative effect of large overpotential steps occurred throughout the temperature range of 25 to 55 °C, and became more pronounced at higher temperatures. Final

step potentials of less than ca. 100 mV vs. NHE, i.e., a potential step of ≤ 422 mV from the starting potential of 522 mV vs. NHE, appeared to have no deleterious effect. This was confirmed by repeatedly stepping to these smaller overpotentials without eliciting a change in response. However, a noticeably smaller response was obtained after returning to a smaller overpotential following a large overpotential step. Also, repeated applications of a large overpotential at elevated temperatures yielded a smaller response with each subsequent experiment. This was most noticeable in the pH 8.0 buffers. Despite these problems, reasonable results were obtained at a particular temperature if the small steps were followed by the diffusion-controlled step and the electrode was not used following the application of a large overpotential step. For both of the pH 7.0 buffers, α is 0.61 ± 0.06 for the temperature range of 25 to 55 °C. This value is slightly higher than the value of 0.50 reported at indium oxide electrodes by earlier work with nonpurified type VI cytochrome c (37). A change of α from 0.5 to 0.6 has little effect on the morphology of a cyclic voltammogram.

At the beginning of this section, the determination of diffusion coefficients by potential step chronocoulometry was discussed. The difficulties encountered with potential step chronoabsorptometry raise questions concerning the reliability of chronocoulometry data. Frankly, a fortuitous selection of experimental conditions avoided the problems

associated with large overpotential steps. The experiments were performed in Tris/cacodylic acid buffer, a solvent in which cytochrome c exhibits quasi-reversible behavior to 65 °C at pH 7.0. The diffusion coefficient was evaluated from 5 to 65 °C. This buffer was chosen since its response to potential steps is more ideal than the phosphate buffer. The negative kinetic effect of large overpotential steps is less pronounced in Tris/cacodylic acid buffer than in phosphate buffer, and the heterogeneous kinetics are faster. Therefore, a smaller potential step was required to achieve diffusion control. The beginning of the cathodic wave observed in background (electrolyte alone) cyclic voltammograms occurs at ca. 100 mV vs. NHE. A final step potential of 122 mV vs. NHE was chosen for the chronocoulometry experiments. This provided an overpotential of at least 100 mV at any temperature, and was sufficient to cause diffusion control. It was found in the chronoabsorptometry work that potential steps to values cathodic of 100 mV vs. NHE resulted in the deterioration of the kinetic response for cytochrome c, especially at elevated temperatures. This potential region was avoided. The nature of the experiment also avoided some of the consequences of large potential steps. Only a few steps were obtained at each temperature, and at least 15 minutes elapsed between temperatures. Thus, few steps were taken, and their size was not large enough to cause a collapse of the system but sufficient to achieve diffusion control. Current was recorded in these experi-

ments and then digitally summed to calculate charge. The current profile consists of a large spike in current which decays exponentially with time. The calculation of the diffusion coefficient required only the slope of the charge versus square root of time relationship. The early spike in current was not recorded in order to gain sensitivity and accuracy at later times and therefore, adsorption data could not be calculated from Q versus $t^{1/2}$ plots.

2. In pH 5.3 Buffer

The temperature dependence of the heterogeneous electron transfer rate constant of cytochrome c in Tris/cacodylic acid buffer was determined from 5 to 75 °C. The variation of rate constant with temperature was less pronounced than at pH 7.0 (Figure 16). This is attributed to the added conformational stability to temperature variation of ferricytochrome c at pH 5.3 relative to pH 7.0. The temperature of maximum kinetics was ca. 55 °C, i.e., the same as at pH 7.0 in Tris/cacodylic acid buffer. The accuracy of the point of maximum kinetics is not as reliable as the pH 7.0 results since the temperature dependence of the electron transfer kinetics was not as pronounced as at pH 7.0. The formal potential at 65 °C is 247 mV vs. NHE, ie., the formal potential at which the maximum kinetics occurs in the pH 7.0 buffers. Some factor is limiting the increase in rate constant with temperature at formal potentials below 247 mV, if this potential represents the optimum conformation for facile electron transfer. The failure of the

system to show a sharp kinetic peak at 247 mV may be due to the inability of ferricytochrome c to bind to the electrode surface at temperatures above 55 °C. Adsorption to an electrode may be a necessary preliminary step preceding electron transfer. The combination of acidic pH and higher temperatures may weaken adsorption to the point that effective binding is precluded. The rates of adsorption, electron transfer, and desorption can each be the rate-limiting step. Above 55 °C, the rate of adsorption may be rate-limiting. Regretfully, no results were obtained for pH 5.3 phosphate buffer, so a comparison could not be made between the kinetics of cytochrome c in the two buffer systems. As mentioned earlier, cytochrome c in pH 5.3 phosphate buffer exhibited irreversible electrochemistry.

Fast scan rate cyclic voltammograms indicated the presence of adsorbed reactant. The surface excess is approximately half that observed at pH 7.0. Simulations of 5 °C and 40 °C, 1 V/s scan rate cyclic voltammograms indicated that the reactant adsorption rate constant is between 4 to 6 X 10^6 L/mole. This corresponds to a free energy of adsorption of ca. 40 kJ/mole, or 9.7 kcal/mole, at 25 °C. A surface excess of ca. 6.0 X 10^{-12} mole/cm^2 is given by these parameters and the Langmuir adsorption isotherm. The decrease in strength of adsorption may be attributed to the decrease in cationic binding sites on the metal oxide electrode surface resulting from the decrease in solution pH. Evidence of adsorbed reactant disappeared at temperatures

above 60 °C.

3. In pH 8.0 Buffer

Fast scan rate cyclic voltammograms of cytochrome c in pH 8.0 buffers demonstrated clearly different behavior than that observed in pH 7.0 and pH 5.3 buffers. The cathodic peak current from quasi-reversible cyclic voltammograms had a more pronounced temperature dependence which was not due to less facile kinetics (Figure 18). Also, the fast scan rate asymmetry of the peak potentials about the formal potential is clearly more evident (Figure 22). Finally, the considerable scan rate dependence of the peak separation meant that the Nicholson method (183) of determining electron transfer rate constants could not be used for this system. The asymmetry of the peak potentials could be caused by an α value of much less than 0.5 at low temperatures and much larger than 0.5 at high temperatures. However, the peak currents support an opposite trend in α. Single potential step chronoabsorptometry experiments indicated an α of ca. 0.56 (± 0.05) below 40 °C and ca. 0.36 (± 0.05) above 40 °C. The low α value above 40 °C is suspect. As discussed below, product adsorption occurs at temperatures above 40 °C. This would limit the absorbance response to a potential step and cause an unrealistically low α to be calculated. Alpha is clearly not the cause of the electrochemical behavior described above. Figure 23 shows a temperature series of quasi-reversible cyclic voltammograms of cytochrome c in pH 8.0 buffer. A maximum current is obtained at ca. 40 °C.

Figure 22. Temperature dependence of the asymmetry of the cyclic voltammetric peak potentials about E°' of cytochrome c in pH 5.3 (upside down triangles), 7.0 (x), and 8.0 (squares) buffers. Scan rate = 509 mV/s for all values. Asymmetry is calculated by: $(E_{p,c} - E°')/(E_{p,a} - E°')$.

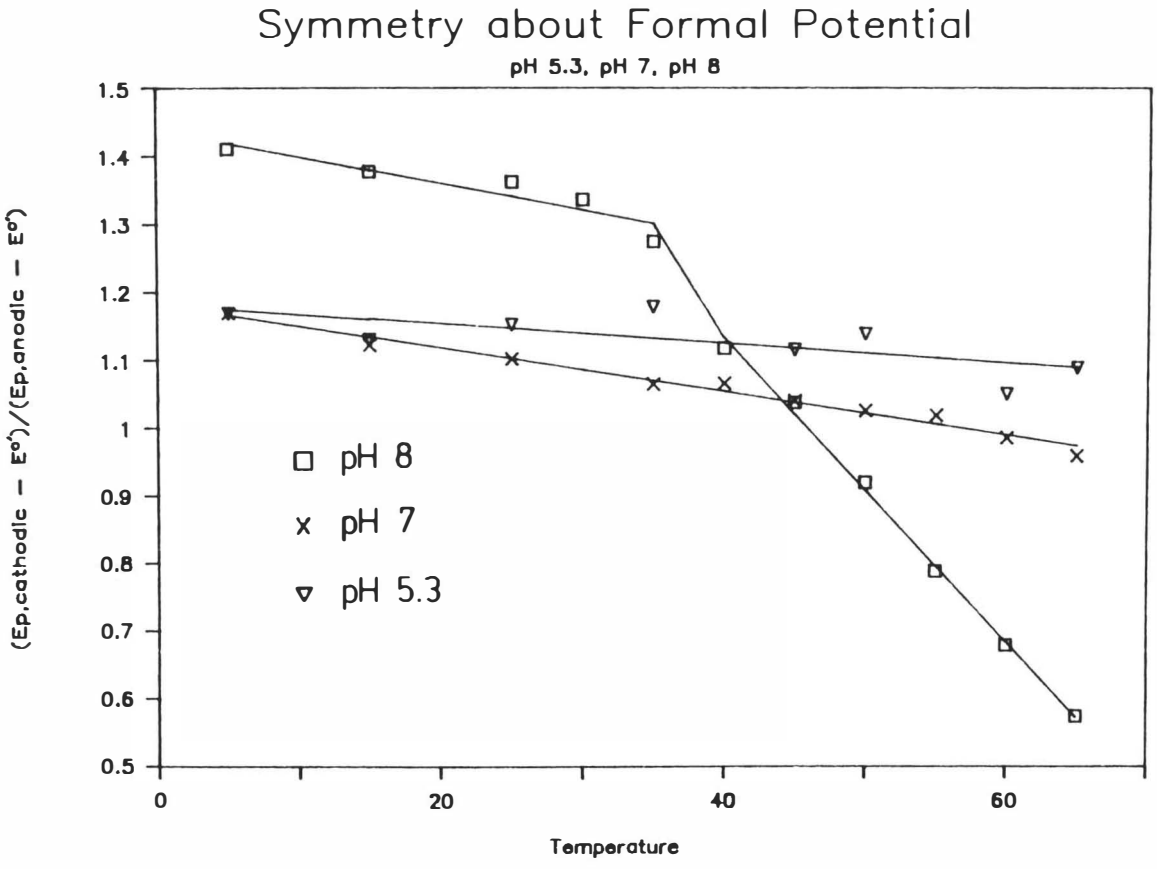
Symmetry about Formal Potential
pH 5.3, pH 7, pH 8
(Ep,cathodic − E°)/(Ep,anodic − E°)
1.5
1.4
1.3
1.2
1.1
1
0.9
0.8
0.7
0.6
0.5
0
20
40
60
Temperature
pH 8
pH 7
pH 5.3

This occurred in both phosphate and Tris/cacodylic acid buffers. The change in current is not attributed to electron transfer kinetics. A considerable change in the temperature dependence of the asymmetry of the peak potentials about the formal potential and the point of maximum current both occur at ca. 40 °C. This is the same temperature at which the break in the temperature dependence of the formal potential occurs. Figure 24 shows a series of cyclic voltammograms obtained at 5 °C. The shift in the cathodic peak potential is larger than that of the anodic peak potential. The low temperature behavior is due to reactant adsorption of weak to moderate strength. The midpoint potential of a 1V/s scan rate cyclic voltammogram is shifted 10 mV negative from the formal potential. For the same scan rate, the corresponding shifts in midpoint potential are 5 and 7 mV in pH 5.3 and pH 7.0 buffers, respectively. The strength of reactant adsorption steadily decreases with increase in temperature. A 40 °C, reactant adsorption is still indicated. Fitting simulations to 5 °C and 40 °C 1 V/s scan rate experiments indicated an adsorption equilibrium rate constant of 8 to 12 X 10^6 L/mole. This is in the same range as at pH 7.0, yet the potential variation at 5 °C indicates that the strength of adsorption is slightly stronger at pH 8.0. The pH 8.0 voltammograms were the most difficult to fit. The experimental peak currents were smaller than expected for the peak potential shift. Fitting to experimental peak potentials yielded an adsorption strength

Figure 23. Temperature dependence of quasi-reversible cyclic voltammograms of cytochrome c in pH 8.0 Tris/cacodylic acid buffer. Scan rate = 1.03 V/s. Temperatures, °C, are 5, 15, 25, 35, 45, 55, 65.

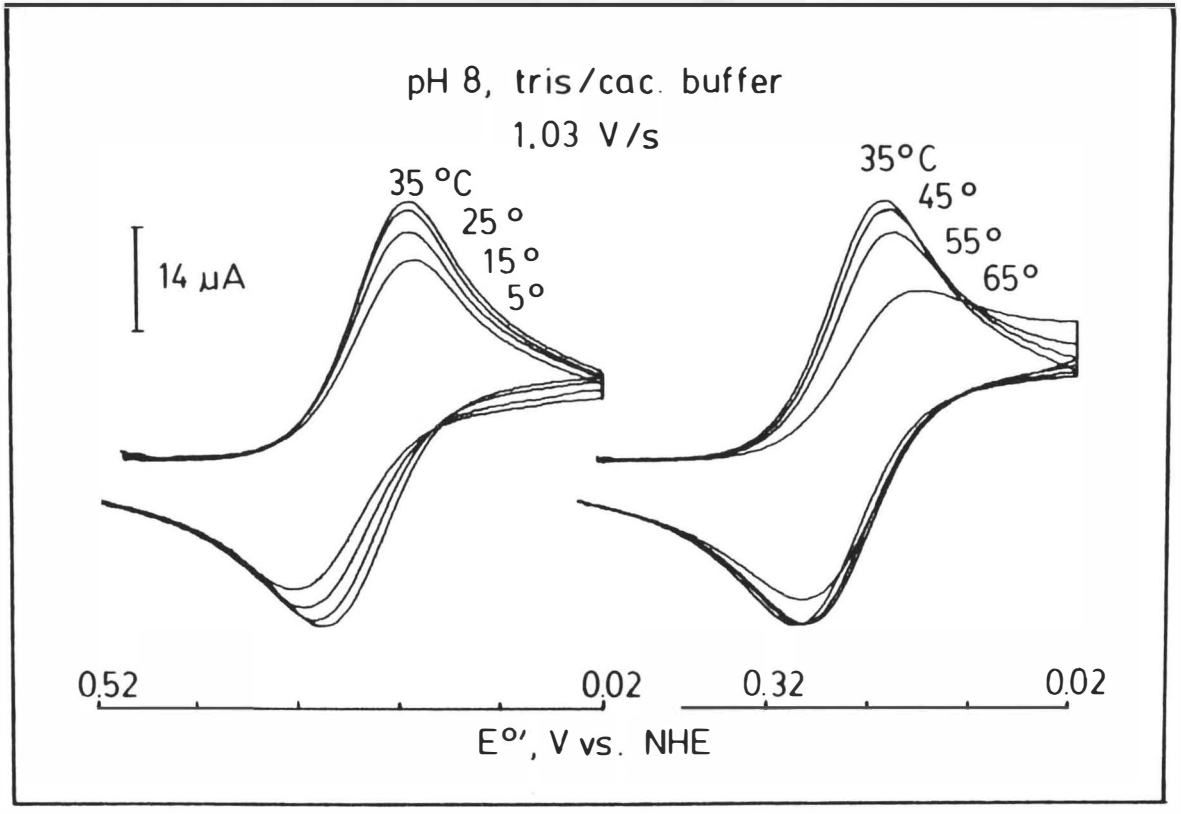
pH 8, tris/cac. buffer
1.03 V/s
35 °C
25 °
15 °
5°
14 µA
35°C
45 °
55°
65°
0.52
0.02
0.32
0.02
E°', V vs. NHE

Figure 24. Scan rate dependence of cyclic voltammmetry of cytochrome c in pH 8.0 Tris/cacodylic acid buffer at 5 °C. Temperature = 5 °C. Scan rates are 0.02, 0.51, and 1.03 V/s.

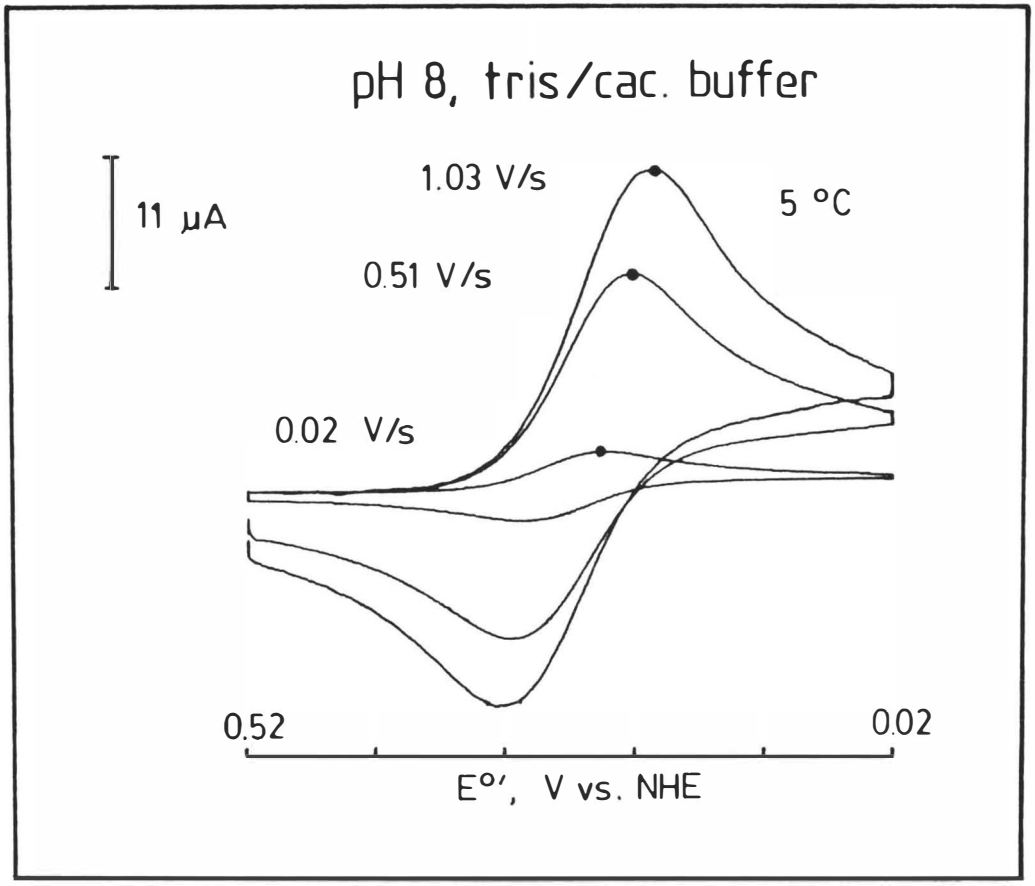
pH 8, tris/cac. buffer
11 µA
1.03 V/s
5 °C
0.51 V/s
0.02 V/s
0.52
0.02
E°', V vs. NHE

stronger than that at pH 7.0, whereas fitting to peak currents indicated weaker reactant adsorption. Product adsorption was also evident. Both product and reactant adsorption are probably stronger at pH 8.0 than in the more acidic solutions, and evaluating the empirical data with a simulation that only considers reactant adsorption is less accurate. Reactant and product adsorption have opposite effects on peak currents and potentials. However, the effect of reactant adsorption clearly dominates at the lower temperatures. There is a difference in the adsorption current between pH 5.3 and 7.0. At pH 5.3, the area occupied by ferricytochrome c is ca. 2800 $Å^2$ (a square with 53 Å sides). This is significantly larger than the 41 Å diameter calculated from the diffusion coefficient. Thus, a moderate increase in adsorption strength would easily increase the surface excess. At pH 7.0, the calculated surface excess indicates that cytochrome c is in a close packed arrangement to dimensions of the solvated structure. Increasing the surface excess would then require a significant increase in adsorption strength to overcome the requirement that some of the solvation sheath of the protein must be removed. Therefore, stronger adsorption would still shift the peak potentials, but a corresponding larger current is not observed since the surface excess has not changed significantly. The simulation used for this work is based on a Langmuir isotherm which does not consider interactions between adsorbed species. A Frumkin isotherm, which does consider adsorbate-

to-adsorbate interactions, probably more accurately describes the adsorption behavior of cytochrome c. A Frumkin isotherm was not simulated due to the added complexity of the algorithm. The present digital simulation algorithm is a qualitative analysis tool, and the addition of more adjustable parameters did not seem suitable for this problem. When the adsorption isotherm of cytochrome c has been determined, it can then be included in the simulation routine to provide further accuracy in evaluating the strength of adsorption and the limiting surface excess.

Figure 25 shows a series of cyclic voltammograms obtained at 60 °C in Tris/cacodylic acid buffer. The cathodic peak potential shift is smaller than the anodic peak potential shift, and the cathodic peak current is much smaller than that which would occur in the absence of adsorption effects. This behavior is attributed to product adsorption of moderate strength. The strength of product adsorption increases with temperature. Temperatures above 40 °C in pH 8.0 buffers are the only experimental conditions in which the effect of product adsorption on fast scan rate cyclic voltammograms is seen to predominate. Simulation of the 1 V/s scan rate cyclic voltammograms in Tris/cacodylic acid buffer above 55 °C proved to be difficult because peak currents were not affected as strongly as the peak potential variation would indicate. The electron transfer kinetics of the reaction are decreasing rapidly above this temperature, which further complicates the evaluation of adsorption

Figure 25. Scan rate dependence of cyclic voltammmetry of cytochrome c in pH 8.0 Tris/cacodylic acid buffer at 60 °C. Temperture = 60 °C. Scan rates are 0.02, 0.51, and 1.03 V/s.

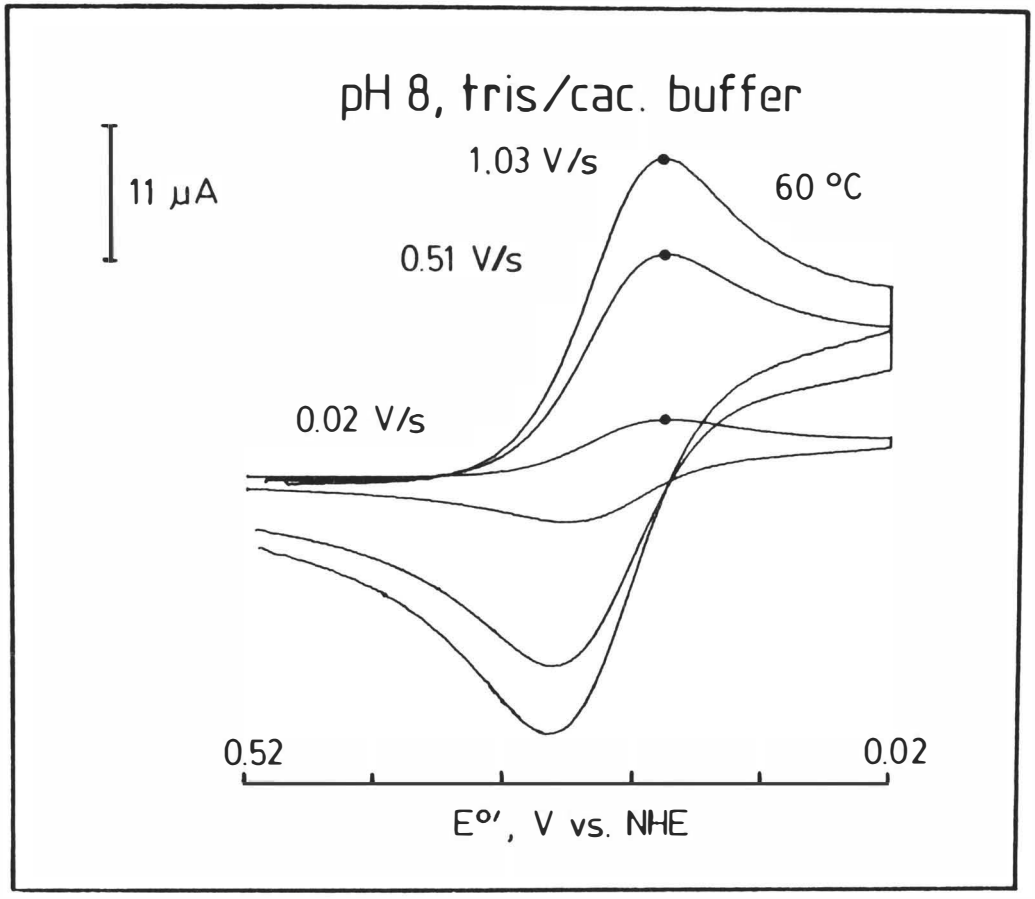
pH 8, tris/cac. buffer
11 µA
1.03 V/s
60 °C
0.51 V/s
0.02 V/s
0.52
0.02
E°′, V vs. NHE

effects. This complication also limits the analysis at low temperatures. The use of the Frumkin isotherm, which accurately includes the interactions between adsorbed molecules, could result in good fits. As mentioned in the discussion of the low temperature, pH 8.0 results, a significant variation in adsorption strength may be required to cause a surface excess above that obtained from close packing of fully solvated structures. A reasonable fit to experimental data was obtained at 55 °C for 1 V/s scan rate cyclic voltammograms using a simulation routine that included the effects of product adsorption. An equilibrium constant of 1.2 to 1.5 X 10^7 L/mole was calculated. This indicates a surface excess of 9.9 X 10^{-12} to 1.1 X 10^{-11} mole/cm^2. This represents a close packed arrangement of fully solvated ferrocytochrome c.

The determination of a temperature of maximum electron transfer kinetics in the pH 8.0 buffers is limited by the occurrence of product adsorption effects in the cyclic voltammograms. The onset of product adsorption behavior occurred at ca. 40 °C in both buffer systems. The maximum electron transfer rate constant in phosphate buffer is clearly lower than in phosphate buffer because irreversible electrochemistry at low scan rates occurred approximately 10 °C to 15 °C earlier in phosphate buffer. This indicates that the formal potential of maximum electron transfer kinetics may be the same in binding and nonbinding pH 8.0 media, since there is an equivalent shift in formal potential between the

two buffers at pH 8.0 and pH 7.0, where a 14 °C difference in maximum kinetics was observed.

The temperature dependence of the formal potentials of cytochrome c in both buffer systems is not affected from 5 to 40 °C by increasing the pH from 7.0 to 8.0. The electron transfer kinetics appear to be nearly equivalent in this temperature range also, although the perturbation of peak potentials from reactant adsorption is more pronounced at low temperatures in the pH 8.0 buffer. The electron transfer rate constant was not evaluated above 40 °C in the pH 8.0 buffers due to the clear dependence of peak potentials on adsorption behavior. The structure of ferricytochrome c may not be affected by changing the pH from 7.0 to 8.0, at least below 40 °C. This is indicated by the lack of effect on the formal potential of the protein. Adsorption strength is stronger at pH 8.0 due to an increase in the number of anionic sites on the electrode.

The onset of product adsorption effects on the electrochemical behavior occurs at the same temperature in both buffer media, but at different formal potentials, indicating that the heme environment is not altered by the change that occurs at 40 °C. This temperature, 40 °C, is the point of the break in the linear temperature dependence of the formal potential which occurs in both buffer media, again, at different formal potentials. As mentioned previously, Taniguchi et al. (51) attributed the break in formal potential at 40 °C to a structural event remote from the heme

environment. This conformational change may be that which reflects the transition from state III to state IIIb described by Myer et al. (90). State IIIb is the intermediate between the alkaline isomerization of state III to state IV, and is produced by a conformational event which does not affect the heme environment. If this is occurring, the change in adsorption effects from reactant to product control may be due to a difference in desorption rates between state III and state IIIb.

The effect of pH and temperature on the electrode must also be considered as a possible cause of the break in the temperature dependence of formal potential and adsorption characteristics. The electrostatic surface characteristics of the electrode may be altered by a change in specific anion binding and/or by a change in the structured solvent layer and the electrode surface. Electrostatically-induced adsorption of cytochrome c may then be strong enough so that the rate of ferrocytochrome c desorption from the electrode becomes slow and product adsorption effects are observed. There is no clear experimental evidence that indicates whether a transition to state IIIb or a change in electrode surface characteristics is causing the observed behavior. The fact that Taniguchi et al. (51) report the same temperature for the break in formal potential temperature dependence at a different electrode suggests that a change in the conformation of cytochrome c is causing the change in electrochemical behavior. It is unlikely that the two different

electrodes would undergo an interfacial change at the same temperature. Whether a change in the electrode or a change in the conformation of cytochrome c occurs ar 40 °C, it is clear that reactant and product adsorption strength is enhanced.

D. Summary

The thermodynamic and kinetic data determined for cytochrome c in pH 7.0 binding and nonbinding media indicate that the formal potential of the protein reflects the conformation of ferricytochrome c about the heme. The observation that a maximum in electron transfer kinetics occurred at the same formal potential (ca. 247 mV vs. NHE) but at different temperatures (42 °C in phosphate buffer and 55 °C in Tris/cacodylic acid buffer) suggests that there is an optimum conformation of ferricytochrome c for facile electron transfer. Adsorption phenomena prevented a similar comparison between formal potential and a maximum in kinetics in pH 8.0 buffers. Cytochrome c was only electrochemically reversible in the nonbinding media at pH 5.3. This disallowed the comparison of the formal potential of maximum kinetics of the protein in acidic binding and nonbinding media.

The difference in formal potential at any temperature between the two pH 7.0 electrolytes is attributed to the effect of anion binding to the positively charged residues in the vicinity of the solvent-exposed heme edge. The formal potential is shifted in a negative direction, and

reflects the enhanced stability of ferricytochrome c when anion binding occurs. The negatively charged anions partially compensate the positive charge of the heme group in its largely hydrophobic environment. Also, binding to the positively charged residues about the solvent-exposed heme edge has been suggested to cause an increase in the size of the heme crevice (133, 173). This greater degree of solvent exposure also stabilizes the positively charged heme group of ferricytochrome.

Fast scan rate cyclic voltammograms indicated the presence of weakly adsorbed reactant and product. The strength of reactant adsorption is larger than the strength of product adsorption under all conditions except for above 40 °C in pH 8.0 buffers. Approximately 1 X 10^{-11} mole/cm^2 of ferricytochrome c was found to be adsorbed to the electrode surface in pH 7.0 buffers. This corresponds to monolayer coverage of a fully solvated structure. Lowering the pH to 5.3 decreased the strength of adsorption, whereas an increase in the strength of adsorption occurred at pH 8.0. The pH dependence of the strength of adsorption is attributed to the pH properties of the indium oxide electrode used for this work. A Langmuir isotherm was used in the digital simulation routine. Adsorption behavior at pH 8.0 suggests that a Frumkin isotherm may be more appropriate. Cytochrome c will follow Langmuirian behavior until the surface is covered with a closely packed layer of fully solvated molecules. The solvation layer probably consists

of several layers of water molecules, each being more loosely held than the preceding layer. Further adsorption requires a larger amount of energy to overcome interadsorbate interaction, i.e., some of the solvation sheath must be removed. At this point, Frumkin isotherm adsorption behavior is observed.

Lowering the solution pH to 5.3 resulted in a decrease in the strength of reactant adsorption to approximately one half of that observed at pH 7.0 in Tris/cacodylic acid media. Cytochrome c was electrochemically irreversible in pH 5.3 phosphate buffer. This may be due to the inability of ferricytochrome c to bind to the electrode under these conditions. The onset of irreversible electrochemistry in pH 5.3 Tris/cacodylic acid buffer occurred at a higher temperature than in the pH 7.0 buffers and at ca. 240 mV vs. NHE, i.e., the same value at which this occurred in the pH 7.0 buffers. The increase in temperature stability is attributed to the added conformational resistance to temperature effects on the opening of the crevice about the solvent-exposed heme edge. The smaller degree of solvent exposure is reflected by the positive shift of the formal potential with change in pH from 7.0 to 5.3. The variation of electron transfer kinetics with change in temperature is not nearly as pronounced at pH 5.3. The optimum in kinetics occurred at the same temperature as in pH 7.0 Tris/cacodylic acid buffer, but at a formal potential of ca. 253 mV vs. NHE. The formal potential of ca. 247 mV vs. NHE, at which

optimum kinetics were obtained the pH 7.0 buffers, did not occur until 65 °C. The failure to observe an optimum electron transfer rate at this same temperature may be due to weaker adsorption in the acidic media.

The temperature dependence of the formal potential and the adsorption behavior of cytochrome c changed at ca. 40 °C in both binding and nonbinding pH 8.0 buffers. These changes in the electrochemical characteristics of the protein may be caused by a conformational transition of ferricytochrome c from state III to state IIIb. The heme environment is not affected by this transition. A change in pH from 7.0 to 8.0 does not affect the thermodynamic and kinetic properties of cytochrome c below 40 °C.

E. Model of Heterogeneous Electron Transfer

Albery and Hill (30, 35) have proposed that there are three essential events for effective electron transfer between an electrode and cytochrome c: adsorption, electron transfer, and desorption. Any of these factors can be a rate-limiting step in the apparent kinetics of the system. The results of this research support this mechanism.

The strength of adsorption depends on the electrode surface characteristics. The electrode should have binding sites of suitable strength for rapid adsorption of ferricytochrome c. The pzzp of the electrode will play a significant role in the initial electrostatic interaction with the protein. The electrode material, solvent pH, and electrolyte determine the pzzp. A negatively charged surface

will attract the positively charged exterior of cytochrome c and interact with the its dipole moment to orient the structure so that the solvent-exposed heme edge is adjacent to the electrode surface. The positively charged lysine residues that surround the active site will then bind to the electrode surface. This binding interaction may serve to enhance electron transfer by holding the structure in the correct orientation for effective orbital overlap with the heme until an appropriate transition state is achieved.

Binding to the active site residues has been proposed to weaken the heme crevice and the Fe-S bond, which may lead to an alteration of the heme environment that activates the complex toward electron transfer (123). This action will also increase the exposure of the hydrophobic interior of the crevice. The combination of a closer approach to the electrode due to binding and an increase in the hydrophobic nature of the domain within the ring of binding sites that surround the heme edge may serve to expel water from the electron transfer site. This model of the binding interaction of ferricytochrome c with an electrode is similar to that reported for the reaction of ferricytochrome c with cytochrome b_5 (118, 123, 139). These studies concluded that charge neutralization resulting from the surface residue interactions and the exclusion of water from the reaction site in the complex both serve to create a hydrophobic, low dielectric environment along the electron transfer path between heme edges. Adsorption decreases with increase in

temperature. The break observed in the heterogeneous electron transfer rate with change in temperature may be due to the strength of adsorption decreasing to the point where an active electron transfer complex becomes difficult to obtain. The inner structured layer of a solvent at an electrode surface is probably not penetrated, or at least is more difficult to remove than that from the heme edge of the cytochrome c physiological redox partners. For this reason, it is unlikely that physiological electron transfer rates will be attained for heterogeneous electron transfer between cytochrome c and an electrode.

While the binding interaction must be strong enough to cause the structural alterations required for a suitable transition state, it must be sufficiently weak to allow the protein to disengage from the electrode following electron transfer. Cytochrome c exhibits irreversible electrochemistry at most electrodes (43). This has been attributed to irreversible adsorption. The strength of adsorption to mercury may be sufficiently strong to denature ferricytochrome c. Weak reactant adsorption and product adsorption occurs at indium oxide electrodes. Thus, an effective electrode/solvent combination for interaction with cytochrome c, or other electron transfer proteins, must have appropriate electrostatic and adsorption characteristics.

As mentioned, binding weakens the crevice and the Fe-S bond in a manner such as to promote the formation of the transition state. The strength of the crevice and the Fe-S

bond are affected by temperature and pH. It seems reasonable that there exists an optimum combination of heme edge exposure, Fe-S bond strength, and adsorption strength for facile electron transfer with an electrode. The formal potential of cytochrome c is an indicator of the heme environment. This dependence is reflected by the temperature and pH dependence of the formal potential of cytochrome c. Thus, there may be an optimum conformation of ferricytochrome c, that is indicated by a specific formal potential, for effective electron transfer with an electrode. This optimum conformation results from a combination of temperature, solvent pH, and anion binding. The formal potential at which this optimum combination occurs may be different for various electrodes since the strength of adsorption is also a factor in the activation process towards electron transfer. The increase in electron transfer rate constant with increase in temperature may be due to a weakening of the heme crevice and Fe-S bond which allows the flexibility required for rapid attainment of the transition state. The break in kinetics may occur at a point where the conformation of ferricytochrome c becomes increasingly removed from the configuration of the transition state. The desorption process may be significantly facilitated by the differences in the conformation of ferri- and ferrocytochrome c. On reduction, the heme moves into the hydrophobic interior of the protein sheath, and the heme crevice closes. The conformational consequence of electron transfer has been

described as a "clamshell-like" opening and closing of the heme crevice (82). The motion of residues in the protein structure are interconnected. The movement of the heme crevice may aid in the desorption of cytochrome c from the electrode surface following electron transfer. A decrease in the strength of this interaction may cause the break to occur in the electron transfer kinetics. Temperature affects the strength of the Fe-S bond and the extent of the heme crevice opening in ferricytochrome c, while having very little effect on ferrocytochrome c. Consequently, the conformational change accompanying electron transfer changes with temperature. The extent of change increases with temperature to the point where ferricytochrome c is denatured. The larger difference in conformation with increase in temperature promotes the rate of desorption through a larger conformational change. As the temperature is increased further, the crevice opening and the strength of the Fe-S bond may have been altered to the point that the driving force to change to the reduced conformational form is not sufficient to overcome the strength of adsorption.

In conclusion, the heme of cytochrome c is contained in the hydrophobic interior of a globular protein structure. The tertiary structure is maintained through an extensive combination of chemical bonds, hydrogen bonds, and hydrophobic interactions. The complex is solubilized by charged surface groups. The residues about the electron transfer site serve as binding sites to reaction partners. The

action of binding serves to alter the conformation of the protein so that the electron transfer transition state is achieved. Electron transfer causes a conformational change which assists desorption through a concerted motion of the interconnected, mobile heme crevice residues. The apparent rate constant of heterogeneous electron transfer of cytochrome c with an electrode is potentially controlled by rates of adsorption, electron transfer, and desorption. As mentioned in the previous discussion, each may play the dominant role under different conditions. It is clear that the processes are interrelated. The strength of adsorption affects the conformation of cytochrome c, which is also affected by temperature, electrolyte, and pH. The ability to desorb from the electrode, depends both on the strength of the adsorption and the conformational difference between ferricytochrome c and ferrocytochrome c. The significant result of this research is that all three processes are clearly a part of the heterogeneous electrochemistry of cytochrome c. The relative contribution of each of these parameters to electron transfer rates with electrodes depends on the electrode material, electrolyte, pH, and temperature.

Selective adsorption, facile electron transfer, and desorption are the critical physiological parameters. Therefore, the mechanism by which cytochrome c, or other electron transfer proteins, interacts with an electrode may be similar to the physiological mechanism. Heterogeneous

electrochemical investigations of enzymes provide a tractable approach to determining physiological reaction mechanisms. An understanding of the electrochemical interaction of a biological substance with an electrode will also assist in the design of electrochemical biological sensors.

REFERENCES

REFERENCES

1. Mathews, F. S., Prog. Biophys. Molecul. Biol. 1985, 45, 1-56.

2. Meyer, T. E.; Kamen, M. D. Adv. Prot. Chem. 1982, 35, 105-212.

3. Salemme, F. R. Ann. Rev. Biochem., 1977, 46, 299-329.

4. Lehninger, A. L. "Principles of Biochemistry"; Worth Publishers, Inc.: New York, 1982; Chapter 17.

5. Rodkey, F. L.; Ball, E. G. J. Biol. Chem. 1949, 182, 17-28.

6. Betso, S. R.; Klapper, M. K.; Anderson, L. B. J. Am. Chem. Soc. 1972, 94, 8197-8204.

7. Margalit, R.; Schejter, A. Eur. J. Biochem. 1973, 32, 492-499.

8. Scheller, F.; Jänchen, M.; Etzold, G.; Will, H. Bioelectrochem. Bioenerg. 1974, 1, 478-486.

9. Scheller, F.; Jänchen, M.; Lampe, J.; Prümke, H.-J.; Blanck, J. Palecek, E. Biochim. Biophys. Acta 1975, 412, 157-167.

10. Scheller, F.; Jänchen, M.; Prümke, H.-J. Biopolymers 1975, 14, 1553-1563.

11. Scheller, F.; Prümke, H.-J.; Schmidt, H. E.; Mohr, P. Bioelectrochem. Bioenerg. 1976, 3, 328-337.

12. Tarasevich, M. R.; Bogdanovskaya, V. A. Bioelectrochem. Bioenerg. 1976, 3, 589-595.

13. Scheller, F. Bioelectrochem. Bioenerg. 1977, 4, 490-499.

14. Anderson, C. W.; Halsall, H. B.; Heineman, W. R.; Kreishman, G. P. Biochem. Biophys. Res. Comm. 1977, 76, 339-344.

15. Yeh, P.; Kuwana, T. Chem. Lett. 1977, 1145-1148.

16. Kuznetsov, B. A.; Shumakovich, G. P.; Mestechkina, N. M. Bioelectrochem. Bioenerg. 1977, 4, 512-521.

17. Kreishman, G. P.; Anderson, C. W.; Su, C.-H.; Halsall, H. B.; Heineman, W. R. Bioelectrochem. Bioenerg. 1978, 5, 196-203.

18. Eddowes, M. J.; Hill, H. A. O. J. Am. Chem. Soc. 1979, 101, 4461-4464.

19. Haladjian, J.; Bianco, P. Serre. P. -A.; Bioelectrochem. Bioenerg. 1979, 6, 555-561.

20. Ikeda, T.; Kinoshita, H.; Yamane, Y. Senda, M. Bull. Chem. Soc. Jap. 1980, 53, 112-117.

21. Ikeda, T.; Yamane, Y.; Kinoshita, H.; Senda, M. Bull. Chem. Soc. Jpn. 1980, 53, 686-690.

22. Haladjian, J.; Bianco. P.; Serre, P. -A. J. Electroanal. Chem. 1980, 106, 397-404.

23. Taniguchi, V. T.; Sailasutu-Scott, N.; Anson, F. C.; Gray, H. B. Pure & Appl. Chem. 1980, 52, 2275-2281.

24. Kreishman, G. P.; Su, C.-H.; Anderson, C. W.; Halsall, H. B.; Heineman, W., R. Adv. Chem. Ser. 1980, No. 188, 169-185.

25. Kuznetsov, B. A. Bioelectrochem. Bioenerg. 1981, 8, 681-690.

26. Serre, P.-A.; Haladjian, J.; Bianco, P. J. Electroanal. Chem. 1981, 122, 327-336.

27. Uosaki, K.; Hill, H. A. O. J. Electroanal. Chem. 1981, 122, 321-326.

28. Senda, M.; Ikeda, T.; Kakutani, T.; Kano, K.; Kinoshita, H. Bioelectrochem. Bioenerg. 1981, 8, 151-165.

29. Bancroft, E. E.; Blount, H. N.; Hawkridge, F. M. Biochem. Biophys. Res. Comm. 1981, 101, 1331-1336.

30. Albery, W. J.; Eddowes, M. J.; Hill, H. A. O.; Hillman, A. R. J. Am. Chem. Soc. 1981, 103, 3901-3910.

31. Haladjian, J.; Pilard, R.; Bianco, P.; Serre, P.-A. Bioelectrochem. Bioenerg. 1982, 9, 91-101.

32. Taniguchi, I.; Murakami, T.; Toyosawa, K.; Yamaguchi,

H.; Yasakouchi, K. J. Electroanal. Chem. 1982, 131, 397-401

33. Dijk, C. V.; Van Leeuwen, J. W.; Veeger, C.; Schreurs, J. P. G. M.; Barendrecht, E. Bioelectrochem. Bioenerg. 1982, 9, 743-759.

34. Hill, H. A. O.; Walton, N. J. J. Am. Chem. Soc. 1982, 104, 6515-6519.

35. Eddowes, M. J.; Hill, H. A. O. Faraday Discuss. Chem. Soc. 1982, 74, 331-341.

36. Taniguchi, I.; Toyosawa, K.; Yamaguchi, H.; Yasukouchi, K. J. Electroanal. Chem. 1982, 140, 187-193.

37. Bowden, E. F.; Hawkridge, F. M.; Blount, H. N. Adv. Chem. Ser. 1982, 201, 159-171.

38. Bowden, E. F.; Hawkridge, F. M.; Chlebowski, J. F.; Bancroft, E. E.; Thorpe, C.; Blount, H. N. J. Am. Chem. Soc. 1982, 104, 7641-7644.

39. Heineman, W. R.; Anderson, C. W.; Halsall, H. B.; Hurst, M. M.; Johnson, J. M.; Kreishman, G. P.; Norris, B. J.; Simone, M. J.; Su, C. Adv. Chem. Ser. 1982, 201, 51-68.

40. Taniguchi, V. T.; Ellis, W. R.; Cammarata, V.; Webb, J.; Anson, F. C.; Gray, H. B. Adv. Chem. Ser. 1982, 201, 51-68.

41. Dhesi, R.; Cotton, T. M.; Timkovich, R. J. Electroanal. Chem. 1983, 154, 129-139.

42. Haladjian, J.; Bianco, P. Pilard, R. Electrochim. Acta 1983, 28, 1823-1828.

43. Hinnen, C.; Parsons, R.; Niki, K. J. Electroanal. Chem. 1983, 147, 329-337.

44. Huang, Y-Y.; Kimura, T. Biochemistry, 1984, 23, 2231-2236.

45. Bowden, E. F.; Hawkridge, F. M.; Blount, H. N. J. Electroanal. Chem., 1984, 161, 355-376.

46. Harmer, M. A.; Hill, H. A. O. J. Electroanal. Chem., 1984, 170, 369-375.

47. Armstrong, F. A.; Hill, H. A. O.; Oliver, B. N.; Walton, N. J. J. Am. Chem. Soc. 1984, 106, 921-923.

48. Arnold, D. J.; Gerchario, K. A.; Anderson, C. W. J. Electroanal. Chem. 1984, 172, 279-382.

49. Razumas, V. J.; Samalius, A. S.; Kulys, J. J. J. Electroanal. Chem. 1984, 164, 195-200.

50. Taniguchi, I.; Iseki, M.; Toyosawa, K.; Yamaguchi, H.; Yasukouchi, K. J. Electroanal. Chem. 1984, 164, 385-391.

51. Taniguchi, I.; Iseki, M., Eto, T.; Toyosawa, K. Yamaguchi, H.; Yasukouchi, K. Bioelectrochem. Bioenerg. 1984, 13, 373-383.

52. Taniguchi, I.; Funatsu, T.; Iseki, M.; Yamaguchi, H.; Yasukouchi, K. J. Electroanal. Chem. 1985, 193, 295-302.

53. Kuznetsov, B. A.; Shumakovich, G. P.; Mutuskin, A. A. Bioelectrochem. Bioenerg. 1985, 14, 347-356.

54. Hill, H. A. O.; Page, D. J.; Walton, N. J.; Whitford, D. J. Electroanal. Chem. 1985, 315-324.

55. Harmer, M. A.; Hill, H. A. O. J. Electroanal. Chem. 1985, 189, 229-246.

56. Koller, K. B.; Hawkridge, F. M. J. Am. Chem. Soc. 1985, 107, 7412-7417.

57. Palmer, G. In "Iron Porphyrins", Lever A. P. B.; Gray H. B., Eds.; Addison-Wesley: Reading, MA., 1983; Vol. II, 43-88.

58. Keller, R. M.; Wüthrich K. Biochim. Biophys. Acta 1978, 533, 195-208.

59. Wüthrich, K.; Aviram, I.; Schejter, A. Biochim. Biophys. Acta 1971, 253, 98-103.

60. Senn, H.; Keller, R. M.; Wuthrich, K. Biochem. Biophys. Res. Commun. 1980, 92, 1362-1369.

61. Dickerson, R. E.; Takano, T.; Eisenberg, D.; Kalli, O. B.; Samson, L.; Cooper, A.; Margoliash, E. J. Bio. Chem. 1971, 246, 1511-1535.

62. Przywarska-Boniecka, H.; Ostropolska, L. J. Inorg. Biochem. 1984, 20, 103-112.

63. Privalov, P. L.; Khechinashvilli, N. N. J. Mol. Biol. 1974, 86, 665-684.

64. Schejter, A.; Zuckerman, M.; Aviram, I. J. Biol. Chem. 1979, 254, 7042-7046.

65. Swanson, R.; Trus, B. L.; Mandel, N.; Mandel, G.; Kallai, O. B.; Dickerson, R. E.; J. Biol. Chem. 1977, 252, 759-775.

66. Takano, T.; Trus, B. L.; Mandel, N.; Mandel G.; Kallai, O. B.; Swanson, R.; Dickerson, R. E. J. Biol. Chem. 1977, 252, 776-785.

67. Takana, T.; Dickerson R. E. Proc. Natl. Acad. Sci. USA 1980, 77, 6371-6375.

68. Poulos, T. L.; Kraut, J. J. Biol. Chem. 1980, 255, 10322-10330.

69. Kassner, R. J. Proc. Natl. Acad. Sci. USA 1972, 69, 2263-2267.

70. Kassner, R. J. J. Am. Chem. Soc. 1973, 95, 2674-2677.

71. Stellwagen, E. Nature 1978, 275, 73-74.

72. Moore, G. R.; Williams, R. J. P. FEBS Lett. 1977, 79, 229-232.

73. Myer, Y. P.; Saturno, A. F.; Verma, B. C.; Pande, A. J. Biol. Chem. 1979, 254, 11202-11207.

74. Ten Kortenaar, P. B. W.; Adams, P. J. H. M.; Tesser, G. I. Proc. Natl. Acad. Sci. USA 1985, 82, 8279-8283.

75. Moore. G. R. Febs 0802, Discussion Letter 1983, 161, 171-175.

76. Moore, G. R.; Williams, R. J. P.; Eur. J. Biochem. 1980, 103, 523-532.

77. Moore, G. R.; Williams, R. J. P.; Eur. J. Biochem. 1980, 103, 513-521.

78. Campbell, I. D.; Dobson, C. M.; Moore, G. R.; Perkins, S. J.; Williams, R. J. P. FEBS Lett. 1976, 70, 96-100.

79. Robinson, M. N.; Boswell, A. P.; Huang, Z.-X.; Eley, C. G. S.; Moore, G. R. Biochem. J. 1983, 213, 687-700.

80. Bosshard, H. R.; Zurrer, M. J. Biol. Chem. 1980, 255, 6694-6699.

81. Harbury, H. A.; Cronin, J. R.; Fanger, N. W.; Hettinger, T. P.; Murphy, A. J.; Myer, Y. P.;

Vinogradox, S. N. Proc. Natl. Acad. Sci. USA 1965, 54, 1658-64.

82. Rackovsky, S.; Goldstein, D. A. Proc. Natl. Acad. Sci. USA 1984, 81, 5901-5905.

83. Schejter, A.; George, P. Biochemistry 1964, 3, 1045-1049.

84. Kaminsky, L. S.; Miller, V. J.;Davison, A. J. Biochemistry 1973, 12, 2215-2221.

85. Pettigrew, G. W.; Aviram, I.; Schejter, A. Biochem. Biophys. Res. Commun. 1976, 68, 807-813.

86. Hines, R. M.; Kreishman, G. P. Bioelectrochem. Bioenerg. 1981, 8, 309-314.

87. Saigo, S. Biochim. Biophys. Acta 1981, 669, 13-20.

88. Moore, G. R.; Huang, Z.-X; Eley, C. G. S.; Barker, H. A.; Williams, G.; Robinson, M. N.; Williams, R. J. P. Faraday Diuscuss. Chem. Soc. 1982, 74, 311-329 and references therein.

89. Theorell, H.; Akesson, A. J. Am. Chem. Soc. 1941, 63, 1804-1827.

90. Myer, Y. P.; Srivastava, R. B.; Swatantar, K.; Raghavendra, K. J. Prot. Chem. 1983, 2, 13-42.

91. Forster, M.; Hester, R. E.; Cartling, B.; Wilbrandt, R. Biophys. J. 1982, 38, 111-116.

92. Cartling, B.; Holton, G. R.; Spiro, T. G. J. Chem. Phys. 1985, 83, 3894-3905.

93. Tabushi, I.; Yamamura, K.; Nishiya, T. Tetrahedron Lett. 1978, 49, 4921-4924.

94. Tabushi, I.; Yamamura, K.; Nishiya, T. J. Am. Chem. Soc. 1979, 101, 2785-2787.

95. Wilting, J.; Van Burren, K. J. H.; Braams, R.; Van Gelder, B. F. Biochim. Biophys. Acta 1975, 376, 285-297.

96. Pecht, I.; Faraggi, M. Proc. Natl. Acad. Sci. USA 1972, 69, 902-906.

97. Smith, H. T.; Millett, F. Biochemistry 1980, 19, 1117-1120.

98. Schejter, A.; Aviram, I.; Sokolovsky, M. Biochemistry 1970, 9, 5118-5122.

99. Bosshard, H. R. J. Mol. Biol. 1981, 153, 1125-1149.

100. Myer, J. P.; Thallam, K. K.; Pande, A. J. Biol. Chem. 1980, 255, 9666-9673.

101. Simone, M. J.; Kreishman, G. P. Anal. Biochem. 1983, 132, 142-146.

102. Hochman, J. H.; Schindler, M.; Jennefer, G. L.; Ferguson-Miller, S. In "The Biochemistry of Metabolic Processes", Lennon, D.; Stratman, F.; Zahlten, R., Eds.; Elsevier Biomedical Press: New York, 1983; 441-450.

103. Hochman, J.; Ferguson-Miller, S.; Schindler, M. Biochemistry 1985, 24, 2509-2516.

104. Theorell, H. Biochem. Z. 1936, 285, 207-218.

105. Gershon, N. D.; Porter, K. R.; Trus, B. L. Proc. Natl. Acad. Sci, USA 1985, 82, 5030-5034.

106. Kawato, S.; Sigel, E.; Carafoli, E. Cherry, R. J. J. Biol. Chem. 1980, 255, 5508-5510.

107. Reference 4, p. 321.

108. Karplus, M.; McCammon, J. A. Scientific American 1986, 254, 42-51.

109. Somogyi, B.; Welch, G. R.; Damjanovich, S. Biochim. Biophys. Acta 1984, 768, 81-112.

110. Salemme, F. R., In "Frontiers of Biological Energetics", Dutton, P. L.; Leigh, J. S.; Scarpa, A., Eds.; Academic Press: New York, 1978; Vol. I, 83-90.

111. Northrup, S. C.; Pear, M. R.; McCammon, J. A.; Karplus, M. Nature 1980, 286, 304-305.

112. Marcus, R. A.; Sutin, N. Biochim. Biophys. Acta 1985, 811, 265-322.

113. Nichols, P. Biochim. Biophys. Acta 1974, 346, 261-310.

114. Wherland, S.; Gray, H. B. Proc. Natl. Acad. Sci. USA 1976, 73, 2950-2954.

115. Goldkorn, T.; Schejter, A. J. Biol. Chem. 1979, 255, 12562-12566.

116. Butler, J.; Chapman, S. K.; Davies, D. M.; Sykes, A. G.; Speck, S.;Osheroff, N.; Margoliash, E. J. Biol. Chem. 1983, 258, 6400-6404.

117. Ragg, E.; Moore, G. R. J. Inorg. Biochem. 1984, 21, 253-261.

118. Ng, S. Smith, M. B.; Smith, H. T.; Millett, F. Biochemistry 1977, 23, 4975-4978.

119. Kang, C. H.; Brautigan, D. L.; Osheroff, N.; Margoliash, E. J. Biol. Chem. 1978, 253, 6502-6510.

120. Smith, M. B.; Stonehuerner, J.; Ahmed, A. J.; Staudenmayer, M.; Millett, F. Biochim. Biophys. Acta 1980, 592, 303-313.

121. Simondsen, R. P.; Weber, P. C.; Salemme, F. R.; Tollin, G. Biochemistry 1982, 24, 6366-6375.

122. Mathew, J. B.; Weber, P. C.; Salemme, F. R. Nature 1983, 301, 169-171.

123. Eley, C. G. S.; Moore, G. R. Biochem. J. 1983, 215, 11-21.

124. Augustin, M. A.; Chapman, S. K.; Davies, D. M.; Sykes, A. G.; Speck, S. H.; Margoliash, E. J. Biol. Chem. 1983, 258, 6405-6409.

125. Veerman, E. C. I.; Wilms, J.; Dekker, H. L.; Muijsers, A. O.; Van Buuren, J. J.; Van Gelder, B. F.; Osheroff, N.; Speck, S. H.; Margoliash, E. J. Biol. Chem. 1983, 258, 5739-5745.

126. Tollin, G.; Cheddar, G.; Watkins, J. A.; Meyer, T. E.; Cusanovich, M. A. Biochemistry 1984, 23, 6345-6349.

127. Smith, H. T.; Staudenmayer, N.; Millet, F. Biochemistry 1977, 16, 4971-4974.

128. Ferguson-Miller, S.; Brautigan, D. L.; Margoliash, E. J. Biol. Chem. 1978, 253, 149-159.

129. Ahmed, A. J.; Smith, H. T.; Smith, M. B.; Millettk F. S. Biochemistry 1978, 17, 2479-2483.

130. Wilms, J.; Dekker, H. L.; Boelens, R.; Van Gelder, B. F. Biochim. Biophys. Acta 1981, 637, 168-176.

131. Pettegrew, G. FEBS Lett. 1978, 86, 14-16.

132. Brautigan, D. L.; Ferguson-Miller, S.; Margoliash, E. J. Biol. Chem. 1978, 253, 130-139.

133. Brautigan, D. L.; Ferguson-Miller, S.; Tarr, G. E.; Margoliash, E. J. Biol. Chem. 1978, 253, 140-148.

134. König, B. W.; Osheroff, N.; Wilms, J.; Muijsers, A. O.; Dekker, H. L.; Margoliash, E. FEBS Lett. 1980, 111, 395-398.

135. Osheroff, J.; Speck, S. J.; Margoliash, E.; Veerman, E. C. I.; Wilms, J.; König, B. W.; Muijsers, A. O. J. Biol. Chem. 1983, 258, 5731-5738.

136. Ferguson-Miller, S.; Brautigan, D. L.; Margoliash, E., In "Tunneling in Biological Systems", Chance, B.; DeVault, D.; Frauenfelder, H., Eds.; Academic Press: New York, 1979; 513-522.

137. Sutin, N. Chem. Brit. 1972, 8, 148-151.

138. Koppenol, W. H.; Margoliash, E. J. Biol. Chem. 1982, 257, 4426-4437.

139. Salemme, F.R. J. Biol. Chem. 1976, 102, 563-568.

140. Yu, C.-A.; Steidl, J. R.; Yu, L. Biochim. Biophys. Acta 1983, 736, 226-234.

141. Speck, S. H.; Daniel, D.; Margoliash, E. Proc. Natl. Acad. Sci. USA 1984, 81, 347-351.

142. Ferguson-Miller, S.; Brautigan, D. L.; Margoliash, E. J. Biol. Chem. 1976, 251, 1104-1115.

143. Speck S. H.; Margoliash, E. J. Biol. Chem. 1984, 259, 1064-1072.

144. Carney, M. J.; Lesniak, J. S.; Likar, M. D.; Pladziewicz, J. R. J. Am. Chem. Soc. 1984, 106, 2565-2569.

145. Taube, H., Adv. Chem. Ser. 1977, 162, 127-144.

146. Hopfield, J. J. Proc. Natl. Acad. Sci. USA 1974, 71, 3640-3644.

147. Marcus, R. A., In "Special Topics in Electrochemistry", Rock, P. A., Ed.; Elsevier Scientific Publishing Co.: Amsterdam, 1977; 161-210.

148. Marcus, R. A.; Sutin, N., Inorg. Chem. 1975, 14, 213-216.

149. Wherland, S.; Gray, H. B. In "Biological Aspects of Inorganic Chemistry", Addison, A. W.; Cullen, W. R.;

Dolphin, D.; James, B. R., Eds.; Wiley-Interscience: New York; 1977, 289-368.

150. Espenson, J. H., "Chemical Kinetics and Reaction Mechanisms," McGraw-Hill Book Company: New York, 1981.

151. Gupta, R. K. Biochim. Biophys. Acta 1973, 292, 291-295.

152. Hupp, J. T. and Weaver, M. J., J. Electroanal. Chem. 1983, 152, 1-14.

153. Bowden, E. F.; Hawkridge, F. M.; Blount, H. N. In "Comprehensive Treatise of Electrochemistry", Srinivasan; Chizmadzhev; Bockris; Conway; Yeager, Eds.; Plenum Publishing Corporation: New York, 1985; Vol. 10, 297-345.

154. Brautigan, D. L.; Ferguson-Miller, S.; Margoliash, E. Methods Enzymol. 1978, 53D, 131-132.

155. Van Buuren, K. J. H.; Van Gelder, B. F.; Wilting, J.; Braams, R. Biochim. Biophys. Acta 1974, 333, 421-429.

156. J. N. Butler "Ionic Equilibrium, A Mathematical Approach", Addison-Wesley Publishing Company, Inc.: New York, 1961.

157. Yee, E. L.; Cave, R. J.; Guyer, K. L.; Tyma, P. D.; Weaver, M. J. J. Am. Chem. Soc. 1979, 101, 1131-1137.

158. Hawkridge, F. M. In "Laboratory Techniques in Electroanalytical Chemistry"; Kissenger, P. T.; Heineman, W. R., Eds.; Marcel Dekker, Inc.: New York, 1984; 337-365.

159. Armstrong, N. R.; Lin, A. W. C.; Fujihira, M.; Kuwana, T. Anal. Chem. 1976, 48, 741-750.

160. Bard, A. J.; Faulkner, L. R. "Electrochemical Methods, Fundamentals and Applications", Wiley, New York, 1980, Chapters 5 and 6, 136-248.

161. Woodard, F. E.; Woodward, W. S.; Reilley, C. N. Anal. Chem. 1981, 53, 1251A-1266A.

162. Thomas, C. E., M. S. Thesis, Virginia Commonwealth University, Richmond, VA., 1982.

163. Savitzkyk, A.; Golay, M. J. E. Anal. Chem. 1964, 36, 1627-1639.

164. Bancroft, E. E.; Sidwell, J. S.; Blount, H. N. Anal. Chem. 1981, 53, 1390-1394.

165. Bancroft, E. E.; Blount, H. N.; Hawkridge, F. M. Anal. Chem. 1981, 53, 1862-1866.

166. Heineman, R. W.; Hawkridge, F. M.; Blount, H. N. In "Electroanalytical Chemistry", Bard, A. J., Ed.; Marcel Dekker, Inc.: New York, 1984; Vol. 13, 1-113.

167. R. N. Adams, "Electrochemistry at Solid Electrodes"; Marcel Dekker, Inc.: New York, 1969; p. 63.

168. M. Abromowitz and I. A. Stegun, eds., "Handbook of Mathematical Functions with Formulas, Graphs, and Mathematical Tables", Dover Publications: New YorK, 1965, p. 299.

169. Hayes, J. W.; Glover, D. E.; Smith, D. E.; Overton, M. W. Anal. Chem. 1973, 45, 277-284.

170. O'Halloran, R. J.; Smith, D. E. Anal. Chem. 1978, 50, 1391-1394.

171. Morrison, S. R., "Electrochemistry at Semiconductor and Oxidized Metal Electrodes"; Plenum Press: New York, 1980; Chapter 2.

172. Osheroff, N.; Brautigan, D. L.; Margoliash, E. Proc. Natl. Acad. Sci. U.S.A. 1980, 77, 4439-4443.

173. Osheroff, N.; Borden, D., Koppenol, W. H.; Margoliash, E. J. Biol. Chem. 1980, 255, 439-449.

174. Lin, J.; Breck, W. G. Can. J. Chem. 1965, 43, 766-771.

175. Hawkridge, F. M.; Kuwana, T. Anal. Chem. 1973, 45, 1021-1027.

176. Bates, R. G. "Determination of pH Theory and Pratice"; Wiley: New York, 1973; pp 90-92.

177. Shaw, R. W.; Hartzell, C. R. Biochemistry 1976, 15, 1909-1914.

178. Andersson, T.; Angstrom, J. Falk, K.-E. Forsen, S. Eur. J. Biochem. 1980, 110, 363-369.

179. Andersson, T.; Thulin, E.; Forsen, S. Biochemistry 1979, 18, 2487-2493.

180. Stellwagen, E.; Shulman, R. G. J. Mol. Biol. 1973, 75, 683-695.

181. Burns, P. D.; La Mar, G. N. J. Am. Chem. Soc. 1979, 101, 5844-5846.

182. Reference 160, p. 506.

183. Nicholson, R. S. Anal. Chem. 1965, 37, 1351-1355.

184. Isied, S. S.; Kuehn, C.; Worosila, G. J. Am. Chem. Soc. 1984, 106, 1722-1726.

185. Norcea, D. G.; Winkler, J. R.; Yocom, K. M.; Bordignon, E.; Gray, H. B. J. Am. Chem. Soc. 1984, 106, 5145-5150.

186. Wopschall, R. H.; Shain, I. Anal. Chem. 1967, 39, 1514-1527.

187. Reference 160, p. 506.

188. Karger, B. L.; Snyder, L. R.; Horwath, C. "An Introduction to Separation Science"; John-Wiley & Sons: New York, 1973; p. 76.

189. Reference 160, pp. 204-206.

APPENDIX - DIGITAL SIMULATION OF CYCLIC VOLTAMMETRY

Digital simulations of the experimental cyclic voltammograms of cytochrome c proved invaluable in detecting and analyzing reactant and product adsorption. Experimentally determined formal potentials ($E^{\circ'}$), diffusion coefficients (D), heterogeneous electron transfer rate constants ($k^{\circ'}$), and electrode areas (A) were used to simulate the experimental results. A simulation program that does not contain adsorption effects, CVSIM, agreed with slow potential scan rate experiments, but did not match fast potential scan rate results where the current arising from electrolysis of adsorbed materials is significant. Analysis of these fast scan rate experiments was facilitated by the use of two simulation programs: CVADOX, which included the effects of adsorbed reactant, and CVADRED, which accounted for adsorbed product effects. These programs are based entirely on the published algorithms of Feldberg (1, 2).

In a process where a reactant, O, is reduced by an electrode to form a product, R, the electron flux, i.e., current, that flows during electrolysis is a function of electrode area, electron transfer kinetics, and the concentration of electroactive species ($C_r(0,t)$ and $C_o(0,t)$) at

the electrode surface. Prior to electrolysis, the surface concentrations equal the bulk concentrations (C_r^* and C_o^*). When the electrode potential is adjusted to a point where electrolysis occurs, the surface concentrations no longer equal the bulk concentrations. At this point, the movement of O toward the electrode and R away from the electrode is determined by a concentration gradient, $C_o(x,t)$. The calculation of the current requires solving the linear diffusion equation (Fick's Second Law):

$$\delta C_o(x,t)/\delta t = D_o \delta^2 C_o(x,t)/\delta x^2$$

This is a parabolic, second-order, partial differential equation. Semi-infinite diffusion is assumed for the outer boundary condition. This condition states that the bulk concentrations are not affected by electrolysis at the electrode surface. The flux of O and R at the electrode surface is described by Fick's First Law:

$$\text{flux} = D[\delta C(x,t)/\delta x]_{x=0}$$

Flux balance is maintained at the electrode surface (in the absence of adsorption); thus, the flux of O equals the flux of R:

$$D_o[\delta C_o(x,t)/\delta x)]_{x=0} - D_r[\delta C_r(x,t)/\delta x)]_{x=0} = 0$$

The current is given by:

$$i = nFAD_o(\delta C_o(x,t)/\delta x)_{x=0}$$

For a reversible system:

$$D_o(\delta C_o(x,t)/\delta x)_{x=0} = C_o(0,t) - C_r(0,t)$$

For a quasi-reversible system:

$$D_o(\delta C_o(x,t)/\delta x)_{x=0} = k_f C_o(0,t) - k_b C_r(0,t)$$

$$k_f = k^{\circ\prime}\exp[-\alpha n(F/RT)(E - E^{\circ\prime})]$$

$$k_b = k^{\circ\prime}\exp[(1-\alpha)n(F/RT)(E - E^{\circ\prime})]$$

Digital simulation determines the concentration gradient at any given time by using a finite difference iterative method. The Feldberg method is an explicit finite difference method. Implicit methods are also used (3), and are inherently more accurate. However, the explicit method is mathematically less sophisticated and therefore, easier to implement. An important point is that the accuracy of the explicit finite difference simulation is at least as good as that of the experimental data (4). Orthogonal collocation (5) has been used as an alternative to finite difference methods to simulate electrochemical problems. This method uses orthogonal polynomials to represent the concentration gradient.

Bard and Faulkner (6) present an excellent overview of explicit finite difference simulations. Explicit methods use a forward difference approximation. Implicit methods use an estimate of the n+1 variable in the calculation of the n+1 variable. This procedure adds complexity to the method, but also increased accuracy. Hanafay et al. (7) and Sandifer and Buck (8) have presented modifications to Feldburg's algorithm that may be of interest to potential users of the simulation routines presented here.

The finite difference method is implemented by establishing discrete distance, $\blacktriangle x$, and discrete time, $\blacktriangle t$, elements. Accuracy is increased by using small $\blacktriangle x$ elements.

Feldburg uses a linear array of evenly spaced boxes, each containing a fractional concentration. (Concentration is normalized.) The finite difference equation is:

$$C(x,t + \triangle t) =$$

$$C(x,t) + (D\triangle t/\triangle x2)[(x+\triangle x,t) - 2C(x,t) + C(x-\triangle x,t)]$$

$D\triangle t/\triangle x^2$ is a dimensionless parameter, D_m, that is the model diffusion coefficient. This parameter determines the size of the space elements. Greater accuracy is achieved with large values, but D_m must be less than 0.5 to avoid oscillations (failure in the model) in the simulation results. During each iteration, diffusion is expected to occur only between adjacent boxes. A value of D_m larger than 0.5 causes $\triangle x$ to be too small for the corresponding $\triangle t$, and the model fails. The distance $\triangle x$ is determined by D_m, the time of the experiment, t_k (sweep time for cyclic voltammetry), and the number of iterations, I, by:

$$\triangle x = (Dt_k/D_mI)^{1/2}$$

The size of the diffuse layer increases with time. The concentrations of only those boxes within the diffuse layer require adjustment with each iteration loop. This distance is estimated by:

$$n = 6(N\triangle tD_m/\triangle x)^{1/2}$$

n = number of space elements

N = iteration number

Thus, the concentrations of only those boxes within the diffuse layer determined for a particular time, $N\triangle t$, are adjusted during each iteration. It is noteworthy that the

difference in concentration between adjacent space elements decreases with distance away from the electrode. Converting from evenly sized boxes to a series of variable size, with the smallest next to the electrode, can significantly decrease the simulation time without sacrificing accuracy (9-11).

Fundamentally, a fraction of O is converted to R (or R to O) at the electrode surface during each iteration. The amount of material converted depends on the overpotential ($E - E^{\circ'}$), surface concentration, and heterogeneous kinetics. The amount of O reduced is subtracted from the box which represents the concentration of reactant adjacent to the electrode surface of the array that represents the concentration gradient of O, and is added to the first box of the R array. Diffusion is then allowed to occur between adjacent boxes throughout the array by use of the finite difference equation. The current corresponding to this iteration is calculated from the amount of O converted to R. The next iteration is begun, and the fraction of O converted to R now depends on a new overpotential and surface concentration. Real currents are calculated from the dimensionless flux by using input electrode areas, reactant concentrations, diffusion coefficients, temperature, and number of electrons transferred per molecule.

The specific details of the algorithm are given by Feldberg (1). Also, a listing of program CVSIM is given at the end of this section. The purpose of including the pro-

gram is two-fold. One is to provide the details of converting normalized flux to real current (not included in Feldberg's listing), and the second reason is to give an example of use of the IBM PC AT system to future members of Dr. Hawkridge's group.

The simulations that include the effects of adsorption are also based on a Feldberg algorithm (2). A Langmuir adsorption isotherm was used. The amount of adsorbed material, T, is related to the maximum surface coverage, T_S, the adsorption equilibrium constant, K, and the bulk concentration, C.

$$T = T_S KC/(1 + KC)$$

This can be rearranged to:

$$KC = T/(Ts - T)$$

Weak adsorption behavior is observed for KC values less than 2. Strong adsorption behavior is indicated by KC values larger than 100. The free energy of adsorption, $\blacktriangle G°$, is calculated from by:

$$K = \exp(\blacktriangle G°/RT).$$

The iteration code for the reactant adsorption program, CVADOX, and product adsorption program, CVADRED, is given at the end of this section. These are included since Feldberg (2) does not give program listings for the adsorption programs. Feldberg (2) presents a general algorithm for the reactant adsorption case. The same procedure was followed to develop the product adsorption simulation, CVADRED. The specific equations are contained in the program listing.

The adsorption equilibrium constant and the current due to adsorbed material were normalized with respect to the bulk solution concentration by:

$$K_{norm} = K/C$$

$$T_{norm} = T/[(RTD/vnF)^{1/2}C]$$

v = scan rate

```
        PROGRAM TITLE:  CVSIM
10 '    THIS IS A CYCLIC VOLTAMMETRIC SIMULATION PROGRAM FOR
20 '    THE SIMPLE PROCESS: O + nE = R.  WHERE ONLY O IS
30 '    INITIALLY PRESENT.    WRITTEN IN BASICA 2.0, MSDOS
40 '    2.0
50 DIM X(250), Y(250), X1(250), Y1(250), E(2500), I(2500)
60 CLS:SCREEN 0:WIDTH 80
70 DEFINT J,K,L,N,P
80 LOCATE 4,35
90 PRINT "CV SIMULATION MENU";
100 LOCATE 8,30
110 PRINT "1.  RETRIEVE DATA FROM DISK";
120 LOCATE 10,30
130 PRINT "2.  RUN SIMULATION";
140 LOCATE 12,30
150 PRINT "3.  TYPED OUTPUT OF DATA";
160 LOCATE 14,30
170 PRINT "4.  STORE DATA ON DISK";
180 LOCATE 16,30
190 PRINT "5.  PLOT CV";
200 LOCATE 18,30
210 PRINT "6.  TERMINATE PROGRAM";
220 LOCATE 20,5
230 PRINT "SELECT OPTION NUMBER";
240 Z$ = INKEY$: IF Z$ = "" THEN 240
250 IF Z$ = "6" THEN CLS: END
260 IF VAL(Z$) < 1 OR VAL(Z$) > 6 THEN GOSUB 300: GOTO 100
```

```
270 PRINT VAL(Z$)
280 ON VAL(Z$) GOSUB 2940,1820,3060,2830,470
290 GOTO 60
300 PRINT: LOCATE 22
310 PRINT "INVALID SELECTION - RE-ENTER";
320 GOSUB 360
330 LOCATE 22
340 PRINT "                              ";
350 RETURN
360 FOR N = 1 TO 1000: NEXT N: RETURN
370 '   THIS FINDS PEAK CURRENTS AND POTENTIALS
380 CLS
390 MAX = 0: MIN = 0
400 FOR J = 1 TO POINTS
410     IF MAX < I(J) THEN MAX = I(J): MAXLOC = J
420     IF MIN > I(J) THEN MIN = I(J): MINLOC = J
430 NEXT J
440 CATPEAKE = E(MAXLOC)
450 ANODPEAKE = E(MINLOC)
460 RETURN
470 '   THIS IS THE SCREEN PLOTTING ROUTINE
480 CLS
490 GOSUB 370
500 LOCATE 8,30
510 PRINT "CATHODIC PEAK CURRENT IS:  ";
520 PRINT USING "####.#";MAX;
530 PRINT "  MICROAMPS"
```

```
540 LOCATE 10,30
550 PRINT "ANODIC PEAK CURRENTS IS:   ";
560 PRINT USING "####.#";MIN;
570 PRINT "  MICROAMPS"
580 LOCATE 14,10
590 INPUT "INPUT CURRENT SCALE FROM 0 TO MAX:   ",ISCALE
600 ISCAL1 = ISCALE/66.5
610 PRINT:PRINT "INITIAL POTENTIAL FOR SIMULATION WAS:";
620 PRINT USING "+#.###"; INITE
630 LOCATE 17,10
640 INPUT "INPUT INITIAL POTENTIAL FOR PLOT:    ",INITE1
650 PRINT:PRINT "SWITCHING POTENTIAL FOR SIMULATION WAS:";
660 PRINT USING "+#.###"; SWITCHE
670 LOCATE 20,10
680 INPUT "INPUT FINAL POTENTIAL FOR PLOT:      ",SWITCHE1
690 KEY OFF: CLS: SCREEN 2
700 ESCALE = ABS(INITE1 - SWITCHE1)
710 ESCAL1 = ESCALE/320
720 IF R0 = -1 THEN 820
730 OFFSET = INITE1 - E(0): SET = OFFSET:IF SET < 0 THEN SET
    = 0
740 PSET (SET/ESCAL1 + 160,74.5 - I(0)/ISCAL1)
750 FOR J = 0 TO (KOUNT - 1)
760     MOVE = (E(0)-E(J))/ESCAL1 + OFFSET/ESCAL1
770     IF MOVE < 0 THEN MOVE = 0
780     IF MOVE > 320 THEN MOVE = 320
790     LINE -(MOVE+160,74.5-I(J)/ISCAL1)
```

```
800 NEXT J
810 GOTO 900
820 OFFSET = INITE1 - E(0): SET = OFFSET: IF SET > 0 THEN
    SET = 0
830 PSET (480 + SET/ESCAL1,74.5 - I(0)/ISCAL1)
840 FOR J = 0 TO (KOUNT - 1)
850 MOVE = (E(0)-E(J))/ESCAL1 + OFFSET/ESCAL1
860     IF MOVE > 0 THEN MOVE = 0
870     IF MOVE < -320 THEN MOVE = -320
880     LINE -(480+MOVE,74.5-I(J)/ISCAL1)
890 NEXT J
900 PSET (160,141)
910 FOR L = 1 TO 4
920     FOR J = 1 TO 10
930         IF L=1 THEN LINE -(160+J*32,141):LINE
            -(160+J*32,137.65):LINE -(160+J*32,141)
940         IF L=2 THEN LINE -(480,141-J*13.3):LINE
            -(472,141-J*13.3):LINE -(480,141-J*13.3)
950         IF L=3 THEN LINE -(480-J*32,8):LINE
            -(480-J*32,11.35):LINE -(480-J*32,8)
960         IF L=4 THEN LINE -(160,8+J*13.3):LINE
            -(168,8+J*13.3):LINE -(160,8+J*13.3)
970     NEXT J
980 NEXT L
990 LOCATE 1,35
1000 PRINT "CV SIMULATION"
1010 LOCATE 21,39: PRINT "VOLTS"
```

```
1020 IF R0 = 1 THEN A = INITE1: B = SWITCHE1
     ELSE A = SWITCHE1: B = INITE1
1030 LOCATE 19,19: PRINT USING "+#.##";A
1040 LOCATE 19,59: PRINT USING "+#.##";B
1050 LOCATE 10,4: PRINT "MICROAMPS"
1060 LOCATE 2,16: PRINT USING "###";ISCALE
1070 LOCATE 10,18: PRINT "0"
1080 LOCATE 22,5
1090 PRINT "SEND TO HP7470A?  (Y/N)"
1100 Z$ = INKEY$: IF Z$ = "" THEN 1100
1110 IF Z$ = "N" OR Z$ = "n" THEN 1150
1120 IF Z$ = "Y" OR Z$ = "y" THEN 1140
1130 GOTO 1080
1140 GOSUB 1160
1150 RETURN
1160 '  SEND TO HP7470A PLOTTER
1170 OPEN "COM1: 9600,S,7,1,RS,CS65535,DS,CD" AS #1
1180 DEFINT X,Y
1190 SCREEN 0:CLS: LOCATE 10,10
1200 PRINT "SELECT RECTANGLE SIZE IN INCHES"
1210 INPUT "INPUT X AXIS:  ", AXISX
1220 INPUT "INPUT Y AXIS:  ", AXISY
1230 X1 = (5.1-AXISX/2)*1010
1240 X2 = (AXISX/2+5.1)*1010
1250 Y1 = (3.75-AXISY/2)*1020
1260 Y2 = (AXISY/2+3.75)*1020
1270 PRINT #1, "IN;IP "X1","Y1","X2","Y2";"
```

```
1280 PRINT #1, "IW "X1","Y1","X2","Y2";"
1290 PRINT #1, "SC 0,10000,-10000,10000;"
1300 IF R0 = -1 THEN 1410
1310 X = (INITE1-E(0))/ESCALE*10000
1320 Y = I(0)/ISCALE*10000
1330 PRINT #1, "SP1;PA "X","Y";PD;"
1340 FOR J = 0 TO (KOUNT-1)
1350    X = ((E(0)-E(J))/ESCALE+(INITE1-E(0))/ESCALE)*10000
1360    Y = I(J)/ISCALE*10000
1370    PRINT #1, "PA "X","Y";"
1380 NEXT J
1390 PRINT #1, "SP;"
1400 GOTO 1500
1410 X = (1+(INITE1-E(0))/ESCALE)*10000
1420 Y = I(0)/ISCALE*10000
1430 PRINT #1, "SP1;PA "X","Y";PD;"
1440 FOR J = 0 TO (KOUNT-1)
1450    X =(((ESCALE+E(0)-E(J))/ESCALE+
        (INITE1-E(0))/ESCALE)*10000
1460    Y = I(J)/ISCALE*10000
1470    PRINT #1, "PA "X","Y";"
1480 NEXT J
1490 PRINT #1, "SP;"
1500 LOCATE 20,10
1510 PRINT "DO YOU WANT TO FRAME THIS GRAPH?  (Y/N)  ";
1520 Z$=INKEY$:IF Z$="" THEN 1520
1530 IF Z$="N" OR Z$="n" THEN 1570
```

```
1540 IF Z$="Y" OR Z$="y" THEN 1560
1550 GOTO 1520
1560 GOSUB 1580
1570 DEFSNG X,Y: CLOSE #1: RETURN
1580 '  FRAME ROUTINE TO HP7470A
1590 PRINT #1, "IW;"
1600 PRINT #1, "SP1;"
1610 PRINT #1, "SC 0,100,0,100;"
1620 PRINT #1, "PAPU 0,0,PD;"
1630 FOR L = 1 TO 4
1640    FOR J = 10 TO 100 STEP 10
1650            IF L = 1 THEN PRINT #1,
                "TL1.5,0;PA"J",0;XT;"
1660            IF L = 2 THEN PRINT #1,
               "TL0,1.5;PA100,"J";YT;"
1670            IF L = 3 THEN P = 100-J:
                PRINT #1, "TL0,1.5;PA"P",100;XT;"
1680            IF L = 4 THEN P = 100-J:
                PRINT #1, "TL1.5,0;PA0,"P";YT;"
1690    NEXT J
1700 NEXT L
1710 A$=STR$(INITE1): B$=STR$(SWITCHE1): C$=STR$(ISCALE)
1720 L = -(LEN(C$)+1)
1730 PRINT #1, "PU;PA0,0;SR2,2;CP-1,-1.5;LB"A$""+CHR$(3)
1740 PRINT #1, "PU;PA100,0;CP-1,-1.5;LB"B$""+CHR$(3)
1750 PRINT #1, "PU;PA50,0;CP-4,-3;LBE (VOLTS)"+CHR$(3)
1760 PRINT #1, "PU;PA0,50;CP-2,0;LB0"+CHR$(3)
```

```
1770 PRINT #1, "PU;PA0,100;CP"L",0;LB"C$""+CHR$(3)
1780 PRINT #1, "PU;PA0,50;CP-5,-4;DI0,90;LBI
     (MICROAMPS)"+CHR$(3)
1790 PRINT #1, "PU;DI;SR3,3;PA50,100;CP-6,1;LBCV
     SIMULATION"+CHR$(3)
1800 PRINT #1, "PA0,0;SP;"
1810 PRINT #1, "SP;": CLOSE #1: RETURN
1820 CLS
1830 INPUT "INPUT VALUE OF REDUCTION POTENTIAL IN VOLTS",E0
1840 PRINT
1850 INPUT "INPUT VALUE OF INITIAL POTENTIAL IN VOLTS",INITE
1860 PRINT
1870 INPUT "INPUT VALUE OF SWITCHING POTENTIAL IN VOLTS",
     SWITCHE
1880 PRINT
1890 INPUT "INPUT SCAN RATE IN VOLTS/SEC", SCANRAT
1900 PRINT
1910 INPUT "INPUT NUMBER OF ELECTRONS TRANSFERRED",N
1920 PRINT
1930 INPUT "INPUT AREA OF ELECTRODE, CM^2",AREA
1940 PRINT
1950 INPUT "INPUT TEMPERATURE IN DEGREES C",TEMP
1960 PRINT
1970 INPUT "CONCENTRATION OF PRECURSOR (MOLAR)",CONC
1980 PRINT
1990 INPUT "DIFFUSION COEFFICENT OF PRECURSOR (CM^2/SEC)",
     DIFFUSE
```

```
2000 PRINT
2010 INPUT "INPUT ALFA",ALFA
2020 PRINT
2030 INPUT "INPUT HETEROGENEOUS RATE CONSTANT (CM/SEC)",
     HETKIN
2040 PRINT
2050 INPUT "INPUT DATA RATE FOR SIMULATION (SEC/PT)", RATE
2060 PRINT
2070 CLS
2080 REM INITIALIZE SIMULATION VARIABLES
2090 F = 96484.6                    'FARADAYS CONSTANT
2100 R = 8.31441                    'GAS CONSTANT
2110 SCANRAT = -SCANRAT
2120 IF SWITCHE = 0 THEN 2170
2130 IF INITE/SWITCHE > O THEN 2170
2140 TEMPE = SWITCHE
2150 INITE = INITE - SWITCHE: E0 = E0 - SWITCHE
2160 SWITCHE = 0
2170 IF INITE > SWITCHE THEN R0 = 1 ELSE R0 = -1
2180 INITE = R0*INITE
2190 E0 = R0*E0
2200 SWITCHE = R0*SWITCHE
2210 TEMP = TEMP + 273
2220 FACTOR = N*F/(R*TEMP)
2230 FACTOR1 = -ALFA*FACTOR
2240 FACTOR2 = (1-ALFA)*FACTOR
2250 M0 = 0
```

```
2260 C1 = 0
2270 KOUNT = 0: G = 0
2280 POINTS = 2*(SWITCHE-INITE)/(RATE*SCANRAT) + 2
2290 V = SCANRAT*RATE
2300 D1 = .45
2310 R2 = SQR(DIFFUSE)
2320 R3 = SQR(D1)
2330 FACTOR3 = HETKIN*SQR(RATE)/R2
2340 FACTOR4 = R2*CONC*1000/(R3*SQR(RATE))
2350 FACTOR5 = 2*D1: INVFACT5 = 1/FACTOR5
2360 FACTOR6 = R0*N*F*AREA
2370 REM SIMULATION ROUTINE
2380 FOR J = 0 TO 250
2390 X(J) = 1
2400 Y(J) = 0
2410 NEXT
2420 CLS: LOCATE 5,5: PRINT "********** ACQUIRING DATA
     **********";
2430 LOCATE 7,5
2440 PRINT "NUMBER OF LOOPS REQUIRED TO COMPLETE
     SIMULATION:"; POINTS;
2450 LOCATE 9,5
2460 PRINT "CURRENT LOOP NUMBER IS:  ";
2470 KOUNT = KOUNT + 1
2480 LOCATE 9,33: PRINT KOUNT;
2490 J1 = 6*SQR(D1*KOUNT)+3
2500 FOR J=2 TO J1
```

```
2510 X1(J) = X(J) + D1*(X(J+1) - 2*X(J) + X(J-1))
2520 Y1(J) = Y(J) + D1*(Y(J+1) - 2*Y(J) + Y(J-1))
2530 NEXT
2540 IF M0 = 1 THEN 2570
2550 E3 = INITE + (KOUNT - 1)*V
2560 GOTO 2590
2570 G = G+1
2580 E3 = SWITCHE + G*V
2590 F1 = EXP(FACTOR1*(E3 - E0))
2600 B1 = EXP(FACTOR2*(E3 - E0))
2610 R5 = F1/B1
2620 B2 = FACTOR3*B1
2630 B3 = 1/(B2*R3) + R5/(FACTOR5) + INVFACT5
2640 Z = (R5*X(1)-Y(1))/B3
2650 F3 = FACTOR4*Z
2660 C1 = FACTOR6*F3
2670 X1(1) = X(1) + D1*(X(2)-X(1)) - Z
2680 Y1(1) = Y(1) + D1*(Y(2)-Y(1)) + Z
2690 E(KOUNT - 1) = E3*R0 + TEMPE: I(KOUNT - 1) = C1
2700 FOR J = 1 TO J1
2710 X(J) = X1(J)
2720 Y(J) = Y1(J)
2730 NEXT
2740 IF M0 = 1 THEN 2780
2750 IF KOUNT < POINTS/2 THEN 2470
2760 V = -V
2770 M0 = 1
```

```
2780 IF KOUNT > (POINTS - 2) THEN 2800
2790 GOTO 2470
2800 INITE = INITE*R0 + TEMPE: SWITCHE = SWITCHE*R0 + TEMPE:
     E0 = E0*R0 + TEMPE
2810 BEEP: CLS
2820 RETURN
2830 '  DISK WRITE SUBROUTINE, SEQUENTIAL FILE
2840 CLS
2850 LOCATE 8,1
2860 INPUT "input file name, include path if required  ",
     FILE$
2870 OPEN FILE$ FOR OUTPUT AS #1
2880 WRITE #1,E0,INITE,SWITCHE,N,AREA,TEMP,CONC,DIFFUSE,
     ALFA,HETKIN,RATE,POINTS,KOUNT,R0,SCANRAT
2890 FOR J = O TO POINTS
2900    WRITE #1, E(J),I(J)
2910 NEXT J
2920 CLOSE #1
2930 RETURN
2940 '  DISK READ SUBROUTINE, SEQUENTIAL FILE
2950 CLS
2960 LOCATE 4,20
2970 LOCATE 10,1
2980 INPUT "input file name, include path if required  ",
     FILE$
2990 OPEN FILE$ FOR INPUT AS #1
3000 INPUT #1, E0,INITE,SWITCHE,N,AREA,TEMP,CONC,DIFFUSE,
```

```
     ALFA,HETKIN,RATE,POINTS,KOUNT,R0,SCANRAT
3010 FOR J = 0 TO POINTS
3020    INPUT #1, E(J),I(J)
3030 NEXT J
3040 CLOSE #1
3050 RETURN
3060 '  WRITE TO SCREEN AND PRINTER SUBROUTINE
3070 CLS
3080 GOSUB 370
3090 SEPPEAK = ABS(E(MAXLOC) - E(MINLOC))
3100 RESOLUTION = ABS(SCANRAT*RATE)
3110 LOCATE 1,35
3120 PRINT "CV SIMULATION"
3130 LOCATE 4,1
3140 PRINT TAB(10) "REDUCTION POTENTIAL  (VOLTS)";
3150 PRINT TAB(59) USING "##.###"; E0
3160 PRINT TAB(10) "INITIAL POTENTIAL  (VOLTS)";
3170 PRINT TAB(59) USING "##.###"; INITE
3180 PRINT TAB(10) "SWITCHING POTENTIAL  (VOLTS)";
3190 PRINT TAB(59) USING "##.###"; SWITCHE
3200 PRINT TAB(10) "SCAN RATE  (VOLTS/SEC)";
3210 PRINT TAB(60) USING "#.###"; ABS(SCANRAT)
3220 PRINT TAB(10) "NUMBER OF ELECTRONS";
3230 PRINT TAB(60) USING "#.###"; N
3240 PRINT TAB(10) "ELECTRODE AREA  (CM^2)";
3250 PRINT TAB(60) USING "#.###"; AREA
3260 PRINT TAB(10) "TEMPERATURE  (DEG C)";
```

```
3270 PRINT TAB(58) USING "###.#"; TEMP-273
3280 PRINT TAB(10) "CONCENTRATION OF PRECURSOR (CM^2/SEC)";
3290 PRINT TAB(59) USING "##.##^^^^"; CONC
3300 PRINT TAB(10) "DIFFUSION COEFFICIENT OF PRECURSUR
     (CM/SEC)";
3310 PRINT TAB(59) USING "##.##^^^^"; DIFFUSE
3320 PRINT TAB(10) "ALFA";
3330 PRINT TAB(60) USING "#.###"; ALFA
3340 PRINT TAB(10) "HETEROGENEOUS RATE CONSTANT";
3350 PRINT TAB(59) USING "##.##^^^^"; HETKIN
3360 PRINT TAB(10) "NUMBER OF POINTS USED IN SIMULATION";
3370 PRINT TAB(59) POINTS
3380 PRINT TAB(10) "SPACING BETWEEN POINTS  (mV)";
3390 PRINT TAB(60) USING "##.#"; RESOLUTION*1000
3400 PRINT TAB(10) "PEAK SEPARATION  (mV)";
3410 PRINT TAB(59) USING "###.###"; SEPPEAK*1000
3420 PRINT TAB(10) "MAXIMUM CATHODIC CURRENT  (MICROAMPS)";
3430 PRINT TAB(58) USING "####.#"; MAX
3440 PRINT TAB(10) "MAXIMUM ANODIC CURRENT  (MICROAMPS)";
3450 PRINT TAB(58) USING "####.#"; MIN
3460 PRINT TAB(10) "CATHODIC PEAK POTENTIAL  (mV)";
3470 PRINT TAB(58) USING "####.###"; E(MAXLOC)*1000
3480 PRINT TAB(10) "ANODIC PEAK POTENTIAL (mV)";
3490 PRINT TAB(58) USING "####.###"; E(MINLOC)*1000
3500 PRINT:PRINT "SEND TO PRINTER?  (Y/N)";
3510 Z$ = INKEY$: IF Z$ = "" THEN 3510
3520 IF Z$ = "N" OR Z$ = "n" THEN 3560
```

```
3530 IF Z$ = "Y" OR Z$ = "y" THEN 3550
3540 GOTO 3500
3550 GOSUB 3570
3560 RETURN
3570 LPRINT:LPRINT
3580 LPRINT TAB(35) "CV SIMULATION"
3590 LPRINT
3600 LPRINT TAB(10) "REDUCTION POTENTIAL  (VOLTS)";
3610 LPRINT TAB(59) USING "##.###"; E0
3620 LPRINT TAB(10) "INITIAL POTENTIAL  (VOLTS)";
3630 LPRINT TAB(59) USING "##.###"; INITE
3640 LPRINT TAB(10) "SWITCHING POTENTIAL  (VOLTS)";
3650 LPRINT TAB(59) USING "##.###"; SWITCHE
3660 LPRINT TAB(10) "SCAN RATE  (VOLTS/SEC)";
3670 LPRINT TAB(60) USING "#.###"; ABS(SCANRAT)
3680 LPRINT TAB(10) "NUMBER OF ELECTRONS";
3690 LPRINT TAB(60) USING "#.###"; N
3700 LPRINT TAB(10) "ELECTRODE AREA  (CM^2)";
3710 LPRINT TAB(60) USING "#.###"; AREA
3720 LPRINT TAB(10) "TEMPERATURE  (DEG C)";
3730 LPRINT TAB(58) USING "###.#"; TEMP-273
3740 LPRINT TAB(10) "CONCENTRATION OF PRECURSOR (CM^2/SEC)";
3750 LPRINT TAB(59) USING "##.##^^^^"; CONC
3760 LPRINT TAB(10) "DIFFUSION COEFFICIENT OF PRECURSUR
     (CM/SEC)";
3770 LPRINT TAB(59) USING "##.##^^^^"; DIFFUSE
3780 LPRINT TAB(10) "ALFA";
```

```
3790 LPRINT TAB(60) USING "#.###"; ALFA
3800 LPRINT TAB(10) "HETEROGENEOUS RATE CONSTANT";
3810 LPRINT TAB(59) USING "##.##^^^^"; HETKIN
3820 LPRINT TAB(10) "NUMBER OF POINTS USED IN SIMULATION";
3830 LPRINT TAB(59) POINTS
3840 LPRINT TAB(10) "SPACING BETWEEN POINTS  (mV)";
3850 LPRINT TAB(60) USING "##.#"; RESOLUTION*1000
3860 LPRINT TAB(10) "PEAK SEPARATION  (mV)";
3870 LPRINT TAB(59) USING "###.###"; SEPPEAK*1000
3880 LPRINT TAB(10) "MAXIMUM CATHODIC CURRENT  (MICROAMPS)";
3890 LPRINT TAB(58) USING "####.#"; MAX
3900 LPRINT TAB(10) "MAXIMUM ANODIC CURRENT  (MICROAMPS)";
3910 LPRINT TAB(58) USING "####.#"; MIN
3920 LPRINT TAB(10) "CATHODIC PEAK POTENTIAL  (mV)";
3930 LPRINT TAB(58) USING "####.###"; E(MAXLOC)*1000
3940 LPRINT TAB(10) "ANODIC PEAK POTENTIAL (mV)";
3950 LPRINT TAB(58) USING "####.###"; E(MINLOC)*1000
3960 RETURN
```

```
          PROGRAM TITLE: CVADOX
10 '      THIS IS A CYCLIC VOLTAMMETRIC SIMULATION PROGRAM FOR
          THE PROCESS OF:  O + nE = R, WHERE O IS ADSORBED TO
          THE ELECTRODE.  ADSORPTION IS CONTROLLED BY A
          LANGMUIR ISOTHERM.  THE ALGORITHM IS FROM S. W.
          FELDBERG, IN "COMPUTERS IN CHEMISTRY".
1840 INPUT "INPUT VALUE OF REDUCTION POTENTIAL IN VOLTS",E0
1850 INPUT "INPUT VALUE OF INITIAL POTENTIAL IN VOLTS",INITE
1860 INPUT "INPUT VALUE OF SWITCHING POTENTIAL IN VOLTS",
     SWITCHE
1870 INPUT "INPUT SCAN RATE IN VOLTS/SEC",SCANRAT
1880 INPUT "INPUT NUMBER OF ELECTRONS TRANSFERRED",N
1890 INPUT "INPUT AREA OF ELECTRODE",AREA
1900 INPUT "INPUT TEMPERATURE IN DEGREES C",TEMP
1910 INPUT "CONCENTRATION OF PRECURSOR (MOLAR)",CONC
1920 INPUT "DIFFUSION COEFFICENT OF PRECURSOR (CM^2/SEC)",
     DIFFUSE
1930 INPUT "INPUT ALFA",ALFA
1940 INPUT "INPUT HETEROGENEOUS RATE CONSTANT (CM/SEC)",
     HETKIN
1950 INPUT "INPUT DATA RATE FOR SIMULATION (SEC/PT)",RATE
1960 INPUT "INPUT OX ADSORPTION EQUILIBRIUM CONSTANT",EOX
1970 INPUT "INPUT RED ADSORPTION EQUILIBRIUM CONSTANT",ERED
1980 INPUT "INPUT ADSORBED ELECTRON TRANSFER RATE CONSTANT",
     HETKINA
1990 INPUT "INPUT MAX SURFACE COVERAGE (MOLE/CM^2)",MAX
2000 CLS
```

```
2010 REM INITIALIZE SIMULATION VARIABLES
2020 F = 96484.6                    'FARADAYS CONSTANT
2030 R = 8.31441                    'GAS CONSTANT
2040 SCANRAT = -SCANRAT
2050 IF SWITCHE = 0 THEN 2100
2060 IF INITE/SWITCHE > 0 THEN 2100
2070 TEMPE = SWITCHE
2080 INITE = INITE - SWITCHE: E0 = E0 - SWITCHE
2090 SWITCHE = 0
2100 IF INITE > SWITCHE THEN R0 = 1 ELSE R0 = -1
2110 INITE = R0*INITE
2120 E0 = R0*E0
2130 SWITCHE = R0*SWITCHE
2140 TEMP = TEMP + 273
2150 D1 = .45
2160 R2 = SQR(DIFFUSE)
2170 R3 = SQR(D1)
2180 FOR J = 0 TO 250
2190 X(J) = 1
2200 Y(J) = 0
2210 NEXT
2220 EOX = EOX*CONC/1000
2230 ERED = ERED*CONC/1000
2240 TMAX = TMAX*1000/(SQR(R*TEMP*DIFFUSE/
           (F*ABS(SCANRAT)))*CONC)
2250 ADSORBX = TMAX*EOX*X(1)/(1+EOX*X(1))
2260 FACTOR = N*F/(R*TEMP)
```

```
2270 FACTOR1 = -ALFA*FACTOR
2280 FACTOR2 = TMAX*(EOX^(1-ALFA))*(ERED^ALFA)*HETKINA
2290 FACTOR4 = R2*CONC*1000/(R3*SQR(RATE))
2300 FACTOR5 = 2*D1
2310 FACTOR6 = R0*N*F*AREA
2320 M0 = 0: C1 = 0: KOUNT = 0: G = 0
2330 POINTS = 2*(SWITCHE-INITE)/(RATE*SCANRAT) + 2
2340 V = SCANRAT*RATE
2350 CLS: LOCATE 5,5: PRINT "********** ACQUIRING DATA
**********";
2360 LOCATE 7,5
2370 PRINT "NUMBER OF LOOPS REQUIRED TO COMPLETE
     SIMULATION:";POINTS;
2380 LOCATE 9,5
2390 PRINT "CURRENT LOOP NUMBER IS:  ";
2400 KOUNT = KOUNT + 1
2410 LOCATE 9,33: PRINT KOUNT;
2420 J1 = 6*SQR(D1*KOUNT)+3
2430 FOR J=2 TO J1
2440 X1(J) = X(J) + D1*(X(J+1) - 2*X(J) + X(J-1))
2450 Y1(J) = Y(J) + D1*(Y(J+1) - 2*Y(J) + Y(J-1))
2460 NEXT
2470 THETA = ADSORBX/TMAX
2480 IF M0=1 THEN 2510
2490 E3 = INITE +(KOUNT-1)*V
2500 GOTO 2530
2510 G = G+1
```

```
2520 E3 = SWITCHE+G*V
2530 F1 = (1-THETA)*(HETKIN+FACTOR2)*EXP(FACTOR1*(E3-E0))
2540 B1 = F1*EXP(FACTOR*(E3-E0))
2550 FAMAX = FACTOR5*X(1)
2560 FAMIN = -FACTOR5*Y(1)-ADSORBX
2570 Z = (FAMAX+FAMIN)/2
2580 DADSORBX =(Z*(1+F1/FACTOR5+B1/FACTOR5)
     +B1*Y(1)-F1*X(1))/(1+B1/FACTOR5)
2590 IF (ADSORBX+DADSORBX)<0 THEN FAMIN = Z:GOTO 2570
2600 IF (ADSORBX+DADSORBX)>TMAX THEN FAMAX = Z:GOTO 2570
2610 FCHECK =(ADSORBX+DADSORBX)/(EOX*(X(1)-Z/FACTOR5)
     *(TMAX-ADSORBX-DADSORBX))
2620 IF FCHECK<.9999 THEN FAMIN=Z: GOTO 2570
2630 IF FCHECK>1.0001 THEN FAMAX=Z: GOTO 2570
2640 ADSORBX = ADSORBX+DADSORBX
2650 ZB = DADSORBX-Z: ZF = Z-DADSORBX
2660 X1(1) = X(1) + D1*(X(2)-X(1)) - Z
2670 Y1(1) = Y(1) + D1*(Y(2)-Y(1)) - ZB
2680 C1 = FACTOR4*FACTOR6*ZF
2690 E(KOUNT - 1) = E3*R0 + TEMPE: I(KOUNT - 1) = C1
2700 FOR J = 1 TO J1
2710 X(J) = X1(J)
2720 Y(J) = Y1(J)
2730 NEXT
2740 IF M0 = 1 THEN 2780
2750 IF KOUNT < POINTS/2 THEN 2400
2760 V = -V
```

```
2770 M0 = 1
2780 IF KOUNT > (POINTS - 2) THEN 2800
2790 GOTO 2400
2800 INITE = INITE*R0 + TEMPE: SWITCHE = SWITCHE*R0 + TEMPE:
     E0 = E0*R0 + TEMPE
2810 BEEP: CLS
2812 EOX = EOX*1000/CONC
2814 ERED = ERED*1000/CONC
2820 RETURN
```

```
        PROGRAM TITLE:  CVADRED
10 '    THIS IS A CYCLIC VOLTAMMETRIC SIMULATION PROGRAM FOR
        THE PROCESS OF:  O + nE = R, WHERE R IS ADSORBED TO
        THE ELECTRODE. ADSORPTION IS CONTROLLED BY A
        LANGMUIR ISOTHERM.  THE ALGORITHM IS FROM  S. W.
        FELDBERG, IN "COMPUTERS IN CHEMISTRY".
1840 INPUT "INPUT VALUE OF REDUCTION POTENTIAL IN VOLTS",E0
1850 INPUT "INPUT VALUE OF INITIAL POTENTIAL IN VOLTS",INITE
1860 INPUT "INPUT VALUE OF SWITCHING POTENTIAL IN VOLTS",
     SWITCHE
1870 INPUT "INPUT SCAN RATE IN VOLTS/SEC",SCANRAT
1880 INPUT "INPUT NUMBER OF ELECTRONS TRANSFERRED",N
1890 INPUT "INPUT AREA OF ELECTRODE",AREA
1900 INPUT "INPUT TEMPERATURE IN DEGREES C",TEMP
1910 INPUT "CONCENTRATION OF PRECURSOR (MOLAR)",CONC
1920 INPUT "DIFFUSION COEFFICENT OF PRECURSOR (CM^2/SEC)",
     DIFFUSE
1930 INPUT "INPUT ALFA",ALFA
1940 INPUT "INPUT HETEROGENEOUS RATE CONSTANT (CM/SEC)",
     HETKIN
1950 INPUT "INPUT DATA RATE FOR SIMULATION (SEC/PT)",RATE
1960 INPUT "INPUT OX ADSORPTION EQUILIBRIUM CONSTANT",EOX
1970 INPUT "INPUT RED ADSORPTION EQUILIBRIUM CONSTANT",ERED
1980 INPUT "INPUT ADSORBED ELECTRON TRANSFER RATE CONSTANT",
     HETKINA
1990 INPUT "INPUT MAX SURFACE COVERAGE (MOLE/CM^2)",MAX
2000 CLS
```

```
2010 REM INITIALIZE SIMULATION VARIABLES
2020 F = 96484.6                    'FARADAYS CONSTANT
2030 R = 8.31441                    'GAS CONSTANT
2040 SCANRAT = -SCANRAT
2050 IF SWITCHE = 0 THEN 2100
2060 IF INITE/SWITCHE > 0 THEN 2100
2070 TEMPE = SWITCHE
2080 INITE = INITE - SWITCHE: E0 = E0 - SWITCHE
2090 SWITCHE = 0
2100 IF INITE > SWITCHE THEN R0 = 1 ELSE R0 = -1
2110 INITE = R0*INITE
2120 E0 = R0*E0
2130 SWITCHE = R0*SWITCHE
2140 TEMP = TEMP + 273
2150 D1 = .45
2160 R2 = SQR(DIFFUSE)
2170 R3 = SQR(D1)
2180 FOR J = 0 TO 250
2190 X(J) = 1
2200 Y(J) = 0
2210 NEXT
2220 EOX = EOX*CONC/1000
2230 ERED = ERED*CONC/1000
2240 TMAX = TMAX*1000/(SQR(R*TEMP*DIFFUSE/
            (F*ABS(SCANRAT)))*CONC)
2250 FACTOR = N*F/(R*TEMP)
2260 FACTOR1 = -ALFA*FACTOR
```

```
2270 FACTOR2 = TMAX*(EOX^(1-ALFA))*(ERED^ALFA)*HETKINA
2280 FACTOR4 = R2*CONC*1000/(R3*SQR(RATE))
2290 FACTOR5 = 2*D1
2300 FACTOR6 = R0*N*F*AREA
2310 M0 = 0: C1 = 0: KOUNT = 0: G = 0
2320 POINTS = 2*(SWITCHE-INITE)/(RATE*SCANRAT) + 2
2330 V = SCANRAT*RATE
2340 CLS: LOCATE 5,5: PRINT "********** ACQUIRING DATA
**********";
2350 LOCATE 7,5
2360 PRINT "NUMBER OF LOOPS REQUIRED TO COMPLETE
     SIMULATION:  ";POINTS;
2370 LOCATE 9,5
2380 PRINT "CURRENT LOOP NUMBER IS:  ";
2390 KOUNT = KOUNT + 1
2400 LOCATE 9,33: PRINT KOUNT;
2410 J1 = 6*SQR(D1*KOUNT)+3
2420 FOR J=2 TO J1
2430 X1(J) = X(J) + D1*(X(J+1) - 2*X(J) + X(J-1))
2440 Y1(J) = Y(J) + D1*(Y(J+1) - 2*Y(J) + Y(J-1))
2450 NEXT
2460 THETA = ADSORBY/TMAX
2470 IF M0=1 THEN 2500
2480 E3 = INITE +(KOUNT-1)*V
2490 GOTO 2520
2500 G = G+1
2510 E3 = SWITCHE+G*V
```

```
2520 F1 = (1-THETA)*(HETKIN+FACTOR2)*EXP(FACTOR1*(E3-E0))
2530 B1 = F1*EXP(FACTOR*(E3-E0))
2540 FAMAX = FACTOR5*Y(1)
2550 FAMIN = -FACTOR5*X(1)-ADSORBY
2560 Z = (FAMAX+FAMIN)/2
2570 DADSORBY = (Z*(1+F1/FACTOR5+B1/FACTOR5)
     -B1*Y(1)+F1*X(1))/(1+F1/FACTOR5)
2580 IF (ADSORBY+DADSORBY)<0 THEN FAMIN = Z:GOTO 2560
2590 IF (ADSORBY+DADSORBY)>TMAX THEN FAMAX = Z:GOTO 2560
2600 FCHECK = (ADSORBY+DADSORBY)/(ERED*(Y(1)
    -Z/FACTOR5)*(TMAX-ADSORBY-DADSORBY))
2610 IF FCHECK<.9999 THEN FAMIN=Z: GOTO 2560
2620 IF FCHECK>1.0001 THEN FAMAX=Z: GOTO 2560
2630 ADSORBY = ADSORBY+DADSORBY
2640 ZF = DADSORBY-Z
2650 X1(1) = X(1) + D1*(X(2)-X(1)) - ZF
2660 Y1(1) = Y(1) + D1*(Y(2)-Y(1)) - Z
2670 C1 = FACTOR4*FACTOR6*ZF
2680 E(KOUNT - 1) = E3*R0 + TEMPE: I(KOUNT - 1) = C1
2690 FOR J = 1 TO J1
2700 X(J) = X1(J)
2710 Y(J) = Y1(J)
2720 NEXT
2730 IF M0 = 1 THEN 2770
2740 IF KOUNT < POINTS/2 THEN 2390
2750 V = -V
2760 M0 = 1
```

```
2770 IF KOUNT > (POINTS - 2) THEN 2790
2780 GOTO 2390
2790 INITE = INITE*R0 + TEMPE: SWITCHE = SWITCHE*R0 + TEMPE:
     E0 = E0*R0 + TEMPE
2800 BEEP: CLS
2802 EOX = EOX*1000/CONC
2804 ERED = ERED*1000/CONC
2810 RETURN
```

APPENDIX REFERENCES

1. Feldberg, S. W. In "Electroanalytical Chemistry", Bard, A. J., Ed.; Marcel Dekker, Inc.: New York, 1969; Vol. 3, 199-297.

2. Feldberg, S. W. In "Computers in Chemistry and Instrumentation", Mattson, J. S.; Mark, H. B., Jr.; MacDonald, H. C. Jr., Eds.; Marcel Dekker, Inc.: New York, 1972; Vol. II, 185-218.

3. Heinze, J.; Storzback, M.; Mortensen, J. J. Electroanal. Chem. 1984, 165, 61-69.

4. Lasia, A. J. Electroanal. Chem. 1983, 146, 397-141.

5. Whitting, L. F.; Carr, P. W. J. Electroanal. Chem. 1977, 81, 1-20.

6. Bard, A. J.; Faulkner, L. R. "Electrochemical Methods, Fundamentals and Applications", Wiley, New York, 1980, Appendix B, 675-698.

7. Hanafey, M. K.; Scott, R. L.; Ridgway, T. H.; Reilley, C. N. Anal. Chem. 1978, 50, 116-137.

8. Sandifer, J. R.; Buck, R. P. J. Electroanal. Chem. 1974, 49, 161-170.

9. Joslin, T.; Pletcher, D. J. Electroanal. Chem. 1974, 49, 171-186.

10. Feldberg, S. W. J. Electroanal. Chem. 1981, 127, 1-10.

11. Seeber, R.; Stefani, S. Anal. Chem. 1981, 53, 1011-1016.

VITA